Swansea University
Prifysgol Abertawe

Medical School
Ysgol Feddygaeth

The development of innervative biomaterials for skeletal tissue regeneration

Inês Sousa dos Santos - [redacted]

Submitted to Swansea University in fulfilment of the requirements for the Degree of Master of Science

ABSTRACT

Innervation is a vital physiological process enabling communication between bodily functions and the central nerve system (CNS). It is expected that innervation plays an important role in tissue regeneration. However, there is a significant knowledge gap on the innervative capacity of synthetic biomaterials for the purposes for skeletal tissue engineering. This study aimed to investigate the innervation potential and improvement of the regenerative capacity of a biomaterial composed of hydroxyapatite/aragonite (HAA). Three main objectives were explored: 1) To assess whether HAA exhibits toxicity with HUMSCs and ReNcells through Alamar Blue assays and live cell imaging, 2) To determine the capacity of HAA to support neuronal growth and proliferation, and 3) To investigate the potential of HAA to enhance bone regeneration in an *in vivo* femoral-defect rat model. Following material preparation and characterization, HAA was tested *in vitro* using a co-culture of ReNcells and HUMSC where cell morphology, proliferation, and differentiation were monitored. HAA scaffolds were implanted into *in vivo* models, where they promoted bone regeneration by increasing bone callus formation, quantified via microCT scanning. The results indicate that HAA is non-toxic towards the co-culture. Through immunofluorescence and live cell imaging, we observed that ReNcells within the co-cultured showed consistent growth and proliferation through the first 7 days and successfully differentiated into matured neurons by day 14. The addition of HAA to the *in vivo* model showed a significant reduction in fracture gap width relative to the untreated. In conclusion, these findings demonstrate the potential to produce an innervative biomaterial for skeletal tissue engineering, offering a promising approach for skeletal tissue regeneration. Future research should aim to optimize cell deposition onto HAA by refining the fabrication methods to produce more uniform scaffold structures, applying techniques to quantify neuronal differentiation markers will also be essential to further clarify HAA's innervative capacity.

DECLARATION

This work has not previously been accepted in substance for any degree and is not being concurrently submitted in candidature for any degree.

Signed .....  ..... (candidate)

Date .....03/06/25.....

STATEMENT 1

This thesis is the result of my own investigations, except where otherwise stated. Where correction services have been used, the extent and nature of the correction is clearly marked in a footnote(s).

Other sources are acknowledged by footnotes giving explicit references. A bibliography is appended.

Signed .....  ..... (candidate)

Date .....03/06/25.....

STATEMENT 2

I hereby give consent for my thesis, if accepted, to be available for photocopying and for inter-library loan, and for the title and summary to be made available to outside organisations.

Signed .....  ..... (candidate)

Date .....03/06/25.....

TABLE OF CONTENTS

LIST OF FIGURES

LIST OF ABBREVIATIONS

3D – Three-Dimensional

ALP – Alkaline Phosphatase

BDNF – Brain-Derived Neurotrophic Factor

BMP – Bone Morphogenetic Protein

BP – Biphosphate

BSP – Bone Sialoprotein

CAD – Computer-Aided Design

cAMP – Cyclic Adenosine Monophosphate

CART – Cocaine- and Amphetamine-Regulated Transcript

CNS – Central Nervous System

Col2a1 – Collagen, type II, alpha 1 chain

CT – Computed Tomography

DBM – Demineralized Bone Matrix

ECM – Extracellular Matrix

EGF – Epidermal Growth Factor

ERK – Extracellular Signal-Regulated Kinase

FGF – Fibroblast Growth Factor

FTIR – Fourier-Transform Infrared Spectroscopy

GPA – Gigapascal

HA – Hydroxyapatite

HAA – Hydroxyapatite-Aragonite

HUMSC – Human Umbilical Mesenchymal Stem Cell

IGF – Insulin-Like Growth Factor

ITAM – Immunoreceptor Tyrosine-Based Activation Motif

KV – Kilovolt

LCP – Locking compression plate

MAP2 – Microtubule-Associated Protein 2

MC4R – Melanocortin 4 Receptor

MHC – Major Histocompatibility Complex

MiRNA – MicroRNA

ml – Millilitre

mm – Millimetre

ms – Millisecond

MSC – Mesenchymal Stem Cell

NE – Norepinephrine

NGS – Normal Goat Serum

Ng – Nanogram

NK1-R – Neurokinin 1 Receptor

NMU – Neuromedin U

NSA – Necrosulfonamide

NSC – Neural Stem Cell

NPY – Neuropeptide Y

OPN – Osteopontin

OSX - Osterix

PBST – Phosphate-Buffered Saline with TritonX100

PE – Polyethylene

PGA – Polyglycolic Acid

PKA – Protein Kinase A

PLA – Polylactic Acid

RFU – Relative Fluorescence Units

ROS – Reactive Oxygen Species

RT – Room Temperature

SD – Standard Deviation

SEM – Scanning Electron Microscopy

Sema3A – Semaphorin 3A

SNS – Sympathetic Nervous System

SP – Substance P

Tph2 – Tryptophan Hydroxylase 2

TO – Topology Optimization

TPMS – Triply Periodic Minimal Surfaces

TCP – Tricalcium Phosphate

TTCP – Tetracalcium Phosphate

μA – Microampere

μg – Microgram

Y1R – Neuropeptide Y Receptor Type 1

°C – Degrees Celsius

β2AR – Beta-2 Adrenergic Receptor

ACKNOWLEDGEMENTS

First and foremost, I want to express my deepest gratitude to my supervisor, Dr. Zhidao Xia, for his unwavering support, guidance, and steady encouragement throughout this entire project. Thank you for believing in me, especially during the moments I struggled to believe in myself, and for offering me opportunities that helped me grow both as a researcher and a person. I'm also sincerely thankful to my secondary supervisor, Dr. Jeffrey Davies, for his insight and kindness, and for helping me navigate the neural side of this work with patience and clarity.

A special thank you to Andrew, for generously providing the mice used in the in vivo studies. I also want to thank Logan for all his help and advice with the mechanical aspects.

To my friend Yadan, sharing lab space with you made this journey far less lonely and infinitely more joyful, I'll always be grateful for your friendship. Thank you as well to Leila for the thoughtful advice, kindness, and encouragement when I needed it most. And to my girls, Bri, Ffion, Meg, and Mos, I can't thank you enough for your patience, support, and for reminding me that life exists beyond experiments and deadlines.

I also want to express my gratitude to my family for always believing in me and encouraging me to aspire for more. And to my beloved granny, who is no longer with us, I hope I've made you proud.

1. INTRODUCTION

Bone is a dynamic, mineralized connective tissue that is essential for structural support, protection of soft tissues, movement, and mineral homeostasis (Florencio-Silva et al., 2015). Its mechanical strength arises from a highly organized composite structure that consists of an inorganic phase, primarily hydroxyapatite (HA) [$Ca_{10}(PO_4)_6(OH)_2$], which provides compressive strength, and an organic matrix dominated by type I collagen, which relays flexibility and tensile resistance (Schlesinger et al., 2019). This extracellular matrix (ECM) houses a coordinated network of bone cells that regulate growth, remodelling, and repair. Osteoprogenitor cells, derived from mesenchymal stem cells (MSCs), serve as precursors that differentiate into osteoblasts, the bone-forming cells responsible for synthesizing and mineralizing new matrix (Clines, 2010). As osteoblasts become embedded within the bone matrix they secrete, some differentiate into osteocytes, the most abundant bone cells. These mature cells reside within lacunae, or cavities within bone, and form an interconnected network via canaliculi, where they function as mechanosensors that detect mechanical strain and orchestrate bone remodelling by regulating both osteoblast and osteoclast activity (Florencio-Silva et al., 2015). Osteoclasts, on the other hand, originate from hematopoietic stem cells and are responsible for bone resorption. These multinucleated cells degrade mineralized bone matrix and facilitate turnover, which enables the release of calcium and phosphate into circulation (Boyce et al., 2009). The coordinated actions of these cells are critical for maintaining skeletal integrity and ensuring the bone retains its capacity to respond to mechanical stress, microdamage, and metabolic demands throughout life (Feng & McDonald, 2011).

Bone defects are a common public health issue worldwide and pose a serious socioeconomic burden (Court-Brown & Caesar, 2006; Polinder et al., 2016; Wu et al., 2021). Most bone defects or injuries can be repaired via natural bone regeneration and remodelling, the continuous process of old bone resorption and new bone formation, which allows for normal fracture healing (Gorter et al., 2021). However, bone defects arise from a variety of causes which can be broadly categorized into traumatic, pathological, and congenital origins (Blokhuis, 2017; Nauth et al., 2018). Trauma is a

leading cause of bone defects and can often result in fractures that extend beyond the bone's natural capacity for repair. In extreme cases of trauma, segmental bone loss, where large portions of bone are destroyed or removed which poses a significant challenge for reconstruction and healing (Adamczyk et al., 2020). Disorders that weaken the structural integrity of bone also contribute to defects, the biggest incidence of this is in osteoporosis. Characterized by low bone mass and microarchitectural deterioration of bone tissue, osteoporosis leads to reduced bone strength and increased risk of low-energy fractures, this is particularly observed in the elderly population (Gorter et al., 2021; Lupsa & Insogna, 2015). Similarly, primary or metastatic bone tumours can also lead to the erosion of bone tissue and significantly increase its fragility, which means that surgical intervention for bone resection and reconstruction is often required (Bădilă et al., 2021; Rajani & Gibbs, 2012). Infections such as osteomyelitis can also compromise bone integrity, resulting in localized defects that are difficult to heal without intervention (Weber et al., 2022). Bone defects can also stem from congenital conditions such as osteogenesis imperfecta. These defects are present from birth and may impair normal bone growth, function, and resorption which leads to a lifelong need for medical intervention (Deguchi et al., 2021).

Severe bone damage, such as non-union fractures, are a significant challenge in orthopaedic medicine. Non-union fractures occur when broken bones fail to heal within the expected timeframe and are often associated with underlying health conditions. These injuries can lead to chronic pain, reduced mobility, and long-term disability, which imposes a substantial socioeconomic burden (GBD 2019, 2021). In such event, the use of bone grafts becomes essential to support healing. Bone grafts provide a framework for regeneration through osteoconduction, osteoinduction, and osteogenesis, facilitating the restoration of structural integrity and function; osteoconduction refers to the graft's ability to serve as a scaffold for new bone growth, osteoinduction involves the recruitment and differentiation of progenitor cells into osteoblasts through signalling molecules, and osteogenesis refers to the formation of new bone by viable cells present within the graft itself (Albrektsson & Johansson, 2001). There has been a rising demand for bone grafts due to factors such as the aging population, increased rates of trauma, and advancements in surgical oncology (Zhao et al., 2021). These have highlighted

limitations in traditional materials, such as the limited availability of autografts and ethical concerns surrounding the use of allografts and xenografts. This unmet demand and need highlights the importance of developing alternative grafting solutions that can address the complex biological and mechanical challenges posed by severe bone injuries.

Autologous bone grafts involve harvesting bone tissue from the patient's own body and are widely regarded as the "gold standard" in bone grafting due to their compatibility and biological functionality (Schmidt, 2021). Typically sourced from sites such as the iliac crest, autografts contain the essential elements required for effective bone healing: osteogenic cells, osteoinductive factors, and an osteoconductive matrix (Miron et al., 2011; Pokharel et al., 2022). These properties make autografts uniquely suited for promoting bone regeneration in a variety of clinical contexts, from trauma to reconstructive surgeries. The primary advantage of autografts lies in their biocompatibility. As the graft material is derived from the patient, the risk of immune rejection is effectively eliminated, thus ensuring a higher success rate in integration and healing (Schmidt, 2021). Furthermore, autografts possess inherent osteogenic potential, which means they directly contribute live osteoblasts and progenitor cells that actively form new bone tissue (Miron et al., 2011). In addition to osteogenesis, autografts provide a natural scaffold for new bone growth (osteoconduction) and release biochemical signals that stimulate the differentiation of progenitor cells into osteoblasts (osteoinduction). These combined properties make autografts a superior choice in complex cases, such as non-union fractures or critical-sized defects. Despite their effectiveness, autografts are not without limitations. A major drawback is the morbidity associated with the donor site. Harvesting bone often results in significant pain, risk of infection, hematoma formation, and even long-term functional impairment at the site of extraction (Shin & Tornetta, 2016). The quantity of bone that can be harvested is limited, particularly in cases where a large bone graft volume is required, such as trauma-derived non-union fractures. This limitation is further worsened in patients with pre-existing conditions such as osteoporosis, where the quality of the natural bone is compromised. Finally, the need for an additional surgical procedure increases operative time,

healthcare costs, and the risk of complications, making autografts a less feasible option for certain patient populations (Schmidt, 2021).

Xenografts and allografts provide valuable alternatives, especially in cases where autograft tissue is insufficient or unavailable. These grafts offer a broader pool of material sources but come with their own set of advantages and challenges. Xenografts involve the use of bone tissue derived from animals, typically bovine or porcine sources, which is processed to reduce antigenicity and prevent immune rejection (Li et al., 2024; Sun et al., 2019). These grafts provide a readily available, cost-effective alternative to autografts and are often used in dental and orthopaedic procedures. The primary benefit of xenografts is their availability as animal-derived bone is often more abundant than human-sourced grafts, which makes xenografts a practical option for when large quantities of graft material are required (Ferraz, 2023). Xenografts also do not require a secondary surgical site for harvesting, which eliminates donor site morbidity and reduces operative time. The lower cost compared to autografts and allografts also makes xenografts an appealing choice for many patients and healthcare systems (Li et al., 2024). The main limitation with xenografts is the potential for immune rejection. Despite extensive processing to remove antigens, xenografts may still elicit an immune response in the human recipient, leading to graft resorption or failure. There is also the risk of transmitting animal-borne diseases, which, although rare, can have serious implications (Sun et al., 2019). In addition, while xenografts can provide a scaffold for bone healing, they lack osteogenic potential, meaning they do not directly contribute to new bone formation unless enhanced with osteogenic factors (Oguić et al., 2023). Another common alternative to bone autographs is allografts, which are primarily sourced from human cadavers. They can be processed as fresh, frozen, or demineralized bone matrix (DBM) to preserve their structural integrity and enhance their osteoinductive properties (Steijvers et al., 2022). Allografts are often used in orthopaedic, spinal, and dental surgeries. Allografts offer several benefits over xenografts, most notably their biological similarity to human bone, as this reduces the likelihood of immune rejection relative to xenografts, particularly when the graft is matched to the recipient's tissue type (Lomas et al., 2013). Allografts can also provide osteoinductive properties, especially when processed into a DBM form, which helps stimulate new bone formation. Allografts

eliminate the need for a second surgical site, reducing the patient's overall surgical burden. Despite their advantages, allografts are not without challenges. One of the primary concerns is the risk of disease transmission, particularly when grafts are not thoroughly screened or processed. Although the risk is low due to stringent protocols, it remains a potential issue. Another limitation is the variability in quality, as the osteogenic potential of allografts can be affected by the age of the donor, the processing method, and the storage conditions (Betz, 2002; Steijvers et al., 2022).

1.1. Skeletal tissue engineering

Synthetic bone allografts have emerged as a promising alternative to traditional grafting strategies, offering a solution to the limitations associated with autografts, allografts, and xenografts. These engineered constructs are designed to closely mimic the structural, mechanical, and biological properties of native bone while providing customizable and scalable options for a wide range of clinical applications. For maximum therapeutic efficacy, an ideal synthetic graft must satisfy a set of requirements that align with that of natural bone tissue. Biocompatibility is essential to prevent immune rejection and cytotoxicity and to establish an environment that supports cellular attachment, proliferation, and differentiation. In addition to mechanical and structural demands, the graft must exhibit osteoconductivity, osteoinductivity, and osteogenesis, the process by which osteoblasts synthesize and deposit the ECM of bone (Albrektsson & Johansson, 2001).

Equally as important is biodegradability or resorbability, the scaffold should degrade at a rate proportional to new bone formation to avoid the persistence of foreign material, while also providing temporary mechanical support. The graft must possess sufficient mechanical strength to bear physiological loads, especially in load-bearing sites, and should match the elastic modulus of native bone to prevent stress shielding. A porous microarchitecture is vital for facilitating tissue ingrowth, nutrient and waste exchange, and vascularization, which is necessary for sustaining metabolic activity within the regenerating tissue (Steijvers et al., 2022). In recent years, the role of innervation in bone regeneration is being acknowledged; grafts that support or promote neural integration

may enhance regulatory signalling, bone remodelling, and sensory feedback, all of which contribute to long-term graft success and skeletal homeostasis As such, the development of synthetic bone allografts involves the intricate balance of mechanical design, biomolecular functionality, and cellular compatibility to replicate the dynamic environment of natural bone as closely as possible.

It is important to recognize that the porous structure of natural bone tissue is inherently non-uniform and highly irregular. To date, no mathematical model has been able to fully describe the complex porous architecture of bone (Kim et al., 2022). While the microscopic arrangement of pores appears random, the macroscopic orientation of trabecular bone aligns with principal stress trajectories, allowing the skeleton to efficiently withstand mechanical loading (Oftadeh et al., 2015). Beyond mechanical support, this intricate porous network plays a vital biological role by providing a favourable environment for cell infiltration, migration, and vascularization (Kusumbe et al., 2014). The distribution of capillaries throughout bone is essential for the delivery of oxygen and nutrients and the removal of metabolic waste, processes that are central to bone health and regeneration. Vascular channels, including Haversian systems, are formed through this vascular invasion and remodelling process (Moreira et al., 2019).

The porous matrix acts as a channel for the diffusion and transport of bioactive molecules that are critical in regulating cellular activities such as differentiation, proliferation, and matrix deposition; these include bone morphogenetic proteins (BMPs), insulin-like growth factors (IGFs), biphosphates (BPs), and components of the ECM (Cui et al., 2019; Oliveira et al., 2021). In the context of scaffold design, mimicking this porous architecture is essential not only for mechanical function but also for providing an optimal interface for cell adhesion, tissue ingrowth, neurogenesis, and angiogenesis (Panseri et al., 2021). Therefore, a well-designed porous surface should enhance scaffold integration by facilitating direct cellular interaction and support the dynamic processes required for bone regeneration.

To address these complex requirements, researchers have increasingly turned to composite biomaterials and scaffold-based approaches. These scaffolds are designed to provide a three-dimensional (3D) porous framework that mimics the natural bone environment, thereby enhancing cell infiltration, vascularization, and nutrient diffusion.

The porosity of the materials is particularly important as most of the mammalian bone is inherently porous. This architecture reduces weight and facilitates cellular activity and blood vessel penetration, but it also imposes a trade-off with mechanical integrity. Thus, optimizing porosity is essential for balancing biological performance and mechanical stability (Qi et al., 2023; Wang et al., 2022). The design and fabrication of 3D scaffolds with optimal porosity and geometry have been revolutionized by computational and imaging technologies. Computer-Aided Design (CAD) software, along with Computed Tomography (CT)-based image analysis, allows for patient-specific modelling and precise fabrication of scaffold architecture (Zopf et al., 2014). Furthermore, advanced modelling techniques such as Triply Periodic Minimal Surface (TPMS) designs and topology optimization (TO) approaches enable the generation of complex, biomimetic internal structures that mimic the anisotropic and hierarchical nature of native bone (Dong & Zhao, 2021; Smit et al., 2021). These methods improve the mechanical performance of porous scaffolds while preserving high surface area and interconnected porosity for biological function, however, each method presents specific challenges. For instance, CT-based designs depend heavily on high-resolution imaging and accurate patient-specific data which can introduce variability; TPMS and TO approaches are powerful for optimizing mechanical and biological performance, though they often require significant computation resources, and may be constrained by current fabrication capabilities, particularly when translating complex geometries into physical scaffolds depending on the material used (Dong & Zhao, 2021; Ngo et al., 2018).

A variety of materials have been explored for bone tissue engineering, including metals, ceramics, polymers, and bioactive glass, each with distinct advantages suited to specific clinical needs. Titanium and its alloys are widely used in orthopaedic implants due to their high mechanical strength, corrosion resistance, and long-term stability. Upon implantation, titanium forms a thin, biologically inert oxide layer that reduces immune response. Its elastic modulus is lower than other metals like stainless steel, providing a closer but still higher match to cortical bone and reducing the risk of stress shielding (Chouirfa et al., 2019; Yılmaz et al., 2018). Advances in surface modification have improved titanium's resistance to bacterial adhesion and biofilm formation, enhancing infection control. However, titanium's stiffness can still negatively affect bone

remodelling in load-bearing situations. Furthermore, corrosion and wear of titanium implants may release alloy particles and ions into surrounding tissues, provoking inflammatory reactions that can cause bone loss and potentially lead to failure of osseointegration (Kim et al., 2019). Other metals used in bone tissue engineering include stainless steel and cobalt-chromium alloys. Stainless steel offers high strength and corrosion resistance but has a higher elastic modulus than titanium, increasing the risk of stress shielding. Cobalt-chromium alloys provide excellent wear resistance and mechanical durability. However, both metals may provoke significant inflammatory responses and have less favorable biocompatibility relative to titanium, which may limit their usage and effectiveness in certain applications (Chouirfa et al., 2019). Other metals like iron, magnesium, and zinc are gaining attention for their resorbable nature and ability to promote bone formation (Chen et al., 2022). Metals are increasingly alloyed to achieve an optimal balance of mechanical strength, osteogenic potential, and controlled resorbability, making them versatile options for bone tissue engineering applications (Herber et al., 2021).

Polymers such as polyethylene (PE), poly(lactic acid) (PLA), and poly(glycolic acid) (PGA) have been extensively explored for biomedical applications, particularly in bone tissue engineering (Fraile-Martínez et al., 2021). These materials are attractive due to their biocompatibility, biodegradation rates, and adaptability to various fabrication techniques. PGA has shown promise as a scaffold material for bone, cartilage, and tooth regeneration, owing to its mechanical properties, which are relatively comparable to those of natural bone. It supports essential cellular activities such as adhesion, proliferation, migration, and differentiation, promoting efficient tissue regeneration. However, one of the key limitations of using polymers alone is that regenerated tissues following severe damage often lack the full structural and functional continuity of the original tissue. To overcome this, polymers are frequently combined with other materials, such as ceramics like HA, to create composites that enhance mechanical strength and biological performance (Nguyen et al., 2022; Yeo et al., 2021). Additionally, polymers are highly compatible with advanced fabrication strategies such as electrospinning, solution mixing, melt extrusion, latex technology, and *in situ* synthesis (Zagho et al., 2018). Among these, 3D printing stands out as a major advantage, allowing

to produce highly customizable scaffolds with controlled porosity and architecture, which is critical for guiding cell behaviour and ensuring tissue integration.

Finally, ceramics are a widely used class of materials in skeletal tissue engineering. Ceramics are typically defined as solid compounds made either from two or more non-metallic elements or from a metallic element combined with one or more nonmetals (Boccaccini, 2005). Since bone tissue is naturally rich in calcium phosphate, many ceramic materials used are designed to mimic that composition.

HA is a crystalline form of calcium phosphate that closely resembles the mineral component of natural bone, comprising roughly two-thirds of the inorganic bone matrix (Mondal et al., 2023). Stoichiometric HA consists primarily of calcium and phosphorus in a Ca/P molar ratio of 1.67, which has been shown to be the most effective for promoting bone regeneration (Firdaus Hussin et al., 2012). This similarity to bone makes HA an attractive material for bone implants, it offers excellent biocompatibility and strong osteoconductive properties. In addition, another advantage HA has over the previously detailed materials is its high compressive strength, with a Young's modulus that can exceed 100 GPa in its dense form; however, it should be noted that this strength diminishes predictably as porosity increases, which is a common trade-off in scaffold design (Osuchukwu et al., 2023). Interestingly, HA has also demonstrated osteoinductive potential *in vivo* in primates, though the underlying mechanism for this is still not fully understood. Some researchers have speculated that this may involve the adsorption of osteoinductive molecules onto its surface following implantation (Ripamonti, 1996). Despite these advantages, HA's inherent brittleness and extremely slow biodegradation rate limit its use as a standalone implant material, especially in applications requiring dynamic mechanical loading or complete scaffold resorption (Campana et al., 2014).

To address these limitations, supplementing HA with $CaCO_3$ has emerged as a promising strategy. This enhances the biodegradability of the material, which allows for faster resorption and replacement by natural bone. In addition, calcium carbonate's ability to neutralize acidic environments can create a more favourable pH for cellular activity,

further supporting bone regeneration. This combination improves the material's mechanical and biological properties, bridging the gap between bioactivity and functionality in dynamic physiological environments.

β-tricalcium phosphate (β-TCP), its amorphous derivatives, and $CaCO_3$ are all significantly more biodegradable than hydroxyapatite. However, these materials can be resorbed by the body within a matter of weeks which makes them unsuitable as the primary structural component of a scaffold, particularly in terms of load-bearing or long-term applications (Campana et al., 2014; Monchau et al., 2013). Due to this rapid degradation, there are risks that affect their mechanical stability before sufficient new bone tissue can form. However, by incorporating HA to $CaCO_3$, it is possible to balance out the limitations of using each material independently as HA contributes mechanical strength and biocompatibility, while calcium carbonate enhances resorbability. A particularly effective form of this combination is seen in hydroxyapatite-aragonite (HAA), in which the $CaCO_3$ is present in its aragonite crystalline polymorph, a naturally occurring form of $CaCO_3$ with an orthorhombic crystal structure that contributes to its bioactivity. (Shi et al., 2020). Aragonite has been shown to support bone regeneration through its bioactivity and rapid remodelling capacity, thus making HAA a promising biomaterial that balances advantageous properties like osteoconductivity, mechanical strength, and controlled biodegradation (Lucas et al., 2001; Shi et al., 2020; Steijvers et al., 2025).

HAA scaffolds can be produced using a variety of approaches depending on the intended application. For powder-based formats, particularly when combined with polymers, the materials can be prepared by mixing commercially available HA and $CaCO_3$ powders in the desired ratio. Alternatively, $CaCO_3$ can be partially converted to HA through hydrothermal treatment in the presence of a phosphate source, which allows for a more precise control over the ratio between the components (Jinawath et al., 2002; Yoshimura et al., 2004). This method has been applied to naturally occurring coral structures due to their trabecular bone-like architecture, though the use of coral is not viable for large-scale production due to their status as endangered species. For clinical applications, it is important for synthetic bone scaffolds to be ethically sourced and able to be scaled according to demand (Ni & Ratner, 2003).

A typical HAA scaffold cement can be produced from a combination of tetracalcium phosphate (TTCP), calcium hydrogen phosphate ($CaHPO_4$), and $CaCO_3$. TTCP and $CaHPO_4$ react in a 1:1 molar ratio to form HA, while $CaCO_3$ is added according to the desired HA to CC ratio. This mixture can be processed into a cement well suited for extrusion-based 3D printing or solvent casting, both are cost-effective technique that allows for precise control over scaffold architecture, including pore size. Gelatine is also introduced in the formulation as a suspending agent, giving the cement a paste-like consistency that facilitates homogeneous mixing and printability. It also stabilizes the structure through crosslinking, which helps maintain the shape and integrity of the printed scaffold before the chemical setting reaction occurs (Shi et al., 2020; Steijvers et al., 2025; Xia et al., 2018)

MSCs are multipotent progenitor cells capable of differentiating into several cell lineages, including osteoblasts, chondrocytes, adipocytes, and neural-like cells. In addition to their differentiation potential, they play an active role in modulating the local microenvironment through the secretion of cytokines, growth factors, and components of the ECM (Arvidson et al., 2011). This paracrine activity can support angiogenesis, recruit host progenitor cells, and stimulate the repair and regeneration of damaged tissue (Watt et al., 2013). These properties allow MSCs to contribute to bone healing even in the absence of full differentiation. Another important feature of MSCs is their low immunogenic profile. They express only low levels of major histocompatibility complex (MHC) class I molecules and lack expression of MHC class II, which reduces the likelihood of triggering an immune response after transplantation (Machado et al., 2013). This allows for greater flexibility in therapeutic applications, including allogeneic cell delivery. Furthermore, MSCs exhibit intrinsic homing capabilities that enable them to migrate towards sites of tissue injury or inflammation, where they can contribute to localised repair in response to biochemical signalling cues (Yuan et al., 2022). When MSCs are integrated into a 3D scaffold such as HAA, the combination offers both structural and biological support for tissue regeneration. The HAA scaffold provides mechanical stability and spatial organisation, while also mimicking key aspects of the native bone matrix. In turn, MSCs populate this matrix and respond to its cues by initiating osteogenic pathways, secreting pro-regenerative factors, and interacting with

host cells *in vivo* (Jamshidi-adegani et al., 2024). By embedding MSCs directly within the scaffold during fabrication or post-printing, the engineered construct becomes not only a passive support for bone regrowth, but also an active participant in the healing process.

1.2. The nervous system in bone regeneration

The central nervous system (CNS) plays a pivotal role in maintaining skeletal integrity and facilitating bone regeneration. This regulation is primarily mediated through hypothalamic centres that integrate various physiological signals and modulate peripheral bone remodelling processes (Lv et al., 2022; Shi & Chen, 2024; Xiao et al., 2023). The hypothalamus, a critical brain region involved in energy homeostasis, appetite control, and hormonal regulation, communicates with bone tissue via neuroendocrine and autonomic pathways, which influence both osteoblast and osteoclast activity (Horsnell & Baldock, 2016; Khor & Baldock, 2012).

Neuropeptide Y (NPY) plays a significant role in energy balance, appetite regulation, and stress response. NPY exerts its effects through a family of G-protein-coupled receptors, notably Y1 and Y2 receptors, which are differentially expressed in central and peripheral tissues, including bone (Chen & Zhang, 2022; Shi & Baldock, 2012). Central NPY signalling, particularly via hypothalamic Y2 receptors, has been shown to inhibit bone formation. Baldock et al. (2002) demonstrated that Y2 receptor knockout mice exhibited increased osteoblast activity and doubled bone trabecular volume due to increased trabecular number and thickness, which suggests that Y2 receptor activation may suppress bone anabolic processes. Further studies revealed that targeted deletion of Y2 receptors in the arcuate nucleus of the hypothalamus led to a significant increase in bone mass (Allison et al., 2006; Qi et al., 2016; Wee et al., 2019). Peripheral NPY can also inhibit bone formation via Y1 receptor signalling on osteoblasts and bone marrow stromal cells (Igwe et al., 2009; Lee et al., 2015). For instance, Igwe et al. (2009) found that mouse calvarial osteoblasts treated with exogenous NPY showed reduced levels of intracellular cyclic AMP (cAMP) and osteoblast differentiation markers such as osteocalcin and bone sialoprotein (BSP). These results indicate an inhibitory effect of NPY on bone formation, as this pathway is mediated through Y1 receptors. Moreover,

mice with osteoblast-specific deletion of Y1 receptors exhibited increased bone mass, which highlights the inhibitory role of peripheral NPY-Y1 signalling on bone formation (Lee et al., 2010). In contrast, some studies suggest that peripheral NPY can promote osteoblast proliferation and differentiation under certain conditions, highlighting its anabolic potential in bone regulation. (Franquinho et al., 2010; Ma et al., 2013).

Central NPY normally inhibits bone formation via Y2 receptors signalling in the hypothalamus. However, under chronic stress conditions, increased hypothalamic NPY expression may serve a protective function by limiting stress-induced bone loss by modulating a corticotropin-releasing factor and sympathetic norepinephrine (NE) release. Baldock et al. (2014) demonstrated that mice lacking Y2 receptors specifically in arcuate neurons exhibited exaggerated bone loss relative to wild-type controls. In global Y2 receptor-deficient mice, stress-induced cancellous bone loss was threefold greater than in wild-type counterparts, associated with reductions in mineral apposition rate (Baldock et al., 2014; Elefteriou, 2018).

Neuromedin U (NMU) is a neuropeptide expressed in the hypothalamus and peripheral tissues, involved in regulating energy balance and stress responses. (De Prins et al., 2020) NMU has been implicated in bone metabolism, with studies showing that NMU-deficient mice exhibit increased bone formation and mass, and that it more pronounced in male mice than female mice. (Born-Evers et al., 2023; Sato et al., 2007) Central administration of NMU decreases bone formation, suggesting that hypothalamic NMU negatively regulates bone anabolic processes. The mechanism involves NMU-mediated activation of the sympathetic nervous system, leading to increased β2-adrenergic receptor signalling in osteoblasts and subsequent suppression of bone formation. (Gianfagna et al., 2013). Cocaine- and amphetamine-regulated transcript (CART) is another example of a neuropeptide expressed in hypothalamic neurons, known primarily for its role in regulating appetite and energy homeostasis. However, increasing evidence suggests CART also plays a significant role in bone metabolism. Specifically, CART has been shown to act as a central inhibitor of bone resorption by suppressing osteoclast differentiation. This effect is particularly evident in models of melanocortin 4 receptor (MC4R) deficiency, where both mice and humans exhibit elevated hypothalamic CART expression, reduced markers of bone resorption, and increased bone mass. Ahn et al.

(2006) suggest that partial deletion of the CART gene in these models is sufficient to restore normal bone resorption, without altering the metabolic disturbances associated with MC4R inactivation. These findings suggest that CART's influence on bone remodelling operates independently of its effects on energy balance, pointing to a distinct central neural pathway through which CART regulates skeletal homeostasis (Ahn et al., 2006; Idelevich et al., 2020)

Semaphorin 3A (Sema3A), first characterized as an axonal guidance cue during neural development has emerged as a unique local regulator of bone remodelling owing to its dual actions on osteoclasts and osteoblasts. (Ferretti et al., 2022; K. Wu et al., 2023) Expressed in both the central nervous system and bone tissue, Sema3A signals primarily through neuropilin-1 and PlexinA1 receptors, which are present on osteoclast precursors and osteoblast lineage cells. Upon binding to Nrp1 on osteoclast precursors, Sema3A suppresses RANKL-induced differentiation by inhibiting immunoreceptor tyrosine-based activation motif (ITAM)-mediated signalling and downstream RhoA activation, thereby reducing bone resorption. (El-Masri et al., 2024; Toyofuku et al., 2005; K. Wu et al., 2023) Simultaneously, Sema3A–Nrp1 engagement in mesenchymal progenitors stimulates the canonical Wnt/β-catenin pathway, thus enhancing osteoblast differentiation and inhibiting adipocyte lineage commitment which are reportedly steps in new bone formation. (El-Masri et al., 2024) A study conducted by Hayashi et al. (2012) provided *in vivo* confirmation of these mechanisms. Through systemic administration of recombinant Sema3A, wild-type mice significantly increased both trabecular and cortical bone mass as well as the trabecular number and thickness. On the other hand, Sema3a-deficient mice, or mice bearing a targeted disruption of the Sema3A-binding domain in Nrp1, showcased an osteopenia phenotype characterized by reduced bone formation and elevated resorption. The intravenous Sema3A delivery accelerated bone regeneration following injury. These findings establish Sema3A as a critical local modulator of bone remodelling and highlight its therapeutic potential for conditions such as osteoporosis and impaired fracture healing. (El-Masri et al., 2024; Hayashi et al., 2012)

The role of serotonin in bone physiology is complex and dependent on its site of production. CNS-derived serotonin, which is synthesized in the brainstem's raphe nuclei via tryptophan hydroxylase 2 (Tph2), acts as a positive regulator of bone formation

through its actions on the hypothalamus and downstream pathways. (Ducy & Karsenty, 2010; Sharan & Yadav, 2014; Shi & Chen, 2024) .

Leptin, an adipocyte-derived hormone that communicates energy status to the CNS, further exemplifies how hypothalamic regulation integrates systemic physiology with skeletal tissue regeneration. The effect of leptin on bone is primarily mediated by hypothalamic centres, particularly the ventromedial hypothalamus, which regulates sympathetic nervous system (SNS) output. Elevated leptin levels stimulate sympathetic tone, activating β2-adrenergic receptors (β2ARs) on osteoblasts and inhibiting their bone-forming activity. (Motyl & Rosen, 2012; Reid et al., 2018) A study by Bertoni et al. (2009) found that maternal administration of high-dose leptin during mid-gestation accelerates the formation and growth of primary ossification centres in foetal long bones. Newborn mice from leptin-treated mothers exhibited significantly larger and longer endochondral and intramembranous ossification regions than their control counterparts. These findings suggest that peripheral leptin can promote both chondrocyte and osteoblast proliferation and differentiation during early bone histogenesis, therefore, leptin may act as a direct growth factor for cartilage and bone, enhancing both endochondral and periosteal bone formation.

Bone tissue engineering has advanced significantly by combining biomaterials, osteoinductive/conductive factors, and scaffold design to best stimulate bone regeneration. However, an essential but overlooked component in these regenerative strategies is innervation, the presence and functional integration of nerve fibres within bone tissue. The nervous system influences bone remodelling through sensory and sympathetic pathways, modulating osteoblast and osteoclast activity, angiogenesis, and immune responses. (Chen et al., 2024; Shi & Chen, 2024) Despite this biological importance, most current bone tissue engineering approaches have neglected biomaterial innervation, leaving behind a significant gap in translational potential.

1.3. Enhancing the innervative capacity of synthetic bone allografts

The skeletal system is highly innervated and intricately regulated by the nervous system. Sensory and autonomic nerve fibres permeate bone tissue, particularly within the periosteum, bone marrow, and cortical regions, where they play a continuous role in bone development, remodelling, and repair through life. Despite the recognized importance of vascularization in bone healing, the role of innervation has often been overlooked in the design of synthetic bone allografts. Current biomaterials, while successful in mimicking the structural and mechanical properties of bone, frequently lack the capacity to support nerve ingrowth and integration. This deficiency can lead to impaired remodelling, delayed healing, and increased risk of chronic pain or sensory dysfunction. In addition, the interplay between nerves and blood vessels is critical for effective bone regeneration. Nerves not only influence vascularization but also modulate the local immune environment, further highlighting their multifaceted role in bone healing. Therefore, incorporating innervative properties into synthetic bone allografts is essential for achieving complete and functional bone regeneration.

Biochemical enhancement strategies aimed at improving the innervative potential of synthetic bone allografts frequently involve the incorporation of neurotrophic factors such as NGF, due to its established roles in both neural regeneration and bone repair. Foundational developmental evidence by (Tomlinson et al., 2016) demonstrated that NGF directly contributes to sensory innervation during skeletal development, which in turn promotes vascularization and osteoprogenitor maturation. In mouse models, TrkA-positive axons were observed adjacent to perichondrial bone surfaces during primary ossification, corresponding with localized NGF expression. Genetic inactivation of TrkA signalling in TrkA(F592A) mice resulted in reduced innervation, impaired vascular invasion of ossification centres, decreased numbers of osterix (Osx)-expressing osteoprogenitors, and overall reduced femoral length and volume. Similarly, conditional deletion of NGF in collagen type II alpha 1 chain (Col2a1)-expressing osteochondral progenitors phenocopied these defects, confirming that endogenous NGF signalling is essential for coordinated innervation and bone development.

Building on this, J. Xu et al. (2022) identified a critical role for NGF–p75 signalling in adult bone repair. In a cranial bone injury model, NGF was shown to act through the p75 neurotrophin receptor on mesenchymal osteogenic precursors, promoting their migration into the defect site. Mice lacking NGF in myeloid cells or p75 in $Pdgfra^{+}$ progenitor cells exhibited delayed bone healing due to impaired precursor recruitment. Although the study did not assess nerve regeneration directly, it emphasized that NGF-mediated signalling is essential for orchestrating the early cellular events in bone repair. Ji et al. (2024) furthered these findings by addressing the therapeutic limitations associated with NGF overexpression. Inflammatory bone environments were shown to trigger pyroptosis in NGF-overexpressing bone marrow MSCs via the p75NTR pathway, compromising cell survival. To counteract this, the researchers co-delivered necrosulfonamide (NSA), a pyroptosis inhibitor, within an allogeneic scaffold. In a rat femoral condylar defect model, this composite system significantly suppressed pyroptosis and enhanced osteogenesis, demonstrating that the co-modulation of inflammatory responses is necessary for effective NGF-based interventions.

Ye and Gong (2020) developed a titanium-based scaffold coated with a composite of NGF, chondroitin sulphate, and HA, aiming to simultaneously promote both osteogenic and neurogenic differentiation. The 65 μm porous coating provided sustained release of bioactive NGF. When bone marrow MSCs were seeded onto the scaffold, there was significant upregulation of both osteogenic and neuronal gene markers, including those related to bone morphogenetic proteins and neural differentiation pathways, as confirmed by RT-qPCR and protein expression analysis. This study offers direct *in vitro* evidence of dual lineage commitment supported by a neurotrophin-functionalized synthetic scaffold. Recent advances have also integrated NGF with exosome-based delivery systems to enhance the ability of exosomes to carry neurotrophic signals in a sustained and targeted manner. This strategy was explored by Lian et al. (2024) by stimulating MSCs with NGF to produce NGF-enhanced exosomes, engineering a vesicle population enriched with neuro-promotive properties. These enhanced exosomes significantly improved neuronal function and neurotrophic signalling *in vitro*, while also enhancing the osteogenic activity of bone-forming cells. Bioinformatic analysis attributed these effects to NGF-induced miRNA cargo that activated MAPK and PI3K-Akt

signalling pathways. When delivered via a 3D-printed hierarchical porous scaffold, the exosomes facilitated sustained bioavailability and promoted robust neovascularization and innervated bone regeneration in a rat femoral defect model. This study not only underscores the potential of NGF as a biochemical modulator of innervation but also positions MSC-derived exosomes as a versatile platform for targeted delivery of neuro-regenerative signals in scaffold-based bone repair. However, despite the development of advanced delivery platforms, a major limitation of exosome-based strategies in bone and nerve regeneration remains their limited stability and retention at the target site. This presents a significant barrier to achieving sustained therapeutic effects and poses a challenge for clinical translation (Lian et al., 2024; Youseflee et al., 2022).

Brain-derived neurotrophic factor (BDNF), released in response to nerve injury, plays a critical role in promoting the natural healing of injured nerves and has been increasingly recognized for its influence on bone regeneration. Ida-Yonemochi et al. (2017) demonstrated that *in vitro*, BDNF enhanced osteocalcin mRNA expression in MC3T3-E1 osteoblast-lineage cells, indicating promoted differentiation, though it did not affect proliferation or migration. The *In vivo* application of BDNF to mandibular corticotomy sites in rats resulted in increased osteopontin-positive new bone formation and sustained bone remodelling involving TrkB-positive osteoblasts and osteocytes, highlighting its role in bone maturation and changes following peripheral nerve injury. Supporting these findings, Park et al. (2024) reported that BDNF significantly elevated alkaline phosphatase (ALP) activity, calcium deposition, and osteoblast differentiation markers both *in vitro* and in their mouse model. Further studies have also confirmed that BDNF enhances osteogenesis and neurogenesis of human bone marrow stem cells, suggesting that its osteogenic effects may be mediated indirectly through increased neurogenesis.

Despite their potent neurotrophic and osteoinductive activity, NGFs face significant translational barriers due to their short half-life, *in vivo* instability, and requirement for supraphysiological. While encapsulation strategies (e.g., PLGA microspheres or emulsion electrospinning) aim to extend release kinetics, these systems can exhibit burst release profiles or uneven distribution. Moreover, unlike growth factors such as BMP-2 that are more established in bone tissue engineering, NGF delivery introduces

additional risks, including hyperalgesia, heterotopic ossification, and even tumorigenesis when delivered at high doses. These adverse effects highlight the importance of tight dosage control and context-specific release kinetics, which many current delivery systems are yet to achieve reliably (Carragee et al., 2013; Subbiah & Guldberg, 2019). To maintain effective local concentrations, supraphysiological doses of NGF are often required, which in turn can give rise to serious adverse outcomes; for instance, high-dose NGF delivery has been associated with abnormal nerve sprouting and neuroma formation, which leads to hyperalgesia. In addition excessive NGF exposure can also cause heterotopic ossification in non-skeletal tissues, promote undesired immune responses, and has even been implicated in promoting tumorigenesis under certain conditions (Safari et al., 2021; Subbiah & Guldberg, 2019).

Substance P (SP) is a neuropeptide involved in pain transmission and neurogenic inflammation, but it has also emerged as a key modulator of bone regeneration. Evidence from a study conducted by Li et al. (2010) in fracture healing mouse models showed that SP-positive nerve fibres infiltrate the fracture callus during early regeneration, peaking around day 21 in regions of active bone formation and cortical bridging. Notably in angulated fractures, this peak occurs earlier on the mechanically loaded side and is delayed on the unloaded side, which suggests that SP activity may be sensitive to biomechanical cues. During the remodelling phase, SP fibres diminished in areas undergoing successful healing but remained in unloaded regions where bone resorption predominated. This is supported by Ding et al. (2010), who demonstrated that mice with osteoporotic bone loss exhibited impaired fracture healing alongside significantly reduced SP levels at the fracture site. Similarly, Hofman et al. (2019) showed that pharmacological inhibition of SP signalling through selective blockade of its neurokinin-1 receptor (NK1-R) suppressed the expression of osteogenic genes such as osteocalcin and collagen types I and II, also significantly reducing the biomechanical strength of the healing bone at both 6 weeks and 3 months post-fracture.

During fracture healing, NPY levels rise significantly, with serum concentrations peaking around the 8th week post-injury, coinciding with active callus formation and remodelling. Tang et al. (2017) demonstrated that inhibition of NPY and CGRP impairs fracture healing and suppresses phosphorylated extracellular signal-regulated kinase (ERK) signalling, a

pathway that is essential for osteoblast proliferation and differentiation. They also observed a substantial accumulation of NPY-positive macrophages at the injury site, bringing attention to the neuroimmune crosstalk in the regenerative process of bone. Sousa et al. (2020) investigated the effects of disrupting the NPY-Y1 receptor (Y1R) signalling pathway and found that Y1R knockout ($Y1R^{-/-}$) mice displayed a high bone mass phenotype accompanied by enhanced ECM matrix quality. Specifically, $Y1R^{-/-}$ bones had more densely packed collagen fibres, accelerated deposition of both mineral and organic components, and overall enhanced mechanical strength without pathological changes in collagen crosslinking or mineral crystallinity. Similarly, L. Ye et al. (2021) demonstrated that implantation of biodegradable magnesium nails into critical-size femoral defects significantly enhanced both bone and blood vessel formation in a rat distraction osteogenesis model. The magnesium-induced repair was accompanied by a marked upregulation of CGRP expression in the newly formed bone. Mechanistically, CGRP promoted endothelial cell migration and angiogenic activity via a CGRP–FAK–VEGFA axis. Inhibitors of this pathway abrogated the beneficial effects of magnesium, thus revealing a direct link between sensory nerve activity, CGRP signalling, and vascularized bone regeneration.

Adhesion peptides have gained increasing interest for their roles in enhancing bone regeneration and, potentially, nerve regeneration. RGD (Arg-Gly-Asp) is an adhesion peptide resent in extracellular matrix proteins like fibronectin, is a well-established ligand for integrin receptors on the cell surface. These integrins are comprised of α and β subunits and play a critical role in mediating cell-ECM interactions necessary for tissue repair; specifically, the α5β1 and αvβ3 integrins have been shown to contribute to bone and cartilage regeneration (Yang et al., 2021). α5β1 facilitates MSC migration to injury sites and promotes osteogenic differentiation *in vitro* while αvβ3 has been implicated in pathological bone resorption (Hamidouche et al., 2009; Martino et al., 2009). *In vivo* studies have demonstrated that αvβ3 overexpression is associated with increased bone destruction, whereas pharmacological inhibition of this integrin attenuates osteolysis (Kwakwa & Sterling, 2017; McCabe et al., 2007).

RGD-functionalised biomaterials such as PCL, hydrogels, phosphate-based composites, and metal alloys have been widely explored to enhance scaffold

biocompatibility and support cellular adhesion and differentiation in skeletal tissue engineering (Alipour et al., 2020; Dard et al., 2000; Jäger et al., 2013; Lin et al., 2019; Yang et al., 2021). While most current applications are not neuro-specific, there is some evidence that suggests that RGD may also contribute to neural cell attachment and axonal regeneration (Ahmed & Jayakumar, 2003). However, the extent to which these findings translate into functional innervation within engineered synthetic bone allografts remains unclear. As such, the use of adhesion peptides like RGD represents a promising but still exploratory strategy that require further investigation to determine their full potential.

Table 1. Summary of biochemical strategies to enhance bone regeneration and innervation

Strategy	**Agent**	**Mechanism**	**Limitation**
Neurotrophins	NGF, BDNF	Activate Trk signalling	Short half-life, dose sensitivity
Neuropeptides	SP, NPY, CGRP	Enhance osteogenesis via NK-1, CGRP-R	Stability, delivery method
Exosomes	MSC secretome	miRNA-driven crosstalk	Stability, delivery method
Adhesion Peptides	RGD	Promote neural adhesion	Not neuro-specific

Surface functionalization with ECM proteins such as laminin or fibronectin has been shown to enhance neurite outgrowth and Schwann cell adhesion by providing integrin-binding domains. In addition, physical modifications such as aligned microgrooves or electrospun nanofibers can guide directional axon extension, while tailoring the mechanical stiffness of the scaffold to match the native nerve and bone interface can support both osteogenesis and neurogenesis. More advanced approaches involve the use of conductive or piezoelectric materials that convert mechanical stimuli into electrical signals, further enhancing cell communication and neural activity.

Piezoelectric scaffolds can generate endogenous electrical stimuli in response to mechanical loading. While their capacity to mimic the natural electroactive environment of bone has been well-documented, the full extent of their role in promoting innervation, particularly within bone defects *in vivo*, remains an evolving area of study. A characterization study carried out by Karanth et al. (2023) focused primarily on utilizing piezoelectric scaffolds for bone regeneration. In this study, 3D-printed PLLA scaffolds were fabricated via fused deposition modelling and shown to generate an electric potential (~25 mV) under cyclic loading. The scaffolds exhibited a compressive modulus comparable to that of natural trabecular bone and supported osteoblast-like cell proliferation following fibrinogen coating, demonstrating both mechanical and cytocompatibility benchmarks essential for craniofacial bone repair. While this study highlighted the retention of piezoelectric properties post-fabrication and confirmed the material's regenerative compatibility, it did not investigate any neural components, thus leaving the potential for innervation enhancement via this mechanism largely speculative in the bone context. In contrast, a more nerve-focused study by (Ma et al., 2023) developed a multi-channel nerve guidance conduit that integrating both piezoelectric and conductive properties to actively support peripheral nerve regeneration. This conduit combined a porous silk fibroin cryogel with a piezoelectric outer layer that enabled delivery of spontaneous electrical cue. This electroactive scaffold significantly enhanced Schwann cell proliferation, maturation, and myelination, while also promoting neuronal differentiation and axon regeneration in PC12 cells *in vitro*. Additional, i*n vivo,* application in a rat sciatic nerve defect model confirmed the scaffold's ability to achieve functional nerve repair comparable to that of autografts. Although this study robustly demonstrated the value of electrical stimulation in peripheral nerve repair, its translational applicability to bone-innervative contexts remains uncertain, as the microenvironment and regeneration dynamics in neural tissues differ substantially from those in osseous defects.

Furthering these findings, Zhao et al. (2025) introduced a bilayer piezoelectric scaffold that mimicked both the bone matrix and periosteum. The periosteum-like outer layer, which comprised of a double network hydrogel embedded with sintered whitlockite nanoparticles, provided viscoelasticity and piezoelectric responsiveness, while the inner

chitosan–hydroxyapatite scaffold supported bone-like porosity and mineralization. When stimulated with low-intensity pulsed ultrasound to activate the piezoelectric effect, this bilayer construct was reported to enhance osteogenesis, angiogenesis, and notably, neurogenesis; thus demonstrating that the scaffold capable of supporting neurovascularized bone regeneration. However, while promising, such studies remain limited in number, and the mechanisms underlying the electrical modulation of nerve in-growth are still not fully understood. For instance, it is unclear how the frequency or duration of piezoelectric stimulation correlate with neural differentiation pathways or axonal guidance in bone-specific contexts. (Pinho et al., 2023; Rajabi et al., 2015)

ReNcell VM are immortalized human neural progenitor cells derived from the ventral mesencephalon of the brain. They are widely recognized for their rapid proliferation and multipotent capacity to differentiate into key neural lineages, including neurons, astrocytes, and oligodendrocytes (Song et al., 2019). These characteristics make them a valuable *in vitro* model for investigating neural behaviour in tissue engineering contexts. Although originally developed for studying neural development and regeneration, ReNcell VM cells have increasingly been explored for their potential use in 3D culture systems and scaffold environments relevant to regenerative medicine. Recent studies have demonstrated that ReNcell VM cells can maintain robust proliferation in three-dimensional hydrogel scaffolds, such as PuraMatrix, with doubling times comparable to those observed in traditional two-dimensional culture systems (Ma & Suh, 2019). Ortinau et al. (2010) found that laminin supplementation within these hydrogels significantly influenced cellular organization. Higher concentrations of laminin (0.5%) promoted the formation of compact, flattened cellular aggregates, whereas lower concentrations (0.15%) facilitated more dispersed and extended growth patterns, suggesting that laminin can modulate the architectural development of neural progenitors in a scaffold environment. This highlights the importance of extracellular matrix components in shaping the spatial and structural integration of neural cells within engineered platforms. The maintenance of ReNcell VM cells in a proliferative, undifferentiated state depends critically on the presence of epidermal growth factor (EGF) and basic fibroblast growth factor (bFGF) in the culture medium. As shown by Nierode et al. (2016), the removal of these mitogens induces spontaneous differentiation into mature neural phenotypes.

This allows for temporal control over differentiation, which makes this cell line highly suitable for studies that require monitoring of both proliferation and lineage commitment in response to biomaterial properties.

In addition to laminin, Matrigel has been widely used as a supportive extracellular matrix for neural precursor cultures. Uemura et al. (2010) demonstrated that Matrigel enhances both the survival and neuronal differentiation of neural precursor cells, and later work by Nierode et al. (2018) confirmed that ReNcell VM cells can adhere, proliferate, and differentiate effectively on Matrigel-coated substrates. While these materials are typically used in developmental neurobiology, their capacity to support neural progenitor growth and differentiation provides a framework for assessing the neurocompatibility of synthetic biomaterials. Although these studies were not designed with biomaterial innervation in mind, their findings form an important foundation for future work exploring how neural progenitor cells behave on engineered surfaces. In the context of synthetic bone allografts, where re-establishing neural connectivity may enhance the success and effective of a bone graft integration, pain modulation, and even bone regeneration. Therefore, incorporating ReNcell VM cells into osteogenic scaffold studies offers a valuable approach to preliminarily evaluate the innervative potential of novel materials like HAA, thus setting the stage for future investigations into scaffold-guided neural regeneration in bone tissue engineering.

Another promising strategy involves the co-culture of neural support cells with osteogenic cells. Schwann cells have been combined with MSCs in three-dimensional scaffolds to enhance neuro-osteogenic crosstalk. Wu et al. (2020) demonstrated that a 3D bioprinted scaffold composed of gelatine/alginate hydrogel with embedded Schwann cells promotes enhanced expression of key neurotrophic factors relative to traditional 2D cultures. The Schwann cells remained viable, adhered well, and continued to express neural markers after implantation, indicating that the 3D scaffold provided a supportive environment for neural cell function. Zhang et al. (2021) reached a similar conclusion as their study highlighted the beneficial effects of integrating neural stem cells (NSCs) into 3D bioprinted bone constructs. The inclusion of neural cells enhanced osteogenic differentiation of human bone marrow MSCs, demonstrated by elevated expression of osteogenic markers such as osteopontin (OPN) and BMP-2, as well as increased ALP

secretion. Bai et al. (2024) demonstrated that co-culturing NSCs with bone MSCs within low-modulus gelatine methacrylate hydrogel scaffolds significantly enhanced neural regeneration in spinal cord injury mouse models. Compared to high-modulus scaffolds, the low-modulus system showed enhancement of various advantageous characteristics such as cell viability, proliferation, migration, and neuronal differentiation. *In vivo*, the NSC/bone MSC co-culture implants promoted motor function recovery, reduced spinal cord cavity formation, and stimulated neuron regeneration. These findings support the therapeutic potential of co-culturing neural and osteogenic-related stem cells within biomaterial scaffolds to improve neural tissue repair.

Recent advances in the functionalization of HA-based biomaterials highlight promising strategies to simultaneously promote bone regeneration and innervation, addressing a critical knowledge gap in bone tissue engineering. Fitzpatrick et al. (2021) demonstrated that 3D-printed silk-HA scaffolds incorporating osteoinductive, pro-angiogenic factors, specifically BMP-2 and NGF, can synergistically enhance osteoblastic differentiation and neural stem cell proliferation *in vitro*. This suggests that the integration of these morphogens creates a conducive microenvironment for coupled osteogenesis and neural support. Complementing these findings, J. Ye et al. (2021) also provided *in vivo* evidence that HA coatings functionalized with NGF and chondroitin sulphate on titanium implants significantly improve early osseointegration and peri-implant nerve fibre formation in a canine mandibular model. Their results revealed increased expression of genes related to both osteogenesis and neurogenesis, as well as enhanced mechanical fixation. Further expanding on this concept, Liu et al. (2021) engineered a nanocellulose-reinforced HA membrane capable of directing mesenchymal stem cells toward osteogenic, neuronal, and endothelial lineages simultaneously, thereby generating a bioactive osteoid tissue *in vitro*. Subsequent *in vivo* heterotopic implantation demonstrated rapid vascularized and innervated bone formation, evidencing the scaffold's potential as a multi-lineage differentiation platform for neurovascularized bone regeneration. Collectively, these studies emphasize the emerging potential of HA-based scaffolds to not only restore bone mass but also reestablish the neural networks critical for functional skeletal tissue regeneration. However, despite these promising results, challenges remain. The complexity of recapitulating native bone's neurovascular

niche means that long-term *in vivo* integration, precise control over neural ingrowth, and standardized approaches for multi-lineage stem cell differentiation require further work (Shi et al., 2022). Furthermore, many of studies have focused on early-stage markers and functional outcomes without extensive mechanistic insight into how the physicochemical properties of HA influence nerve growth and signalling pathways. Future research must therefore address these limitations by combining advanced biomaterial design with in-depth biological evaluation to unlock the full regenerative and innervative capacity of HA-based bone substitutes.

1.4. Research aims and objectives

Despite substantial advances in biomaterials for bone regeneration, the capacity of synthetic bone allografts to support neural integration remains poorly understood, particularly with HAA. Despite these materials having been widely studied for their osteoconductive properties, their potential to support innervation, which is a critical component of functional bone healing, remains as a significant and underexplored knowledge gap. Innervation is increasingly recognized as essential not only for bone development and remodelling, but also for orchestrating the cellular and vascular dynamics required for complete success of bone regeneration. There is an expanding body of research focused on electrically active scaffolds, bioactive coatings, and co-culture systems that encourage both nerve regeneration and bone repair. However, few studies have directly evaluated HA-based materials in this dual context of osteogenesis and innervation, particularly in combination with co-culture systems.

As such, there is a pressing need to investigate whether HAA can be optimized to support neural cell growth, axonal extension, and functional integration, alongside its established osteogenic performance. This study addresses that gap by exploring the *in vitro* response of neural and mesenchymal stem cells to functionalized HAA scaffolds, contributing to the foundational knowledge needed to design next-generation biomaterials capable of supporting neuro-osteogenic tissue regeneration. The aim of this study is to optimize the innervation potential of HAA scaffolds and evaluate their

feasibility for supporting *in vitro* neuro-osteogenic integration, with the long-term goal of advancing biomaterial strategies for complex tissue regeneration.

The first objective is to investigate the i*n vitro* response of ReNCells to HAA scaffolds. The second objective is to evaluate the effects of functionalized HAA in co-culture models of ReNcell neural progenitor cells and human umbilical cord-derived MSCs (HUMSCs) to assess proliferation and interaction. The third objective is to analyse key biomarkers of osteogenesis and innervation using immunofluorescence and imaging techniques to characterize how the scaffold environment influences lineage-specific differentiation and tissue-specific signalling. And finally, to identify and validate optimized HAA scaffold conditions with dual osteogenic and neurogenic support and test their performance either in bone explant cultures or through collaboration with *in vivo* research groups.

2. MATERIALS AND METHODS

2.1 Material preparation and characterization

2.1.1 HAA scaffold preparation

To produce HAA scaffolds, tetracalcium phosphate (TTCP, Matexcel, China) and Emprove Essential $CaHPO_4$ (Sigma-Aldrich, USA) were mixed in a 1:1 molar ratio. This mixture was then combined with $CaCO_3$ (Sigma-Aldrich, USA) in a 1:1 weight ratio. The powders were ground using a mortar and pestle for five minutes to ensure a homogeneous mixture before introducing 10% EMPROVE Essential Gelatin powder (Sigma-Aldrich, USA) in water was added to form a paste. The paste was poured into cylindrical silicone moulds and left to dry at room temperature. Once fully dry, the material was removed from the moulds, and a drill was used to bore holes into the scaffolds. The material was then cut into cylindrical shapes with a diameter of 5 mm and a height of 3 mm. To ensure the HA-forming reaction was complete and to stabilize the scaffolds, they were submerged in 0.1% glutaraldehyde (Sigma-Aldrich, UK) for 24 hours to crosslink the material and prevent dissolution. The scaffolds were then washed thoroughly with water and soaked in phosphate-buffered saline (PBS, Gibco, UK) at 37°C for an additional 24 hours. After soaking, the scaffolds were air-dried at room

temperature or at 37°C and subsequently sterilized via autoclaving before being used for tissue culture experiments.

2.1.2 FTIR spectroscopy

FTIR spectroscopy was conducted to determine the concentrations of compounds present in the scaffolds at different stages of preparation. The individual starting powders, including $CaCO_3$, TTCP, and $CaHPO_4$, were first analyzed. Additionally, the prepared HAA scaffolds were tested at various stages: untreated (as prepared), after crosslinking in 0.1% glutaraldehyde for 24 hours, and following soaking in PBS for 24 hours. For each analysis, the scaffolds were crushed into a fine powder by mortar and pestle. Spectra were recorded using a Perkin Elmer Spectrum 100 FTIR spectrophotometer (PerkinElmer, Connecticut, USA).

2.1.3 Mechanical testing

The compressive strength of the HAA scaffolds were evaluated mechanical testing was performed using a Tinius Olsen H25KS universal testing machine (Tinius Olsen Limited, Surrey, UK). This analysis aimed to assess the mechanical integrity of the scaffolds and to determine whether crosslinking and PBS treatment enhanced their strength. Scaffolds were tested in two conditions: untreated (as prepared) and treated (post-crosslinking in 0.1% glutaraldehyde and soaking in PBS for 24 hours). Individual cylindrical samples were placed between the compression plates of the testing machine, and a compressive load was applied at a constant rate until the scaffold cracked or fractured. The maximum load each scaffold could withstand before failure was recorded, and the compressive strength values were analyzed to compare the mechanical performance of untreated versus treated scaffolds.

2.2 *in vitro* work

2.2.1 HUMSC isolation

Human umbilical cord samples were provided by Singleton Hospital, Swansea with informed consent of anonymous donors; the research ethics was approved by the South West Wales Research Ethics Committee (REC 11/WA/0040). The umbilical cords were transported in PBS (Gibco, UK) and processed upon arrival. The veins and artery were removed, and the cord tissue was finely chopped to a paste-like

consistency. The paste was spread onto T25 culture flasks and incubated at 37°C for 10 minutes to enhance surface adherence. Following incubation, 0.5 mL of fetal bovine serum (FBS, Gibco, UK) was added to each flask prior to an overnight incubation at 37°C.

The following day, 1.5 mL of culture medium (1:1 DMEM:F12 (Gibco, UK) supplemented with 10% FBS and 1% penicillin/streptomycin (Gibco, UK)) was added to each flask, with the volume increased to 5 mL after one additional day. The medium was replaced every 2–3 days.

HUMSCs began adhering to the flask surface after approximately one week. When cells reached ~50% confluence, subculturing was performed. Cells were washed with PBS (Gibco, UK), detached using 0.25% Trypsin-EDTA (Gibco, UK), and the Trypsin-EDTA was neutralized with an equal volume of the culture medium. Detached cells were centrifuged at 1200 rpm for 5 minutes (Eppendorf 5810 R, Eppendorf, Hamburg, Germany), then either reseeded in new flasks, cryopreserved in FBS with 10% dimethyl sulfoxide (DMSO, Sigma-Aldrich, UK) for future use, or immediately used in experiments.

2.2.2 HUMSC/ReNCell co-culture

The ReNcell® VM human neural progenitor cell line (Merk-Millipore, UK) was cultured and maintained under specific conditions following the manufacturer's protocol. Differentiation media (ADM) was prepared Advanced DMEM/F12 (Gibco, UK), 1% penicillin-streptomycin, 4 mM glutamine, 1× B27 supplement (Gibco, UK), 50 µg/mL gentamicin (Gibco, UK), and 10 U/mL heparin (Sigma, UK). The solution was sterile-filtered (0.22 µm) and stored at 4°C. Proliferation media (APM) was prepared by supplementing ADM with 20 ng/mL bFGF (Peprotech, UK) and 20 ng/mL EGF (Peprotech, UK).

The ReNcells required coated flasks for attachment. Laminin-coated flasks were prepared by adding 20 µg/mL laminin (AMSbio, UK) to DMEM/F12 (Gibco, UK). Matrigel-coated flasks were prepared using DMEM/F12 supplemented with Matrigel (Corning, UK) diluted 1:100 (v/v). Both coating solutions were incubated at 37°C with

5% CO_2 for 24 hours. Prior to cell seeding, the flasks were washed with sterile PBS and fresh APM was added. Cryopreserved cells were thawed and seeded into coated flasks containing APM. Cultures were incubated at 37°C with 5% CO_2, and media changes were performed every 3–4 days. Cells were monitored daily to check proliferation and morphology.

A co-culture of HUMSC and ReNcells were established in 48-well plates (Corning, UK). HUMSCs were seeded at a density of approximately 2,000 cells/mm^2 in 48-well plates, either uncoated or coated with laminin or Matrigel as previously described. The cells were maintained in HUMSC culture medium for one week to allow for adherence and proliferation. After one week, ReNcells were seeded directly onto the HUMSC layer at a density of approximately 2,000 cells/mm^2. The culture medium was replaced with APM to support ReNcell growth, and the co-cultures were incubated at 37°C with 5% CO_2. Media changes were performed every 2-3 days, and cultures were monitored daily for cell morphology and growth.

2.2.3. Alamar Blue assay

The Alamar Blue assay (Invitrogen, USA) was used to evaluate cell viability and metabolic activity over a 7-day period in three experimental groups: HUMSC monocultures, ReNcell monocultures, and HUMSC/ReNcell co-cultures. For each group, three conditions were assessed: (1) cells cultured on standard tissue culture plastic, (2) cells seeded directly onto HAA scaffold material, and (3) HAA scaffold alone without cells, which served as a negative control. The assay was conducted at 1, 4, and 7 days post-seeding. At each time point, the culture medium in each well was replaced with fresh medium containing 10% Alamar Blue reagent. Plates were returned to the incubator (37°C, 5% CO_2) for 4 hours. Once a visible colour change was observed, 100–200 µl of the medium was transferred from each well to a new 96-well plate for analysis. Absorbance was measured at 570 nm using a microplate reader (BMG Labtech, Germany), and values were normalised to the untreated control wells to evaluate relative viability. In addition, a supplementary experiment was performed to evaluate whether different coatings affected ReNcell viability on the HAA scaffold. ReNcells were seeded onto HAA scaffolds pre-treated with either laminin or Matrigel, and their metabolic activity was assessed using the same

Alamar Blue protocol described above. Culture medium was refreshed every three days throughout the assay period. All conditions were performed in triplicate, and average values were used for analysis.

2.2.4. Immunofluorescence

Immunofluorescence was performed to evaluate the differentiation of ReNcells into neurons when co-cultured with HUMSCs in uncoated 48-well plates. At the experimental endpoint, the media was removed, and cells were fixed with 10% formalin (300 µL/well) for 15 minutes at room temperature (RT). After fixation, cells were washed twice with PBS and permeabilized with 0.15% PBS-Triton X-100 (PBST) for 15 minutes at RT. Following permeabilization, cells were blocked with 5% normal goat serum (NGS [Sigma], UK) in PBST for 1 hour at RT. Primary antibodies were prepared in PBST and incubated with the samples overnight at 4°C in a covered container. The primary antibodies used were β3-Tubulin (D71G9) XP® Rabbit mAb (Cell Signalling Technology, UK) at a 1:400 dilution and Anti-GFAP Rabbit pAb (Abcam) at a 1:1000 dilution. PBS was used in place of primary antibodies for negative controls. After primary antibody incubation, cells were washed twice with PBS and incubated with the secondary antibody, Goat Anti-Rabbit Alexa Fluor™ 488 (ThermoScientific, UK), at a 1:500 dilution in PBST for 1 hour at RT in a covered container. Cells were then washed twice with PBS, followed by incubation with Hoechst 33342 (Invitrogen, UK) at a 1:5000 dilution in PBS for 5 minutes at RT.

2.2.5. Live cell imaging

Live cell imaging was conducted to evaluate the interactions, spatial arrangement, and proliferation of HUMSCs and ReNcells in monoculture and co-culture on HAA discs. HUMSCs were labeled with DiD (red fluorescence), and ReNcells were labelled with DiO (green fluorescence) using the Invitrogen Vybrant™ Multicolor Cell-Labeling Kit (DiO, DiI, DiD Solutions), following the manufacturer's instructions for staining cells in suspension.

For HUMSC and ReNcell monoculture experiments, cells were seeded at a density of 20,000 cells per well in a 48-well plate. To ensure accurate cell placement onto the HAA discs, the cells were suspended in 80 µL of their respective media (culture medium for HUMSC, and APM for ReNcells) and carefully pipetted directly onto the surface of the discs (laminin-coated HAA for ReNcell monoculture). After 30 minutes of incubation to allow for attachment, an additional 300 µL of culture medium was gently added along the well walls to fully submerge the discs and ensure minimum disruption to the seeded cells. The plates were then returned to a 37°C, 5% CO_2 incubator, and medium was replenished every 2–3 days to maintain optimal cell viability and growth.

For co-culture experiments, HUMSCs were seeded first. DiD-labelled HUMSCs were suspended in culture medium and seeded onto the HAA discs at a density of 20,000 cells per well in 48-well plates. The cells were allowed to grow undisturbed for seven days to establish a monolayer of approximately 80% confluence, with culture medium replenished every 2–3 days to support healthy proliferation. Following this, ReNcells were stained with DiO while in suspension and seeded at the same density of 20,000 cells per well. To promote accurate placement, the cells were suspended in 80 µL of medium and pipetted carefully onto the DiD-labelled, HUMSC-covered HAA discs. With the introduction of DiO-labelled ReNcells, every well was replenished with APM which was replenished every 2-3 days to account for the high cell density of the co-culture.

To visualize nuclei and assess cell viability, Hoechst 33342 (Invitrogen, USA) was used as a nuclear counterstain. The dye was diluted 1:2000 in culture medium and added to each well at the respective time points, prior to imaging. Cells were incubated with Hoechst for 10 minutes at room temperature. Following staining, the medium was aspirated, and the HAA discs were carefully removed and inverted with the use of lab-grade tweezers so that the cell-seeded surface faced the glass bottom of a 96-well fluorescence imaging plate. Fluorescence imaging was performed at days 1, 4, 7, and 14 using confocal microscopy to evaluate the distribution, attachment, and interactions of the fluorescently labelled cells across the HAA scaffold. Images captured the progression of cell proliferation and morphology in both monoculture and co-culture conditions. The DiD and DiO dyes served as lipophilic tracers to specifically label live

cells, while Hoechst 33342 (DAPI) provided a nuclear counterstain for additional visualization of cell localization.

2.2.6. Confocal microscopy

Confocal microscopy was conducted using a Zeiss LSM710 imaging system (Carl Zeiss, Germany), with imaging controlled through ZEISS ZEN software (version 3.10). This technique was utilized to capture images of immunofluorescence-stained co-culture samples, as well as for live cell imaging of both HUMSC and ReNcell monocultures, and the co-culture.

2.2.7. Scanning Electron Microscopy

Samples prepared for SEM were initially fixed in 4% glutaraldehyde (Sigma-Aldrich) and subsequently dehydrated through an ethanol series: 40%, 70%, 80%, 90%, 95%, and 100%, with each step lasting one hour. Following ethanol dehydration, samples were submerged in a 50:50 ethanol/hexamethyldisilane solution, then moved to 100% hexamethyldisilane for two consecutive soaks. The final immersion in 100% hexamethyldisilane was followed by overnight evaporation to ensure thorough drying. Dried samples were finally coated with chromium using a Quorum Q150T ES sputter-coater to enhance conductivity (Quorum Technologies Ltd, Sussex, UK). Imaging was performed on a Hitachi S-4800 scanning electron microscope (Hitachi High-Tech Corporation, Tokyo, Japan).

2.3. *in-vivo* work

2.3.1. In vivo model preparation

The *in vivo* implantation was performed at Huazhong University (Wuhan, China) (Research Ethics Approval; IACUC#3294). A total of 6 Sprague-Dawley (SD) rats aged 8-weeks old (weighing 290–320 g) were randomly divided into 2 groups, a treatment group (HAA implant) and a control group (no HAA implant). Following grouping, an ear punch

was performed for identification and record-keeping purposes. The rats were housed in the animal experimental facility where cages were cleaned every 3 days, food and water was provided on a scheduled basis and their activity was monitored.

2.3.2. Implantation

The rats were anesthetized using an RWD Isoflurane R580 gas anaesthesia machine, with a flow rate of 3 L/min isoflurane and 0.5 L/min oxygen. Following induction, the rats were placed on the surgical table, where anaesthesia was maintained via a mask at the same flow rates. A triangular notch was made on the left ear for identification. The fur around the thigh was shaved and further removed using Nair Hair Remover Lotion, followed by disinfection with medical alcohol.

A longitudinal incision of approximately 3.5 cm was made along the lateral side of the thigh, and the quadriceps muscle was bluntly separated and retracted to expose the femur. A 3 cm mini locking compression plate (LCP) was fixed to the anterolateral femur using four 5 mm screws, ensuring that the two central plate holes remained unoccupied. A 2 mm defect was then created between these two central holes using a saw. In the treatment group the defect was filled with a paste-like HAA material, which allowed for precise placement within the defect site and easy handling during surgery, whereas the remaining 3 rats in the control group received no implant.

Following implantation, the muscle was sutured using a surgical bent needle, and the skin was closed with sutures. To prevent dehydration, 10 mL of saline was administered subcutaneously. The rats were monitored in an experimental cage until full recovery from anaesthesia, ensuring normal limb function before being returned to the animal housing facility. The rats were sacrificed 14 days, 28 days, and 56 days following the surgical procedure by humane euthanasia via cervical dislocation. The experimental limb was dissected, with skin and fur removed while preserving muscle, and subsequently fixed in 4% formaldehyde in PBS for further fixation and further analysis.

2.3.3. Micro-CT

After fixation, each left tibia was individually wrapped in parafilm and scanned using a SkyScan 1176 X-ray microtomography system (Bruker MicroCT, Kontich, Belgium). Scanning was conducted at 58 kV and 431 µA, with a pixel resolution of 9 µm, a rotation step of 0.3°, and a high-resolution exposure time of 1,000 ms. Following scanning, the specimens were unwrapped and placed back into 10% formalin for storage at 4°C. The resulting micro-CT data were used to generate three-dimensional models and perform quantitative assessments of new bone formation

2.3.4. Bone imaging

Fixed bone samples were embedded in London Resin Gold (Agar Scientific) containing 1% w/v benzoyl peroxide (Agar Scientific, UK) as per the manufacturer's protocol. Each bone sample was secured to a metal plate using four screws per sample to ensure stability during the embedding process. Aluminium foil was used to correctly position the samples within the resin blocks, which were then cured at room temperature. The cured blocks were sanded using 600- and 1200-grit sandpaper and polished to 6- and 3-micron finishes.

Micro-CT imaging was performed to analyse two key parameters. Firstly, fracture width was assessed in both control samples and the experimental group implanted with HAA scaffolds. Measurements were taken at three distinct locations along the fracture site, and the average of these triplicate measurements was calculated to track changes in fracture width across time points of 14-, 28-, and 56-days following implantation. Secondly, HAA biomaterial volume was quantified in the experimental group to evaluate biodegradation. This was determined by measuring the volume of the biomaterial at each time point and assessing its reduction over time. The decrease in volume was used as an indicator of scaffold biodegradation.

2.3.5. Statistical analysis

Statistical analyses were performed using GraphPad Prism version 10.4.1 (Graphpad Software, San Diego, USA). Data are presented as mean ± standard deviation (SD). For comparisons between two groups, a t-test was employed. One-way ANOVA was used for comparisons involving more than two groups, while two-way ANOVA was conducted to assess interactions between multiple groups across different time points or conditions. A p-value of < 0.05 was considered statistically significant.

3. RESULTS

3.1 HAA scaffold successfully produced

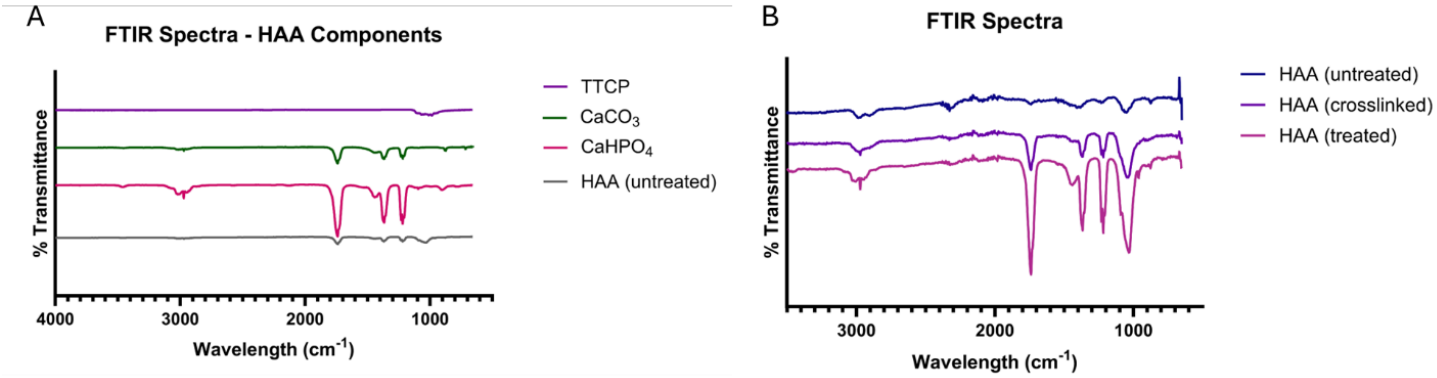

Figure 1. FTIR Spectra of HAA Components and Treatment Stages.
(A) FTIR spectra of untreated HAA, showing characteristic peaks of its functional groups. (B) FTIR spectra of HAA at different treatment stages: (i) untreated, (ii) crosslinked with 0.1% glutaraldehyde for 24 hours, and (iii) post-crosslinking followed by a 24-hour PBS soak. Graph generated using GraphPad Prism version 10.4.1.

The FTIR spectra (Figure 1A) shows the untreated HAA material, with peaks corresponding to the main components of the mixture: TTCP, $CaCO_3$, and $CaHPO_4$. The phosphate peak around 1000 cm^{-1} is relatively weak, suggesting minimal hydroxyapatite formation. Additionally, the carbonate-related peaks at approximately 1200 cm^{-1} and 1400 cm^{-1}, along with a weak hydroxyl peak near 3500 cm^{-1}, reflect the presence of $CaCO_3$ and $CaHPO_4$. These findings indicate that in the untreated state, hydroxyapatite formation is limited, with the material predominantly containing unreacted $CaCO_3$ and $CaHPO_4$. Following crosslinking with 0.1% glutaraldehyde, as shown in Figure 1B, the spectra reveal a more defined peak around 1000 cm^{-1}, which suggests a slight increase

in hydroxyapatite formation. In addition, the peaks at 1200 cm^{-1} and 1400 cm^{-1}, which are characteristic of carbonate groups, are more prominent, and the hydroxyl peak near 3500 cm^{-1} becomes more discernible. These changes indicate that crosslinking may promote partial conversion of $CaCO_3$ and $CaHPO_4$ into hydroxyapatite, as well as some degree of carbonate substitution within the material. Upon further treatment with PBS for 24 hours, the FTIR spectra of the treated HAA show a significant increase in peak intensity, particularly at 1000 cm^{-1}, corresponding to phosphate groups. The carbonate peaks at 1200 cm^{-1} and 1400 cm^{-1}, along with the hydroxyl peak near 3500 cm^{-1}, are also much more defined, suggesting a substantial increase in HA formation. These intensified peaks indicate that the combined crosslinking and PBS treatment significantly enhance phosphate mineralization, the incorporation of phosphate groups into HA, and carbonate incorporation, thus supporting the formation of a more HA-rich structure. The clearer, more defined peaks overall imply that the PBS soak effectively facilitates HA production, leading to a more mature and crystallized biomaterial. Thus, it could be determined that while untreated HAA still consists of its three main compounds, HA was formed in all samples soaked in PBS. As the scaffold is soaked for a longer period, the HA peak becomes larger than the $CaCO_3$ peaks. This indicates the possibility that HA formation is a slow process, and more HA has formed in the samples that were soaked longer.

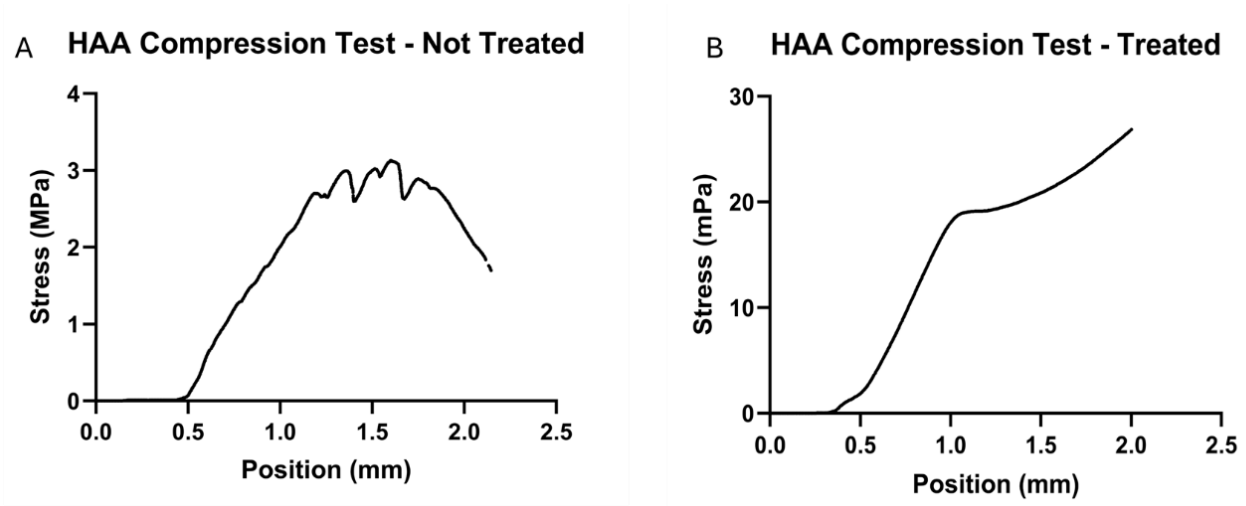

Figure 2: Compression tests of HAA.
(A) Stress-position curve of untreated HAA showing its mechanical response under compression. (B) Stress-position curve of treated HAA, demonstrating the mechanical properties post-treatment. Differences in the curves highlight the impact of treatment on the material's compressive strength and deformation behaviour. Graph generated using GraphPad Prism version 10.4.1.

In the compression testing of both untreated and treated HAA scaffolds, the results from the compression test of untreated and treated HAA scaffolds demonstrate a noticeable difference in mechanical strength. For the untreated HAA scaffold (Figure 2A), the stress-strain curve begins at 0.5 mm, with points of inflection observed around 1.3 mPA, 1.7 mPA, and a distinct inflection at just over 3.6 mPA, at which point the material shows significant signs of crumbling, indicating failure. In contrast, the treated HAA scaffold (Figure 2B), which underwent crosslinking and PBS soaking, experienced no failure or crumbling until it reached its point of inflection at around 20 mPA, which is considerably higher than that of the untreated sample. This was followed by a brief plateau in stress before the experiment was halted due to the material breakage. Overall, these results suggest that treatment supports the strengthening of HAA, thus improving its compressive strength as evidenced by the higher stress tolerance prior to failure.

During optimization of the HAA scaffold production method, an investigation was conducted to determine if different drying methods influenced the occurrence and distribution of naturally occurring pores. Specifically, the effect of air-drying versus freeze-drying was assessed. However, the results indicated no significant difference between the two methods, with air-drying proving to be just as effective at retaining pores throughout the structure. As such, air-drying was selected as the preferred method for further scaffold production.

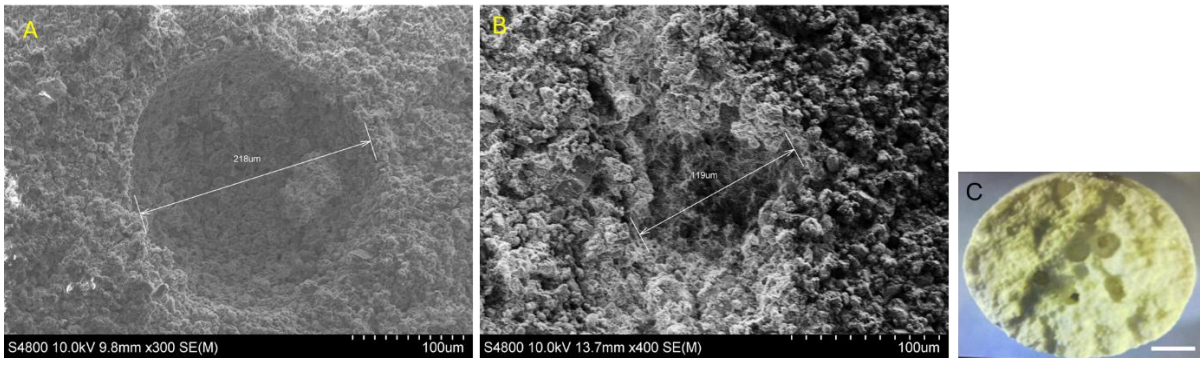

Figure 3: Imaging of Final Treated HAA Disc Product.
SEM images showing the surface of the treated HAA disc with well-defined pores measuring (A) 218 µm in diameter and (B) 119 µm in diameter. (C) Gross image of the final treated HAA disc taken using a Tomlov TM-DM10 imaging system, providing a visual representation of the disc's overall structure, scale bar represents 1 mm.

The surface structure of the treated HAA scaffold was examined under SEM (Figure 3A and 3B). Pores were observed on the surface of the HAA, measuring 218 µm and 119 µm in diameter, respectively. The structure of the material appeared rugged in texture, and while these pores are not highlighted in the images, many irregularly shaped gaps were also observed across the surface. The gross image shown in Figure 3C reveals voids up to 1 mm in diameter, visible to the naked eye. These observations indicate that the material exhibits heterogeneity and incidental gaps, though it is unclear whether these reflect controlled porosity or arise from trapped air during the fabrication process.

3.2 HUMSC/ReNCell VM co-culture established

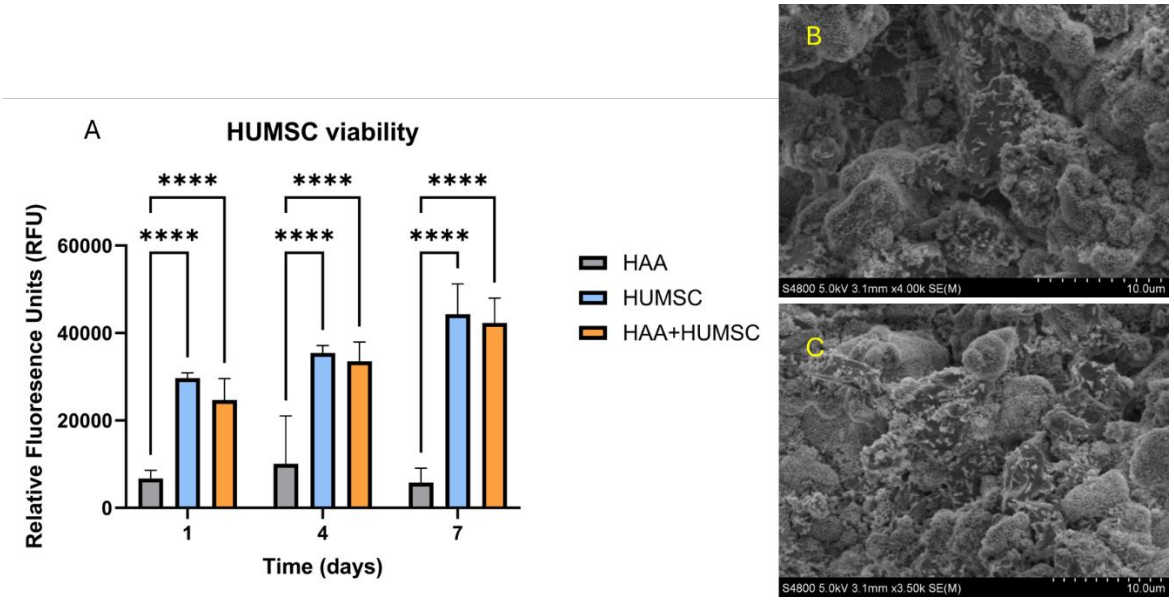

Figure 4. HUMSC Cell Culture on HAA.
(A) Bar chart showing Alamar Blue Assay results for HUMSC viability after 4 and 7 days of culture on HAA. (B) SEM image of HUMSC seeded on HAA for 4 days, highlighting cellular morphology. (C) SEM image of HUMSC seeded on HAA for 7 days, showing the continued adherence and growth of cells on the material. Graph generated using GraphPad Prism version 10.4.1.

To assess the cytotoxicity of the HAA scaffold, an Alamar Blue assay was performed following the seeding of 10,000 HUMSC per well on a 96-well plate. The experiment included three groups: a positive control consisting of only HUMSC, a negative control consisting of only HAA, and an experimental group consisting of HUMSC seeded on top of HAA. The assay was conducted at three time points: day 1, day 4, and day 7 after seeding. A two-way ANOVA was performed with Tukey's multiple comparisons test as

the post-hoc analysis. Statistically significant differences were observed between the HAA and HUMSC groups ($p < 0.0001$), as well as between the HAA and HAA+HUMSC groups across all time points. However, no significant difference was found between the HUMSC and HAA+HUMSC groups on day 1 ($p = 0.2538$), day 4 ($p = 0.8177$), and day 7 ($p = 0.8006$), suggesting that the HAA scaffold does not exert cytotoxic effects on the HUMSCs. Furthermore, the relative fluorescence units (RFU) steadily increased over the course of the experiment, indicating that HUMSCs continued to proliferate and grow in the presence of HAA. These results suggest that HAA is biocompatible and does not inhibit the growth or proliferation of HUMSCs over the 7-day period.

In addition, the attachment of HUMSC to the HAA scaffold was further confirmed through SEM imaging, as shown in Figure 4B. Images were taken on day 4 following the initial seeding, and they clearly show HUMSCs attached to the surface of the HAA as well as within the structural pores of the material. These observations support the notion that HUMSCs can interact with and adhere to the HAA scaffold, allowing for proper cell attachment and integration with the material.

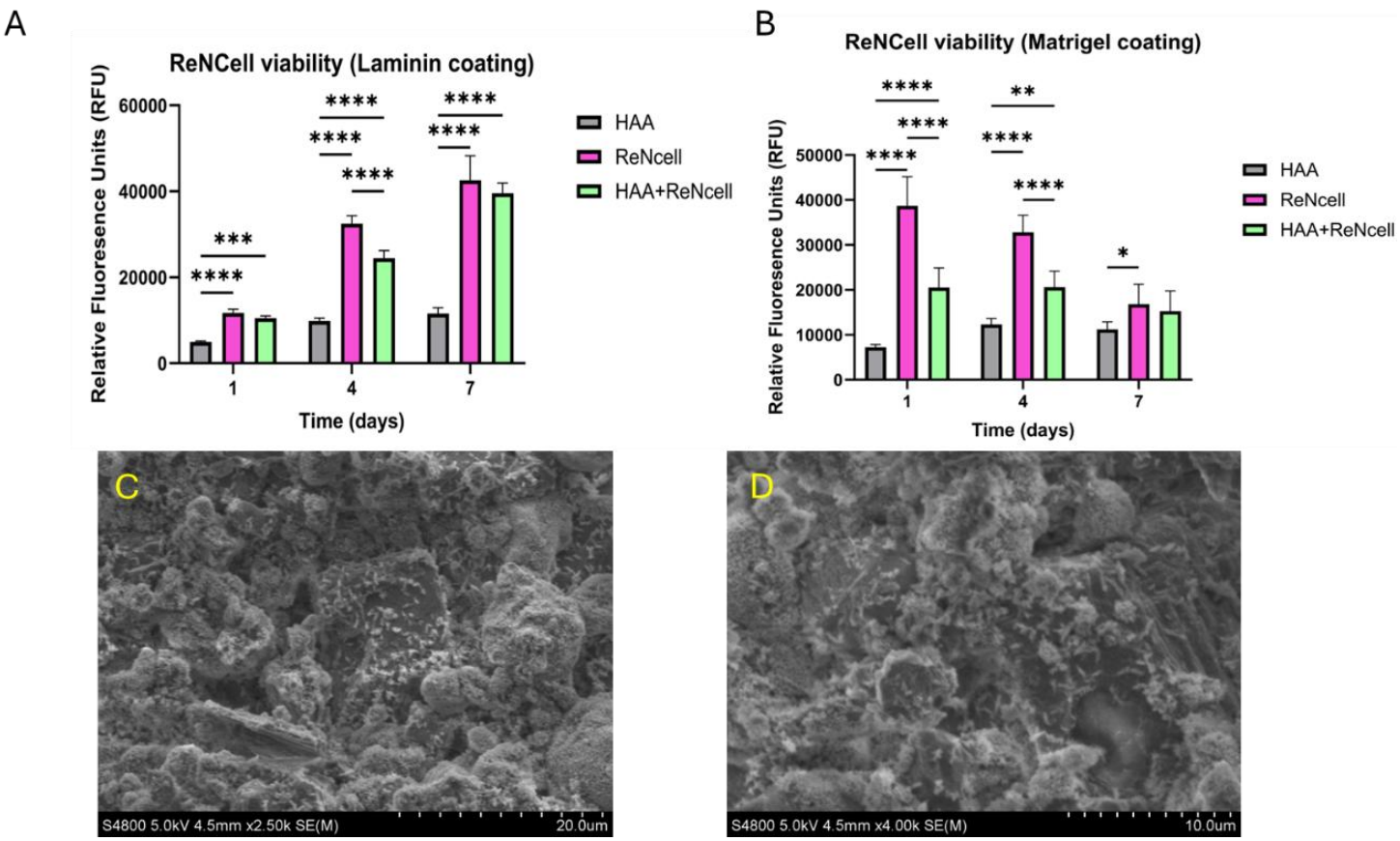

Figure 5. ReNcell Culture on HAA.
(A) Bar chart showing Alamar Blue Assay results for ReNcell viability on laminin-coated HAA over 4 and 7 days. (B) Alamar Blue Assay results for ReNcell viability on Matrigel-coated HAA over 4 and 7 days. (C) SEM image of ReNcells seeded on laminin-coated HAA for 4 days, showing cellular adherence and spacing. (D) SEM image of ReNcells seeded on Matrigel-coated HAA for 4 days, displaying similar adhesion and morphology. Graphs generated using GraphPad Prism version 10.4.1.

The cytotoxicity of HAA to ReNcells was assessed using the Alamar Blue assay over a 7-day period, with ReNcells cultured either on HAA alone or on HAA coated with laminin or Matrigel. In the laminin-coated group (Figure 5A), the results showed a significant difference between the HAA group and the ReNcell group on day 1 ($p < 0.001$), as well as between HAA and the ReNcell/HAA group ($p = 0.004$). However, on day 4, significant differences ($p < 0.001$) were observed across all three groups, which is notable. By day 7, only the HAA versus ReNcell comparison and the HAA versus HAA+ReNcell comparison were statistically significant ($p < 0.001$). The lack of significant difference between the ReNcell and HAA+ReNcell groups on day 7 ($p = 0.0733$) suggests that ReNcells cultured on laminin-coated HAA were compatible and not significantly affected by the material. The data observed on day 4 may indicate a temporary disruption in cell viability, this was possibly due to early-stage cell stress or adjustment to the culture conditions, though further investigation would be needed to confirm the cause.

Cell viability in the Matrigel-coated HAA experiment (Figure 5C) was assessed using the Alamar Blue assay across 3 groups: HAA, ReNcells, and HAA+ReNcell. On day 1, there was a statistically significant difference between all three groups ($p < 0.001$), with the ReNcell-only group exhibiting a notably higher RFU compared to both the HAA and HAA+ReNcell groups. This trend persisted on day 4, where the ReNcell group remained significantly different from the other groups ($p < 0.001$). However, in contrast to the laminin-coated experiment (Figure 5A), the RFU values in the Matrigel-coated experiment progressively decreased over time. For example, on day 1, the ReNcell group had the highest mean RFU of 38695.5 ± 6484.1 (N=6), which dropped to 32824.3 ± 3,788.0 on day 4 and further declined to 16800.8 ± 4482.7 on day 7. Despite this decline, statistical significance between the groups was still observed on day 4 ($p = 0.0016$). By day 7, however, significant differences were only observed between the HAA and ReNcell groups ($p = 0.0411$). These findings suggest that while ReNcells show initial compatibility with Matrigel-coated HAA, there is a decline in cell viability over time, which may suggest some form of cell stress or suboptimal growth conditions in the Matrigel-coated group, such an inadequate coating volume.

The morphology of ReNcells seeded on both laminin- and Matrigel-coated HAA was assessed by SEM on day 7, as shown in Figures 5B and 5D, respectively. The SEM images clearly depict the attachment and spreading of ReNcells across the surface of the HAA material. On the laminin-coated HAA (Figure 5B), ReNcells form a continuous monolayer, with individual cells visibly stretched and elongated along the surface. In a similar manner, on the Matrigel-coated HAA (Figure 5D), ReNcells adhere to and extend across the material's surface, exhibiting characteristics of mid-confluency morphology. It should be noted that in certain regions and crevices of the HAA structure, a higher density of ReNcells is observed, where cells appear to be more compact and show areas of cell-to-cell contact. In these regions, the ReNcells adopt a more polygonal shape, likely due to these cellular interactions. However, due to the 3D nature of the HAA scaffold and its relatively large surface area, several regions of the material exhibit sparse cell coverage. These areas display individual ReNcells with elongated, fibroblast-like morphology and minimal or no cell-to-cell contact, with cells appearing more spread out across the surface.

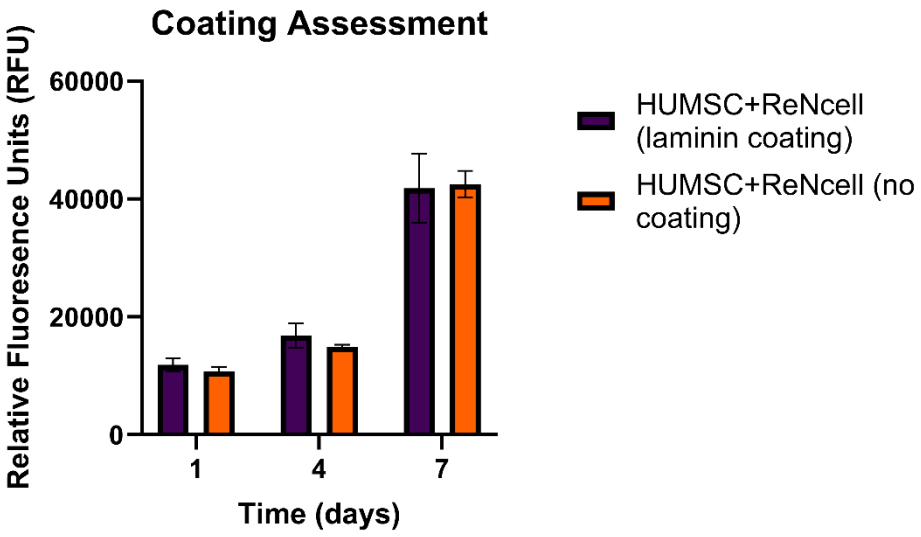

Figure 6. Comparison of ReNcell Viability on Laminin-Coated Plates vs. HUMSC monolayer for co-culture.
Bar chart displaying Alamar Blue Assay results comparing ReNcell viability on laminin-coated plates and HUMSC monolayer over a 7-day period. No statistically significant differences were observed at any timepoint, suggesting that the HUMSC monolayer effectively supports ReNcell viability, making it a viable alternative to the laminin coating for co-culture systems. Graphs generated using GraphPad Prism version 10.4.1.

To evaluate the impact of laminin coating on the performance of the co-culture system, a coating assessment was performed (Figure 6). In this experiment, 10,000 HUMSCs were seeded per well in a 96-well tissue culture plate and allowed to proliferate for one week. Regular checks and media changes were carried out every 2–3 days to maintain cell health. Once the HUMSC monolayer reached approximately 80% confluence, 10,000 ReNcells were seeded per well. The cells were allowed to attach overnight before undergoing the Alamar Blue assay to assess cell viability across both groups. In one group, ReNcells were seeded directly onto the HUMSC monolayer, while the other group coated condition utilized a laminin-coated plate for co-culture preparation. Results showed a trend of increasing RFU over time, with the highest values recorded on day 7 in both groups, indicating continuous cell growth throughout the experiment.

Importantly, no statistically significant differences were observed between the laminin-coated and uncoated groups at any time point. These findings suggest that laminin coating does not confer any additional advantage in this co-culture setup. This supports the feasibility of culturing ReNcells without the need for laminin coating, which simplifies the protocol and reduces preparation costs without compromising cell viability or growth outcomes.

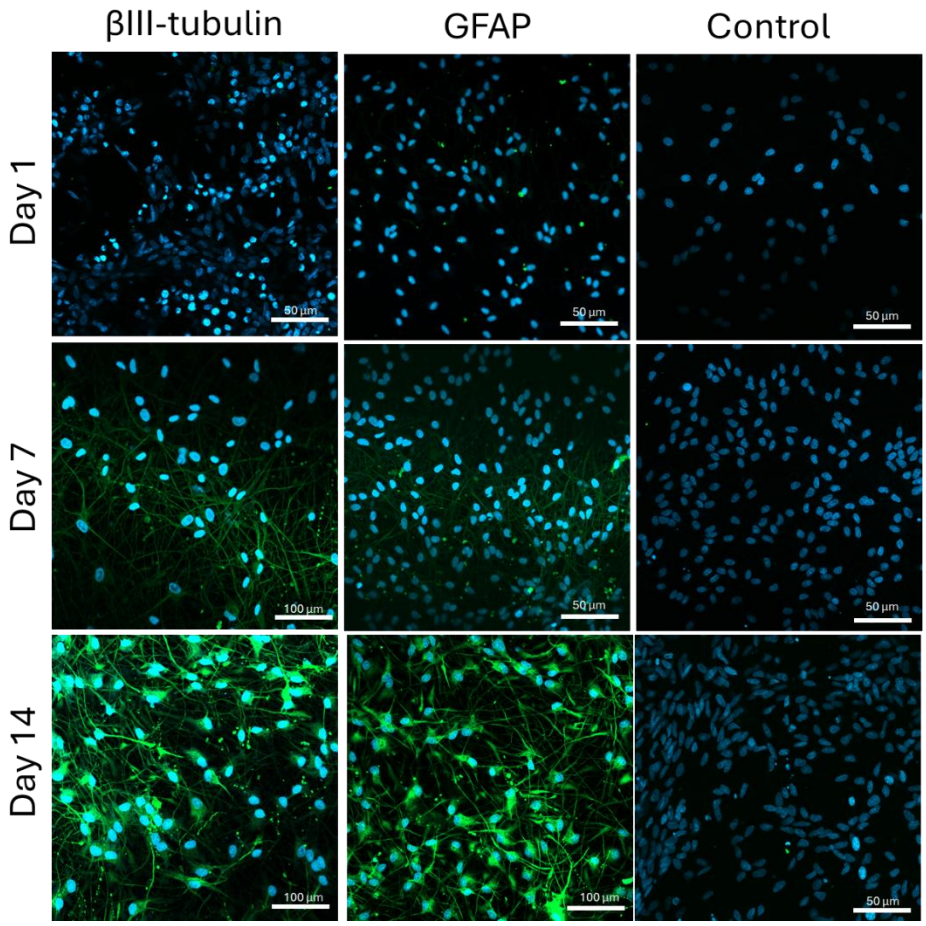

Figure 7. Immunofluorescence images of neural differentiation in ReNcells cultured on HUMSC monolayer.
Series of immunofluorescence images taken at days 1, 7, and 14 to track neural differentiation of ReNcells seeded on a HUMSC monolayer in co-culture, supplemented with ADM. Primary antibodies used were βIII-tubulin as a marker for neurons and GFAP for astrocytes. The images show the progressive differentiation of ReNcells into neural cell types, with increased expression of both

To assess the differentiation potential of ReNcells when co-cultured on a HUMSC monolayer, immunofluorescence staining was performed following supplementation with ADM. The co-culture model was established by first allowing the HUMSC to grow to approximately 80% confluency over 7 days, after which ReNcells were seeded and permitted to adhere for 3 days before initiating differentiation.

On Day 1 of differentiation, no fluorescence indicative of βIII-tubulin or GFAP expression was detected in any of the experimental groups. This was expected, given the early time point and the limited duration for differentiation to occur. The negative control, which was processed without primary antibodies and incubated with PBS only,

displayed no fluorescence, confirming the specificity of the staining protocol. However, positive Hoechst staining confirmed the presence of viable cell nuclei from both the HUMSC monolayer and the overlying ReNcells, verifying the integrity of the co-culture system. By Day 7, distinct morphological and immunofluorescent changes were evident. In the βIII-tubulin-stained group, robust neural networks were observed, with a green fluorescence signal indicating the presence of the Alexa Fluor 488-conjugated secondary antibody to βIII-tubulin. These networks displayed intricate branching and layering, with overlapping neural processes forming a complex, interconnected structure. Furthermore, some Hoechst-stained nuclei were associated with neuronal cell bodies, confirming the differentiation of ReNcells into neurons. Other nuclei, which did not overlap with the neuronal structures, were presumed to correspond to the underlying HUMSC monolayer, serving as a supportive substrate for the developing neural network.

A similar result was observed in the GFAP-stained group on day 7, where a mature astrocyte network was evident, marked by the Alexa Fluor 488-conjugated secondary antibody specific to GFAP, an astrocyte marker. This was consistent with expectations, as ReNcells are human neural progenitor cells with the potential to differentiate into both neurons and glial cells, such as astrocytes, under appropriate conditions. The dense and interconnected astrocytic network further reinforced the successful differentiation of ReNcells in the co-culture model. These findings were further corroborated on day 14, with both βIII-tubulin and GFAP staining continuing to reveal neural and astrocytic networks, respectively. However, fluorescence intensity appeared slightly reduced compared to Day 7. This was attributed to natural cell death, a phenomenon commonly observed during prolonged differentiation phases. Additionally, images from this time point were not consistently taken at equivalent objectives or cell-dense regions, which may have influenced the perceived density of the networks. Nonetheless, the persistence of both neuronal and astrocytic structures indicates the stability of differentiation over the two-week co-culture period.

In conclusion, these results demonstrate that ReNcells seeded onto a HUMSC monolayer can differentiate into both mature neurons and astrocytes when

supplemented with ADM, forming robust, interconnected networks that remain throughout the differentiation phase.

3.3 Co-culture adheres to HAA

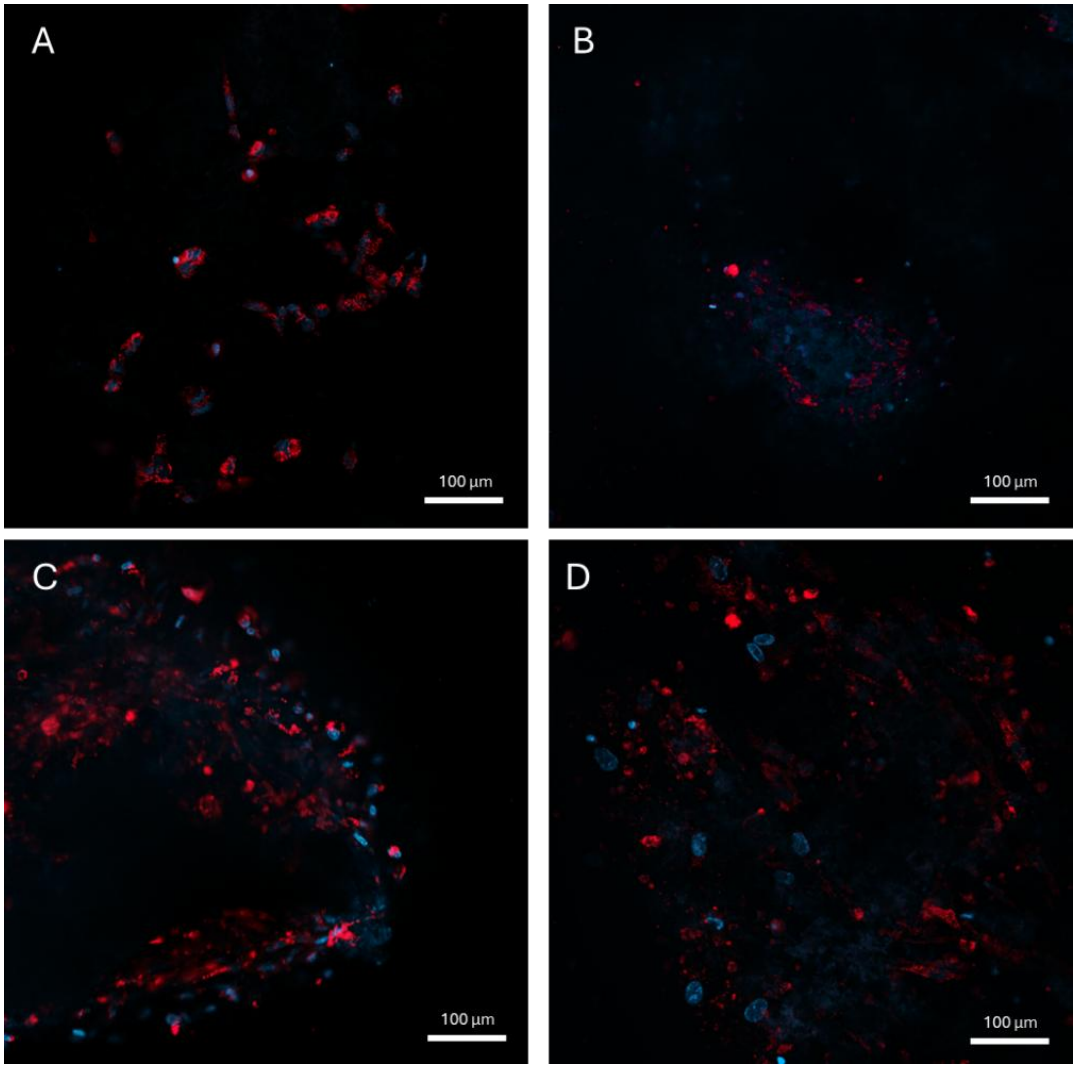

Figure 8. Live Cell Staining of HUMSC with DiD.
Live cell imaging using DiD staining to track HUMSC proliferation over a 14-day period. (A-D) show images taken on days 1, 4, 7, and 14, respectively. The red fluorescent regions indicate HUMSCs, and an increase in cell number is observed as the culture progresses, highlighting cell growth and proliferation. The fluorescence intensity and coverage visibly expand from day 1 to day 14, demonstrating the dynamic cellular activity within the co-culture system. DAPI staining marks cell nuclei blue.

Figure 8 illustrates the progression of HUMSC proliferation and distribution on HAA discs across the timepoints of day 1, day 4, day 7, and day 14. A general trend of

increasing fluorescence is observed over time, signifying the growth and proliferation of DiD-labelled HUMSC seeded onto the material.

On day 1, blue fluorescence from the Hoechst nuclear stain is visible as distinct specks scattered across the HAA surface. These nuclei are enveloped or overlap with specks of red fluorescence, indicating the presence of live DiD-labelled HUMSCs. At this early stage, the red fluorescence is observed as discrete, brighter specks that are well-separated with minimal overlap between them. This pattern suggests that the HUMSCs are in the initial stages of adhesion and have not yet fully spread or proliferated across the material. The cell bodies, although labelled with red fluorescence, appear localized and spread out as they begin the adhering onto the highly porous, 3D structure of the HAA disc. By day 4, an increase in fluorescence intensity is evident, particularly in regions corresponding to the pores of the HAA material. The selected image focuses on a pore where blue fluorescence (nuclei) is concentrated in the centre and surrounded by overlapping red fluorescence. This overlap further confirms the presence of viable HUMSCs adhering to and spreading across the pore surface. However, the number of distinct nuclei remains relatively low at this stage, implying that while adhesion has progressed, cell proliferation is still limited. Importantly, the observed overlap likely reflects spatial proximity rather than active cell-cell interactions. On day 7, significant changes in the fluorescence pattern can be observed. Both the number of nuclei and the extent of red fluorescence have noticeably increased. The red fluorescence begins to extend over a larger portion of the focal plane, indicating that the cells are not only proliferating but are also actively spreading across the porous structure of the HAA. The morphology of the cells appears more stretched and elongated, especially in smaller pores, suggesting that the cells are adapting to the topography and 3D nature of the material. By day 14, the fluorescence intensity and distribution reach their peak, highlighting robust cell proliferation and spreading. The number of nuclei has substantially increased, accompanied by a widespread and bright red fluorescence that overlaps with the nuclei. The DiD-labelled cell bodies exhibit an elongated, fibroblast-like morphology, further signifying their adaptation to the porous and irregular surface of the HAA material. This morphology, combined with the widespread

fluorescence, indicates that the HUMSCs are actively proliferating and successfully colonizing the material over the two-week period.

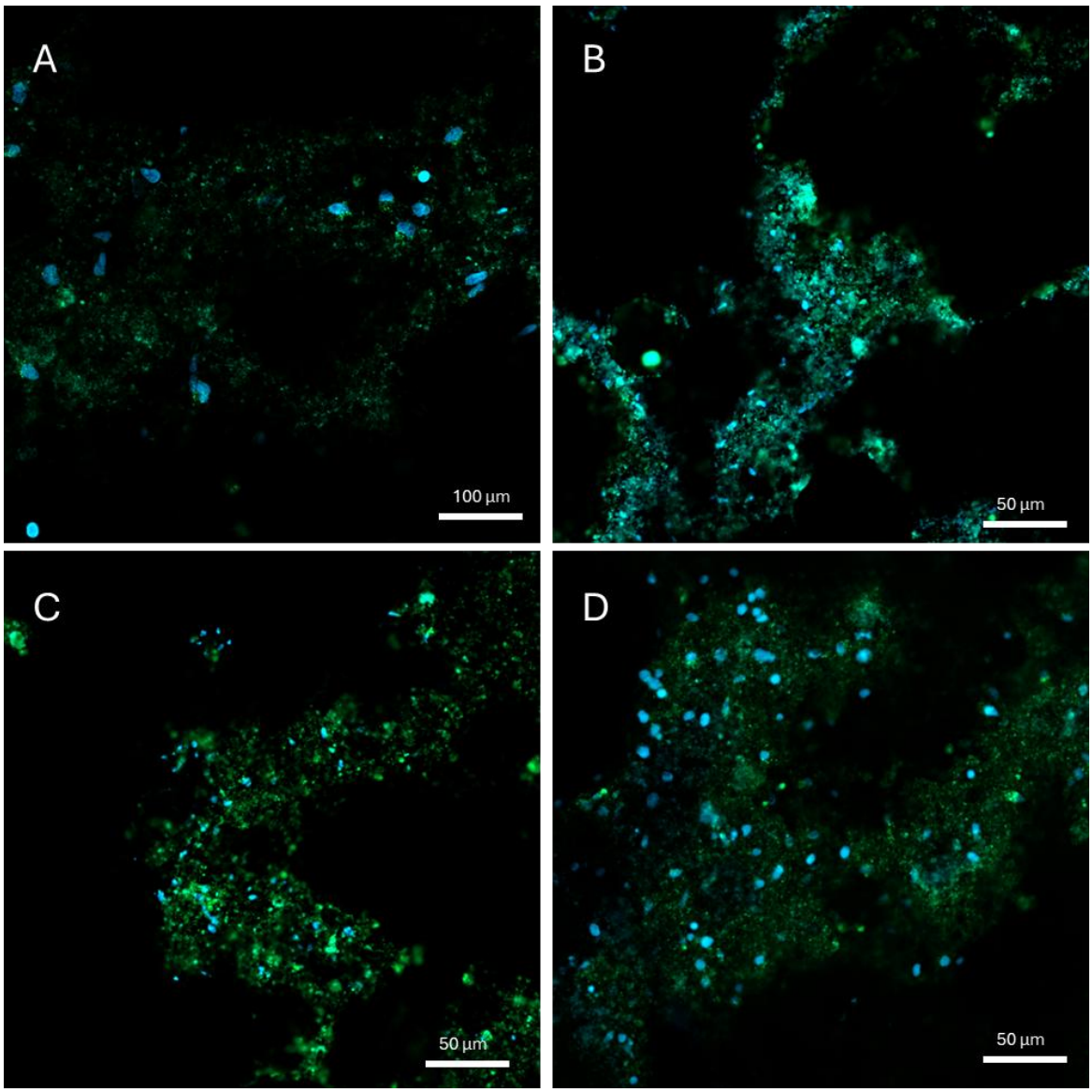

Figure 9. Live Cell Staining of ReNcells with DiO.
Live cell imaging of ReNcells stained with DiO, tracking cell proliferation and viability over a 14-day period. The green fluorescence (DiO) highlights ReNcell populations, with DAPI nuclear staining in blue marking cell nuclei. The images provide a clear representation of ReNcell growth and expansion, with increased cell density over time.

Figure 9 illustrates the progression of ReNcell adhesion, proliferation, and spatial distribution on laminin-coated HAA discs over the timepoints of day 1, day 4, day 7, and day 14. While a general trend of increasing fluorescence intensity and cell coverage is observed, a key feature of these results is the notable autofluorescence of the HAA

material, particularly at the DiO wavelength. This autofluorescence presented a challenge in distinguishing signal originating from cells versus the material; however, the inclusion of the nuclear counterstain (Hoechst 33342) was critical in confirming cell presence. Specifically, regions where the blue nuclear fluorescence overlaps with green DiO fluorescence provide clear evidence of viable, proliferating ReNcells.

On day 1, scattered blue-stained nuclei are visible, along with discrete green fluorescence corresponding to DiO-labelled ReNcells. At this early stage, the cells appear as isolated signals with minimal overlap between nuclei and green fluorescence. This pattern suggests that the cells have adhered to the laminin-coated HAA but have not yet begun substantial proliferation. Autofluorescence of the HAA is apparent at this wavelength, but the presence of blue-stained nuclei overlapping with green fluorescence allows us to definitively identify live, deposited ReNcells. A modest increase in green fluorescence and nuclear count was observed on day 4, indicating the onset of ReNcell proliferation and spreading. In focal planes where the porous HAA surface is clearly visible, the green fluorescence extends across more of the material, often overlapping with nuclei, which reinforces the presence of viable cells. Despite the autofluorescence, the combined fluorescence signals effectively highlight regions of cell attachment and growth on the material surface. By day 7, substantial changes are apparent, with an increased number of nuclei and more extensive green fluorescence spanning across larger portions of the HAA disc. The fluorescence signal becomes more diffuse in some areas, reflecting ReNcell proliferation and spreading across the complex 3D architecture of the material. Cells exhibit an elongated morphology, consistent with adaptation to the porous surface. Notably, regions where the blue fluorescence aligns with green fluorescence provide clear confirmation that viable ReNcells are actively growing and colonizing the material, even in areas where autofluorescence is more prominent.

By day 14, the ReNcells reach their highest observed density, with a pronounced increase in both nuclear and green fluorescence. The green fluorescence appears interconnected, covering extensive portions of the material's surface. Cells display a mix of elongated and clustered morphologies, indicative of robust proliferation and adaptation to the laminin-coated HAA. Although autofluorescence remains a

confounding factor at this stage, the consistent overlap between nuclei and DiO fluorescence validates the presence of live ReNcells. The combination of signals confirms that the ReNcells have proliferated successfully, extensively covering the porous surface of the material.

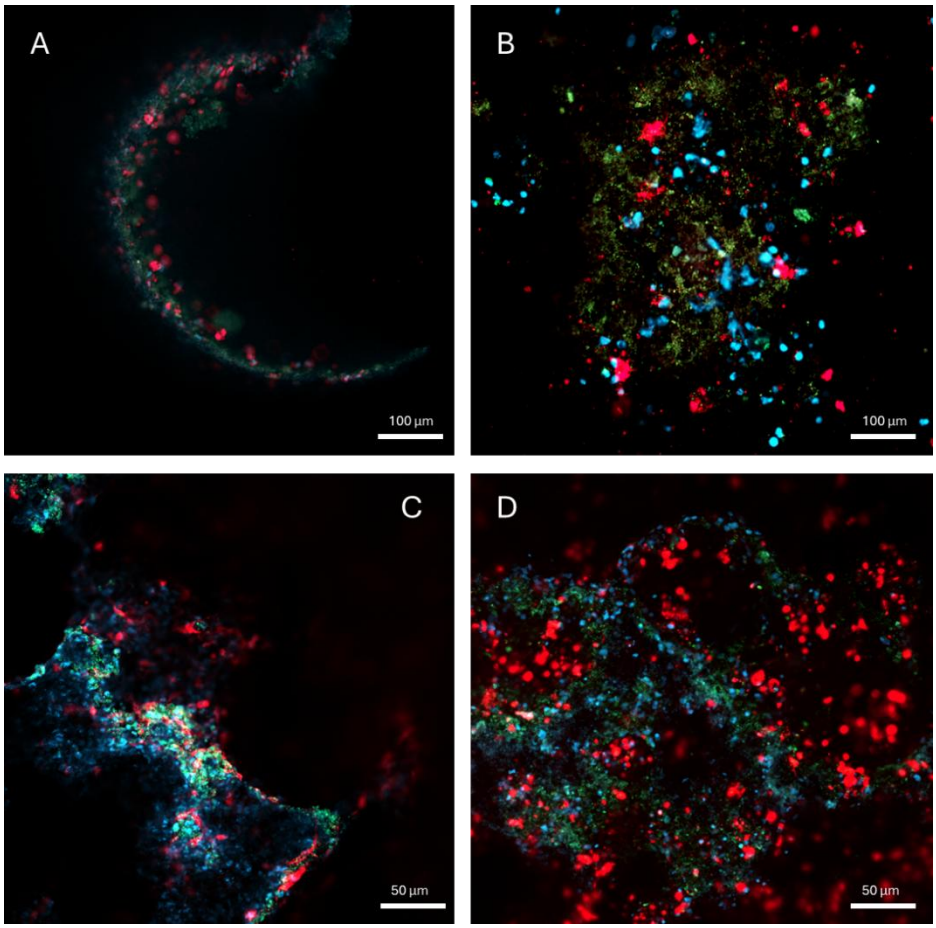

Figure 10: Co-culture Live Cell Staining.
Live cell imaging of the co-culture system consisting of HUMSC (stained with DiD) and ReNcells (stained with DiO) over a 14-day period. DiD staining in red marks HUMSCs, while DiO staining in green highlights ReNcells, with both cell types identified alongside blue DAPI nuclear staining. The images show the growth and interaction of both cell types within the co-culture, with increasing cell density and co-

Figure 10 presents the progression of the co-culture on HAA discs. On day 1, sparse nuclei are visible, along with faint red and green fluorescence. Despite the relatively high seeding density (40,000 cells per well combined), the observed fluorescence is less concentrated than expected. This may reflect imaging challenges, such as the selection of a suboptimal focal plane, rather than a lack of initial adhesion. Nevertheless, areas where fluorescence signals overlap with nuclei provide evidence of

early cell attachment. By day 4, the images show more robust cell coverage, with a notable increase in both fluorescence intensity and the number of nuclei. The fluorescence signals align closely with the nuclei, highlighting areas where HUMSCs and ReNcells have adhered and begun to proliferate. While autofluorescence from the HAA material remains a contributing factor, the specific overlap of red and green fluorescence with nuclei allows for reliable identification of cell locations. The images from day 7 demonstrate significant cell proliferation and distribution across the HAA surface. Both fluorescence signals and nuclei extend across broader regions, with cells showing an affinity for areas surrounding the micropores. The red and green fluorescence often overlap, suggesting a degree of interaction or co-localization between the two cell types. The elongated appearance of fluorescence patterns indicates that cells are adapting to the porous architecture and forming interconnected networks. The surface of the HAA disc is shown to be densely covered with cells by day 14. The high concentration of nuclei and overlapping fluorescence signals reflects extensive proliferation and the establishment of a cohesive cell layer. The distribution of cells around and within the pores is particularly evident, with the clear overlap of fluorescence signals and nuclei demonstrating the success of the co-culture system in supporting growth and interaction between HUMSCs and ReNcells on the 3D scaffold.

3.4. HAA enhances bone regeneration *in vivo*

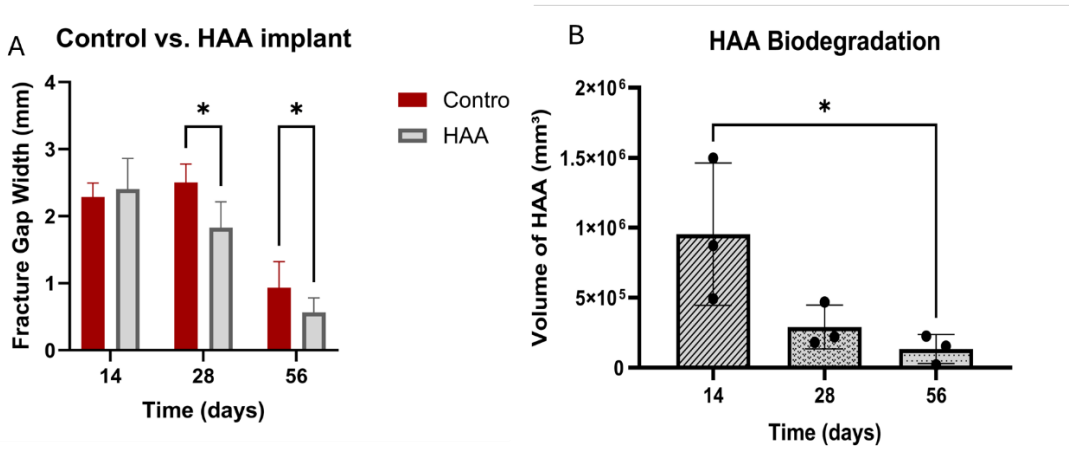

Figure 11: In Vivo Murine Model Analysis of HAA Implants.
(A) Bar chart comparing fracture width measurements between the control and HAA implant groups at days 14, 28, and 56, demonstrating the impact of HAA on bone regeneration over time. (B) Bar chart showing the average volume of HAA implants across the same time points, indicating biodegradation of the material over the 56-day period. Both sets of data highlight the progressive changes in HAA implants and their potential for enhancing bone healing. Graphs generated using GraphPad Prism version 10.4.1.

The *in vivo* rat models were used to evaluate the impact of HAA on bone regeneration at surgically induced femoral fracture sites. Fracture gap widths were compared between control and HAA-treated groups at 14-, 28-, and 56-days post-surgery. Although a total of 6 rats were used in the study (n = 3 per group), three independent measurements were taken from distinct regions within each bone and averaged to account for biological variability. This approach yielded a sample size of N = 9 per group per timepoint for statistical analysis. An unpaired t-test with individual variance at each timepoint was used, and the Holm-Šídák method was applied to correct for multiple comparisons

On day 14, no statistically significant difference in fracture gap width was observed between the control group (mean: 2.288 ± 0.207 mm) and the HAA-treated group (mean: 2.404 ± 0.457 mm) ($p = 0.4957$). This indicates that the addition of HAA had not yet markedly influenced bone regeneration relative to natural healing during the initial two weeks post-implantation. On day 28, a significant difference was evident between the two groups ($p = 0.000560$). The mean fracture gap width in the HAA-treated group decreased to 1.829 ± 0.387 mm, whereas the control group showed a slight, non-significant increase to 2.506 ± 0.272 mm. This suggests that the addition of HAA accelerates fracture gap closure compared to natural bone regeneration at this intermediate stage. At day 56, a further reduction in fracture gap width was observed in both groups. The control group exhibited an average gap width of 0.935 ± 0.386 mm, while the HAA-treated group displayed a significantly smaller width of 0.565 ± 0.217 mm ($p = 0.023528$). These results highlight the enhanced regenerative capacity provided by the addition of HAA into the fracture site, as it facilitated a greater reduction in fracture gap size compared to the control. Overall, these findings demonstrate that HAA significantly promotes bone regeneration by accelerating fracture gap closure, particularly at later stages of healing, compared to natural bone repair alone.

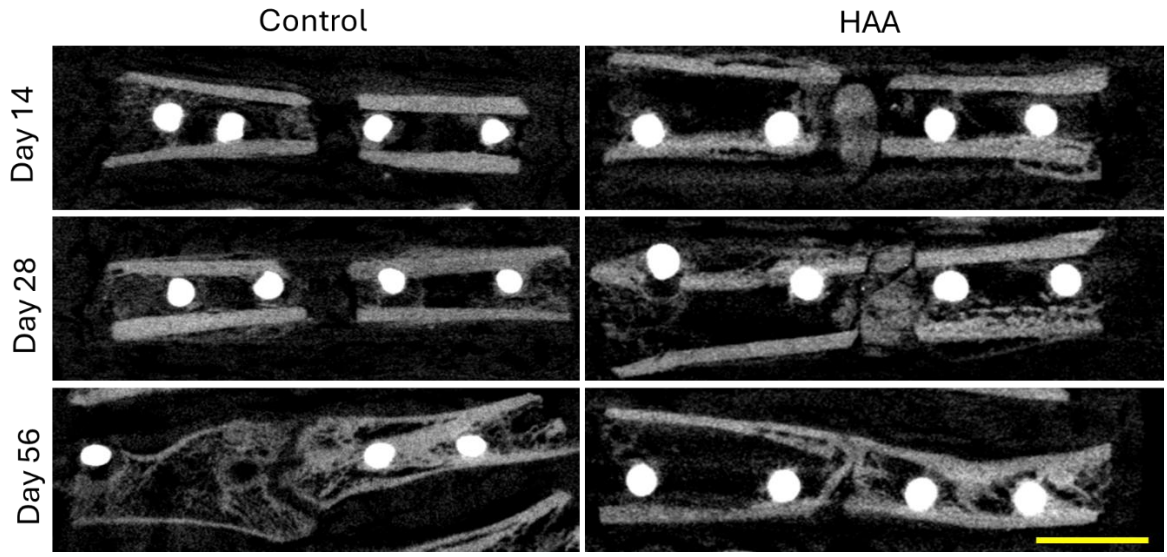

Figure 12. MicroCT scan images of mouse bone fracture repair.
MicroCT scan images of control and HAA-treated mouse bones at days 14, 28, and 56 post-fracture. The images show the progression of fracture repair, with natural healing observed in the control group and enhanced bone regeneration in the HAA-treated group. Scans were obtained using Neoscan60. Scale bar set to 1 mm.

To evaluate the biodegradation of HAA *in vivo,* the change in material volume was assessed over the timepoints of 14-, 28-, and 56-days post-implantation in mouse fracture models. As HAA was only present in the treated group, this analysis focused exclusively on plotting average HAA volumes over time to visualize trends in material degradation. At day 14, the HAA material showed the highest volume, with an average of 954,281 ± 507,712 mm^3 (N = 3). By day 28, a sharp decrease in volume was observed, with an average of 290,948 ± 156,334 mm^3 (N = 3). This reduction continued through day 56, where the average volume reached its lowest value of 133,758 ± 103,939 mm^3 (N = 3). A one-way ANOVA was conducted to assess statistical differences across timepoints, followed by Tukey's multiple comparisons test for pairwise analysis. A statistically significant difference was identified between day 14 and day 56 ($p = 0.0418$), indicating a measurable reduction in HAA volume over the full duration of the study. Despite the large reduction in volume between day 14 and day 28, this change did not reach statistical significance ($p = 0.0899$), and the subsequent decrease between day 28 and day 56 was also not statistically significant ($p = 0.8171$). Representative micro-CT images of both control and HAA-treated bone samples, illustrating the fracture appearance and the integration of HAA within the defect site, are presented in Figure 13 to visually

complement the quantitative data. These results suggest that the HAA material undergoes a substantial degradation process over time.

4. DISCUSSION

The aim of this study was to investigate the *in vitro* response of human neurons to the HAA biomaterial to assess its potential for innervation, with the long-term goal of contributing to the development of enhanced synthetic bone allografts. Innervation, alongside vascularization, is an essential feature in the regeneration of bone, and thus, understanding the innervative capacity of biomaterials holds significant promise for improving bone healing outcomes. Existing literature primarily highlights the osteogenic and osteoconductive properties of materials like HAA, but there is limited research on their ability to facilitate innervation. Therefore, this study sought to address a crucial knowledge gap by evaluating the interaction between HAA and human neural progenitor cell line, ReNcell) in a controlled *in vitro* environment, followed by *in vivo* validation through a murine model to assess the impact of HAA on bone regeneration.

This research aimed to explore three main objectives: 1) To assess whether HAA exhibits cytocompatibility with HUMSCs and ReNcells through Alamar Blue assays and live cell imaging. 2) To determine the capacity of HAA to support neuronal growth and proliferation, both in monoculture and in co-culture with HUMSCs. 3) To investigate the potential of HAA to enhance bone regeneration in an *in vivo* murine model.

The results of this study contribute to a deeper understanding of the properties of HAA and suggest that the material may possess not only osteogenic and osteoconductive qualities, but also the potential to support innervation and enhance bone regeneration. The findings have implications for the design of advanced synthetic bone allografts, capable of supporting both cellular growth and functional tissue regeneration. However, while promising, the conclusions drawn from this research should be interpreted with caution, as further studies are required to establish the long-term effects and full therapeutic potential of HAA in bone regeneration and innervation.

4.1. HAA is cytocompatible with HUMSCs and ReNcells

Alamar Blue assays were used to evaluate the cytocompatibility of HAA scaffolds with both HUMSCs and ReNcells, providing an essential first indicator of material biocompatibility and its potential to support neural and mesenchymal cell populations *in vitro*. The Alamar Blue assay is widely recognized as a well-established, cost-effective, and sensitive method for assessing cytotoxicity and cell viability *in vitro* (Longhin et al., 2022; Nociari et al., 1998). The absence of significant cytotoxicity observed for both cell types suggests that HAA does not exert harmful effects on these cells, supporting its suitability for further *in vitro* investigations. Regarding HUMSCs, the data indicated robust cell viability and proliferation, consistent with previous findings that demonstrate the biocompatibility of HAA with mesenchymal stem cells as shown in Figure 4 (Vuola et al., 1996; Watanabe & Akashi, 2008; Y. Wu et al., 2023)

The Alamar Blue assay results indicated that ReNcells cultured on laminin-coated HAA exhibited levels of viability comparable to that of HUMSC, with no statistically significant differences observed on day 1 or 7. However, it is important to note that on day 4 (Figure 5A), there was a temporary disruption in cell viability on day 4, as indicated by the statistically significant dip in RFU values. While this may reflect a transient stage of cellular stress during adaptation to the HAA scaffold, it is also worth considering other possible biological interpretations. For instance, ReNcells may exhibit delayed adaptation to ECM proteins coated on the surface of HAA, particularly given the complex and non-uniform presentation of laminin in a 3D porous environment relative to a 2D culture. In 3D matrices, cells have been reported to reorganize their cytoskeleton and adjust their adhesion dynamics, often leading to a short-term decrease in viability before stabilization (Baraniak & McDevitt, 2012; Huang et al., 2010). This dip in RFU could also signal the onset of differentiation, as neural stem cells often undergo metabolic and morphological shifts during early lineage commitment (Meli et al., 2014). While the overall trends in cell activity remained relatively stable over time, the dip in RFU observed at this timepoint may reflect a temporary stage of cell stress due to the adjustment to the HAA's 3D, highly porous surface; cell viability can be affected by a variety of factors including stress and environmental factors (H.-Q. Xu et al., 2022). Such early-stage

disruptions are not uncommon in *in vitro* studies, as cells may initially experience some degree of stress when adapting to new substrates, particularly in 3D cell cultures (Baruffaldi et al., 2021). The surface characteristics of HAA are its high porosity, irregular roughness, and brittle ceramic texture, and these have been shown to play a significant role in influencing cellular behaviour. These physical cues are known to regulate stem cell fate through mechanotransduction pathways, and substrate topography can directly affect cell polarity, neurite outgrowth, and clustering patterns (Kim et al., 2020; Kulangara et al., 2014). Porous materials with interconnected pores provide more anchoring points for cell adhesion and allow for neurite extension in multiple directions, which may encourage synaptic-like interactions or early neural network formation (Gonzalez-Perez et al., 2018). However, excessive roughness or irregular surfaces can also induce mechanical stresses or hinder uniform cell spreading, thus potentially delaying early neuronal development. Although not directly evaluated in this study, the inherent physical features of HAA may either support or inhibit the early stages of neural lineage progression depending on how ReNcells respond to these biomechanical inputs. Future investigations could include monitoring early differentiation markers or stress response genes at this timepoint to clarify whether the observed RFU dip is specifically attributed to cell stress, differentiation, or ECM-related mechanical adaptation.

On the other hand, while the Alamar Blue assay is widely supported as a reliable method for assessing cell viability and cytotoxicity, it is important to consider potential limitations associated with employing this technique. One such limitation could involve the oxidative stress imposed on cells by the assay itself, particularly during prolonged or repeated exposure to the reagent (Erikstein et al., 2011). To address this, future work could include the quantification of specific cell stress markers to better understand the underlying causes of the out-of-trend result on day 4. For example, measuring reactive oxygen species (ROS) levels could provide insights into whether oxidative stress induced by the assay or other environmental factors contributed to the observed dip in viability. Another limitation of this assay has been observed where the interaction between the Alamar Blue reagent and cell culture media can result in artificially elevated fluorescence readings even in the absence of cells, potentially leading to false positives or overestimations of cellular metabolic activity (Munshi et al., 2014). To work around the

limitation of potential false positives, it is critical to include media-only controls treated with the 5% Alamar Blue reagent under the same incubation conditions as this can help identify baseline fluorescence levels not related to cellular activity. This would allow for background signals to be detected and removed, thus ensuring a higher degree of accuracy and reliability for the fluorescence readings.

The results from Figure 6, which compared the viability of ReNcells seeded on a laminin-coated plate versus a confluent monolayer of HUMSCs over a 7-day period, provides insight into the adaptability of ReNcells in alternative culture environments. The absence of statistically significant differences in cell viability across all timepoints suggests that the HUMSC monolayer can effectively substitute the laminin coating, which is traditionally used in studies centring ReNcells (Hall et al., 2008; Li et al., 2014). This finding aligns with existing literature, which highlights that MSCs secrete a variety of growth factors, such as EGF and bFGF (Kim et al., 2009; Kim et al., 2018; Yoon et al., 2009) that are integral to neural cell function and growth. These factors play a pivotal role in promoting cellular proliferation, adhesion, and survival, making MSC monolayers an adequate substrate for ReNcell culture.

In this study, a preliminary assessment was carried out to compare the effect of using a laminin or Matrigel coating on the HAA, ahead of introducing ReNcells into the 3D cell culture. Both laminin and Matrigel are widely recognized for their ability to facilitate cell adhesion, proliferation, and differentiation due to their ECM components. The purified mouse laminin and Matrigel employed in this study were both isolated from Engelbreth-Holm-Swarm mouse sarcoma, which is a common source for these substrates.

Despite their efficacy, there are significant drawbacks associated with their use. For instance, their sarcoma-source introduces variability in composition between batches (Kleinman & Martin, 2005), leading to inconsistencies in experimental reproducibility (Kane et al., 2018; Talbot & Caperna, 2015). This variability is a particular concern for research applications that require standardized and reliable results. Furthermore, their animal origin poses challenges for clinical translation, as concerns regarding immunogenicity and regulatory approval are heightened (Aisenbrey & Murphy, 2020).

These limitations emphasize the need for alternative substrates that are reproducible, cost-effective, and scalable for both research and clinical applications; there has been an increase in the exploration of alternatives including the development of extracellular matrix hydrogels derived from decellularized gastrointestinal tissue (Kim et al., 2022), and synthetic polymer alternatives such as scaffolds derived from polyacrylamide (Tse & Engler, 2010) and polyethylene glycol (Aisenbrey & Murphy, 2020; Zustiak & Leach, 2010).

4.2. Neuronal growth and attachment to HAA

The live cell imaging results provide a detailed assessment of ReNcell proliferation and interaction with laminin-coated HAA in monoculture (Figure 9) and with HUMSCs in co-culture (Figure 10). In the monoculture setup, early observations on day 1 revealed scattered ReNcells adhering to the HAA surface, identified by DiO fluorescence and DAPI-stained nuclei. Minimal overlap between nuclei and fluorescence signals suggested initial adhesion without substantial proliferation. By day 4, fluorescence intensity and nuclear count increased, indicating the onset of ReNcell proliferation and spreading across the porous HAA surface. This may reflect the adaptation within HAA's 3D microenvironment. This aligns with known behaviour of cells adapting to bioactive surfaces, wherein lag phases are followed by increased spreading and lineage commitment (Baraniak & McDevitt, 2012; Meli et al., 2014). This trend continued through day 7, with cells exhibiting an elongated morphology and covering larger areas of the scaffold, adapting well to the 3D architecture. By day 14, ReNcells achieved extensive coverage, forming interconnected networks across the scaffold, with robust proliferation evidenced by high fluorescence intensity and nuclear density.

In the co-culture setup, early imaging on day 1 showed sparse fluorescence signals for both DiD and DiO, with limited overlap and sparse nuclei. By day 4, increased fluorescence intensity and nuclear density indicated successful adhesion and proliferation of both cell types. The overlap between red and green fluorescence suggested initial interactions between the two cell populations. Significant changes were observed by day 7, with widespread cell distribution and pronounced co-localization of

fluorescence signals, reflecting interaction and adaptation to the porous architecture. By day 14, the co-culture system displayed dense cellular coverage with extensive overlap between DiD and DiO signals, demonstrating a cohesive and integrated cell layer across the surface of HAA. The pronounced co-localization of DiO- and DiD-labelled cells observed by day 14 suggests more than mere spatial proximity. While the overlap in fluorescence could indicate physical cohabitation of ReNcells and HUMSCs on the HAA surface, the increasing density and integration of signals over time may also reflect a more meaningful interaction. One possibility is the formation of a supportive microenvironment in which HUMSCs influence ReNcell behaviour through biochemical signalling and matrix interactions. MSCs are known to secrete a variety of neurotrophic factors including BDNF and NGF that are known promote neuronal survival, differentiation, and synapse formation. In addition, MSCs are also capable of remodelling the ECM, releasing exosomes, and influencing local stiffness, all of which can shape the fate and function of neighbouring ReNcells (Doeppner et al., 2015; Ma et al., 2020). The increasing overlap of DiO and DiD signals over time may suggest that the two cell types are not just growing side by side, but rather that they are beginning to interact more directly. This interaction could involve the exchange of signalling molecules or other forms of communication that help the cells adapt to each other and the 3D environment of the HAA scaffold. In native tissue, support cells like glia and stromal cells are known to influence how neurons grow and develop, so a similar process might be happening here (Snyder et al., 2010). However, since this study did not include measurement of signalling molecule expression, it is not possible to say for certain what kind of interaction is taking place. Therefore, future studies should aim to pair live cell imaging with immunocytochemical or molecular analyses at defined time points. This could involve quantifying expression of neuronal markers like βIII-tubulin, astrocytic markers like GFAP to delineate how HUMSCs influence ReNcell fate over time. Furthermore, single-cell RNA sequencing or spatial transcriptomics could provide high-resolution insights into the heterogeneity of cellular responses within the scaffold and the spatial dynamics of differentiation.

Previous studies have successfully utilized lipophilic dyes such as DiO and DiD for tracking intercellular interactions. For instance, Lehmann et al. (2016) employed these

dyes in a human chondrosarcoma cell co-culture model and found that both DiO and DiD did not affect cell proliferation, and their degradation rates were comparable. Additionally, the crossover effects between the two dyes were negligible, indicating that they could be used independently for tracking cellular behaviours without interference. These findings support the use of DiO and DiD in our study, as these dyes possess similar properties that allow for reliable labelling of cells without disrupting their normal biological functions. DiO and DiD are lipophilic and readily integrate into the cell membrane, where they label cells in a stable and non-invasive manner which makes them ideal for live cell imaging experiments (Lehmann et al., 2016).

Despite the promising observations of ReNcell adhesion and proliferation on the HAA discs, there are limitations to consider. One major challenge in this study was the autofluorescence of the HAA material, which made it difficult to isolate the specific fluorescence signals from ReNcells. The DiO dye was excited at 488 nm, with an emission of approximately 501 nm. However, autofluorescence from the HAA was observed within this same emission range, which interfered with the DiO signal. This was not observed with DiD, as its emission of approximately 665 nm did not overlap with the autofluorescence of the HAA. The autofluorescence of HAA presented a challenge in imaging at earlier time points, such as day 1 and day 4, when the ReNcells were sparsely distributed on the material surface. This interference obscured the DiO signal and made it difficult to accurately assess cell location and density, as there were not enough DAPI-stained nuclei to reliably visualize cell distribution. To reduce autofluorescence, future studies could incorporate spectral unmixing or use fluorophores with far-red or near-infrared emission spectra to bypass overlapping ranges. Alternatively, pre-treatment of the scaffold with quenching agents such as Sudan Black B may also help to further reduce background signal, as used in autofluorescence-rich materials like bone (Schnell et al., 1999).

Another limitation of this study was the difficulty in obtaining consistent imaging of the highly porous structure of the HAA scaffold. The complex surface architecture was by gas entrapment and irregular crystal growth due to the fabrication process, which resulted in multiple focal planes which made it challenging to capture a full image of the material in 2D. This not only hindered visualization but may have also affected how

uniformly cells adhered, as surface roughness and topographical variation can influence attachment points and local microenvironments. Future studies could benefit from z-stack imaging to better assess cell distribution across different depths of the scaffold.

The immunofluorescence data presented in Figure 7 demonstrated that ReNcells cultured atop a HUMSC monolayer expressed key markers of neuronal (β3-tubulin) and glial (GFAP) differentiation. This finding supports the notion that ReNcells retain the capacity to differentiate into multiple neural lineages when exposed to appropriate microenvironmental cues. The presence of these markers, confirmed through specific primary antibody staining, suggests that the co-culture system can provide at least some of the instructive signals required for neural lineage commitment. However, while these results are encouraging, they represent only a preliminary step in evaluating the broader hypothesis that HAA supports innervation.

Critically, this immunostaining was not extended to ReNcells cultured directly on the HAA scaffold. Due to resource constraints and the high cost of antibodies, this limits the strength of conclusions that can be drawn about the effect of HAA on neural differentiation. Without confirming that ReNcells maintain or enhance neural differentiation when cultured within the 3D environment of HAA, particularly in the presence of HUMSCs, the innervative potential of HAA remains suggestive rather than established. Additionally, while β3-tubulin and GFAP are widely used as markers for early neuronal and astrocytic differentiation, they do not provide insight into the functional maturity of the cells. Therefore, additional markers such as microtubule-associated protein 2 (MAP2) for dendritic development or Synapsin-1 for synaptogenesis, would be necessary to evaluate whether these cells progress beyond early fate commitment toward functional integration (Castejón et al., 2004; Iwata et al., 2005). The inclusion of such markers would also allow for a more detailed spatial and temporal analysis of how the scaffold environment influences lineage specification and maturation.

To complement imaging-based approaches, future studies should integrate molecular techniques such as qPCR to track gene expression changes in neural differentiation markers over time. This would enable statistically robust comparisons across conditions and help distinguish between transient expression and sustained lineage progression. Similarly, protein-level quantification using qPCR, ELISA, or even Western blotting could

validate and expand upon the immunofluorescence findings, providing a more complete understanding of the differentiation dynamics within the HAA scaffold. While the initial immunofluorescence results validate the potential for differentiation in co-culture, additional work is still needed to fully determine the innervative capacity of the HAA scaffold. Nonetheless, this offers a strong starting point and justify further, more detailed investigation and establishing the HAA's capacity to guide and maintain neural differentiation will be essential for substantiating its potential role in promoting innervation in synthetic bone grafts.

4.3. Potential for innervated HAA scaffolds to enhance new bone formation

The *in vivo* model assessed the osteoregeneration and degradative properties of HAA paste when applied to surgically induced femoral fractures. While these experiments provide valuable translational insight, they diverge substantially from the *in vitro* system developed in this study. Notably, the HAA used *in vivo* was delivered in paste form, without embedded ReNcells or HUMSCs, and therefore lacks the structural and biological components central to the innervation-focused *in vitro* design. This limits the extent to which the *in vivo* findings can inform conclusions about HAA's neuro-supportive potential. Despite these differences, the *in vivo* data offer relevant evidence regarding the biocompatibility, resorbability, and bone-healing capacity of HAA. Across the 56-day observation period, HAA-treated fractures exhibited enhanced closure compared to controls, particularly at days 28 and 56. The absence of significant differences at day 14 suggests limited influence during early healing, but a strong osteogenic effect as healing progresses. This delayed, yet accelerated closure profile may reflect the time-dependent resorption of HAA and its role in providing early mechanical stability followed by gradual replacement with native bone.

The biodegradation results further support this interpretation, showing a substantial reduction in material volume over time. Although the greatest change occurred between day 14 and 28, significance was only reached when comparing day 14 to day 56, indicating a progressive and possibly tapering degradation process. This profile is consistent with resorbable graft materials that aim to balance scaffold function with eventual replacement by host tissue. However, the lack of neural markers or innervation-

related endpoints in the *in vivo* study severely limits its relevance to the core hypothesis of this dissertation: that HAA supports not only bone regeneration but also the conditions necessary for neural integration. The absence of co-delivered neural or glial cells, as well as the paste formulation's differing surface architecture, makes it unlikely that the material's behaviour *in vivo* reflects the same cell–material interactions observed *in vitro*. Furthermore, no immunohistochemical or molecular data were collected to assess potential nerve ingrowth, axon guidance, or neurotrophic signalling within the regenerated tissue. Nevertheless, these findings indirectly support the translational relevance of HAA by confirming that the base material is osteoconductive and biodegradable within a living system. If future studies were to incorporate neuro-supportive elements into the *in vivo* model such as co-delivery of HUMSCs, neural precursors like ReNcells, and even neurotrophic factors to further enhance innervation. This model could be adapted to test HAA's ability to support functional innervation during bone repair. This component should be interpreted as a complementary validation of the material's regenerative potential, rather than as direct evidence of its neuro-supportive properties. Its inclusion strengthens the case for HAA as a promising scaffold candidate but also highlights the need for future work to unify osteogenic and neurogenic endpoints in a single *in vivo* system.

While the *in vivo* study provides useful preliminary data on HAA's bone regenerative capacity, it is important to acknowledge the limited sample size used as only 6 rats were included in total. Having such a small cohort restricts the statistical power of the analysis and increases the risk that observed trends may not reliably represent biological variability. A larger sample size would be necessary to confirm the robustness of the fracture gap closure and biodegradation findings. However, it should also be noted that increase animal numbers must be carefully balanced against ethical considerations inherent to vertebrate research. The use of a limited number of animals aligns with the principles of the 3Rs (Replacement, Reduction, and Refinement), which seek to minimize animal use and suffering while maximizing scientific output. Given the preliminary nature of this study and the invasive surgical procedures involved, the choice of a small cohort also reflects a responsible approach to animal welfare. In addition, the rat femoral fracture model, while well-established for studying bone healing, has inherent

limitations in replicating the full complexity of human bone repair and neuro-osteogenic interactions. Differences in bone physiology, healing kinetics, and scale limit the direct translatability of findings.

The absence of direct measures of innervation or neural integration further reduces the model's suitability for evaluating the neuro-supportive aspects of HAA. Therefore, it is crucial for future studies to consider using larger, more comprehensive cohorts combined with refined endpoints to better explain the role of HAA in supporting both osteogenesis and innervation; for instance, this could be achieved by including histological and molecular assessments of nerve ingrowth and functional recovery. Alternative or complementary animal models, potentially with genetically modified reporters for neural tissue, could also improve mechanistic understanding while addressing ethical and scientific challenges.

To build on these preliminary findings and more effectively evaluate HAA's neuro-supportive potential, future *in vivo* studies should address several current limitations. Incorporating the co-delivery of neural or glial cells, such as ReNcells or HUMSCs, would better reflect the bioactive environment modelled *in vitro*. Additionally, future work should explore how differences in surface architecture between scaffold and paste formulations influence neural interactions. Crucially, histological and molecular analyses targeting nerve ingrowth are needed to assess innervation directly. This includes the use of established immunohistochemical markers such as PGP9.5, NF200, and βIII-tubulin, alongside functional assays of nerve regeneration like electrophysiology and gait analysis (Castañeda-Corral et al., 2012; Heinzel et al., 2020; Madsen et al., 1996; Ronchi et al., 2023). Without these elements, conclusions about HAA's capacity to support neural integration during bone repair remain speculative.

4.4. Limitations and future directions

This study offers preliminary insight into the innervative capacity of HAA as a scaffold for bone regeneration, however, several methodological and conceptual limitations must be acknowledged. These limitations span both the *in vitro* and *in vivo* components of the study and highlight important considerations for future work.

The *in vitro* limitations were primarily technical and resource-related. The highly porous, autofluorescent structure of HAA made live cell and immunofluorescence imaging challenging. The 3D architecture of HAA restricted the resolution and clarity needed for robust characterization. While attempts were made to solve these issues by sanding the surface of the HAA scaffold disc and ROI-based imaging, these adaptations did not fully resolve the imaging challenges. Future work could explore strategies to overcome the challenges, such as applying autofluorescence quenchers such as Sudan Black B to reduce background signal and acquiring Z-stack images could improve 3D visualization and analysis of cellular structures within the scaffold. Expanding the panel of immunofluorescent markers, which was limited here due to resource constraints, would also enable a more comprehensive characterization of neural subtypes and maturity stages. Future studies should expand this panel to include markers of glial and neuronal differentiation (e.g., GFAP, MAP2, B3-Tubulin), as well as markers of synaptic formation and neurotrophic signalling, for deeper insight into neural maturation on HAA.

The *in vivo* component demonstrated the osteogenic and biodegradable properties of HAA. The material used in the rat fracture model differed significantly from the *in vitro* design, which altered surface architecture and degradation dynamics. Furthermore, no molecular or histological analyses relevant to nerve ingrowth were performed. Future work would benefit from using immunohistochemical markers such as βIII-tubulin, PGP9.5, or NF200, as well electrophysiology or gait analysis.

It should also be noted that this study did not extensively assess immunogenicity or inflammatory responses to HAA implantation. While osteocompatibility and bioresorbability were demonstrated, biocompatibility encompasses a broader scope, which includes the scaffold's interactions with the host immune system. The absence of cytokine profiling, immune cell infiltration histology, and long-term inflammatory assessments limits understanding of potential adverse immune reactions or chronic inflammation that could impair healing or scaffold integration. Therefore, future work should incorporate detailed immunological evaluations over extended time points to ensure HAA elicits a favorable host response, thereby supporting safe clinical translation. Additionally, the relatively short experimental timeline restricts insight into long-term functional outcomes of bone repair and neural integration. Successful clinical

translation not only requires structural bone regeneration, but also restoration of mechanical integrity and functional neural circuitry. For this reason, longer-term *in vivo* studies are necessary to evaluate sustained scaffold stability, biomechanical strength recovery, innervation. These assessments will better model the clinical scenario where scaffold degradation must be balanced with new tissue formation to maintain load-bearing capacity and neural connectivity. Future work could assess these by implementing behavioural or electrophysiological assays alongside with the immunohistology and imaging analyses to provide a comprehensive understanding of HAA performance over clinically relevant time scales. The sample size in the *in vivo* study (n = 6) also represents a key limitation. While aligned with ethical principles under the 3Rs (Replacement, Reduction, and Refinement), the small cohort limits statistical power and increases variability risk (Hubrecht & Carter, 2019).

Although the findings presented here highlight the potential of HAA as a scaffold for skeletal tissue regeneration, there are several important factors must be considered when evaluating the clinical applicability of this material. The formulation used in this study, which used a ratio of 1:1 between the HA and $CaCO_3$ were specifically developed with the *in vitro* culture in mind, however, this may not fully replicate the form or function required for *in vivo* implantation in human critical-sized bone defects. The paste formulation used in the rat femur defect model demonstrates improved clinical relevance in terms of delivery, but it lacks the complex architecture necessary for controlled cell infiltration, nutrient diffusion, as well as the eventual innervation and vascularization which are all essential properties for integration in large-scale defects. Overall, *in vivo* implantation testing using larger animal models would be more useful as there is a notable size difference between humans and rat models, particularly with the size of their critical bone defects, which makes rats a suboptimal animal for these experimental purposes. However, it is important to take into consideration that despite a larger animal model, such as miniature pigs (Ruehe et al., 2009) being more useful, the costs associated with it would be significantly higher so to justify this and the animal suffering, it would be critical to thoroughly test HAA and its innervative capacity on much smaller scales before scaling up. For successful clinical translation of HAA, it is crucial to recognize that bone healing rates vary significantly depending on the anatomical

location of the injury. For example, femoral fractures typically require 3 to 6 months to heal (Lim et al., 2016), while fibular fractures tend to heal faster, within 7 to 9 weeks (Encinas et al., 2023). This variability indicates that scaffold resorption rates should be customized to the specific injury site rather than applying a universal approach. In addition, the regenerative capacity of bone declines with age, meaning elderly patients may benefit from scaffolds that degrade more slowly to provide sustained mechanical support and promote effective new bone formation compared to younger individuals (Clark et al., 2017). This consideration is particularly relevant in bone-related pathologies such as osteoporosis, where healing dynamics are further compromised (Cheung et al., 2016). Therefore, future research must carefully account for injury location, patient age, and underlying bone pathologies to optimize scaffold design and enhance clinical outcomes in bone repair.

Scaffold reproducibility and reliability also remain a critical barrier to clinical translation. The current fabrication process, while sufficient for laboratory-scale experimentation, produces a highly porous and irregular surface architecture due to the solvent casting technique employed. The formation of air bubbles during solvent casting fabrication method contributes to non-uniform porosity across both macro- and microscopic scales. While this contributes to high surface area which may be beneficial for cell attachment, it introduces variability in mechanical integrity and may hinder the controlled spatial distribution of cells or signalling molecules, and it may also lead to a weaker mechanical integrity and structure damage over time. Inconsistent topography and pore size may also influence cellular behaviour unpredictably, potentially limiting reproducibility between batches and increasing the risk of uneven tissue ingrowth or inflammatory responses *in vivo*. Moreover, such surface irregularities may complicate sterilisation, coating, or cell-seeding processes, which are all critical for clinical application.

Future work should therefore prioritise refinement of the scaffold architecture to balance mechanical strength with mass transport properties. This may involve transitioning toward advanced fabrication techniques such as extrusion-based 3D printing or freeze-casting to generate more controlled pore structures. For example, variants such as honeycomb or gradient-based structures could enhance mechanical integrity while

improving cell migration and nutrient diffusion across the scaffold (Roohani-Esfahani et al., 2016).

CONCLUSION

This study provides preliminary insight into the innervative capacity of HAA as a scaffold for bone regeneration. Both *in vitro* and *in vivo* experiments demonstrated that HAA supports osteogenesis and exhibits promising biocompatibility. Alamar Blue assays revealed that HAA promotes cell adhesion, proliferation, and growth in both HUMSCs and ReNcell neural progenitors. Notably, ReNcells were able to attach, grow, and proliferate effectively when seeded on a HUMSC base layer, even without the laminin or Matrigel coatings typically used to support neural cell cultures. This finding was supported by live cell imaging, which showed increasing live cell staining over time. While the highly porous architecture of HAA facilitated cell growth and proliferation, it also introduced challenges for imaging, limiting detailed visualization of neural structures. However, the complex porous architecture of HAA, thought beneficial for cell adhesion and deposition, posed a significant challenge for detailed imaging. Similarly, the limitation neural markers and the absence of functional assays for nerve regeneration, further restricted conclusions about HAA's innervative properties. The *in vivo* studies confirmed the osteoconductive and biodegradable nature of HAA but lacked targeted evaluation of nerve ingrowth or functional neural integration, this prevents a full validation of the material's innervative potential. In addition to this, immunogenicity and inflammatory responses were not comprehensively assessed, and the relatively short study timeline limited observation of long-term scaffold integration and functional recovery.

Future research should prioritize overcoming these limitations by employing advanced imaging techniques, such as the use of autofluorescence quenchers, Z-stack confocal microscopy to improve visualization within the scaffold. Expanding immunohistochemical marker panels to include a broader range of neuronal and glial markers, coupled with functional assessments like electrophysiology, will also be

crucial for confirming neural integration. Overall, this study supports existing literature confirming HAA's osteogenic potential and suitability as a bone scaffold. Preliminary data exploring its innervative capacity was generated at an *in vitro* scale, so these findings are not sufficient to draw definitive conclusions. Therefore, further rigorous investigation is essential to fully understand and optimize the innervative potential of HAA. This work lays a foundation for future studies aimed at enhancing the design of synthetic bone allografts and functional outcomes in bone regeneration.

APPENDIX

Glossary

Osteoconductivity: The capacity to support the attachment, migration, and growth of new bone-forming cells.

Osteoinductivity: The capacity of a material to induce undifferentiated stem cells or progenitor cells into osteoblasts (bone-forming cells).

Neurogenesis: The process by which new neurons are generated from neural stem or progenitor cells, typically occurring in the central nervous system.

Angiogenesis: The process by which new blood vessels form from pre-existing vasculature, which is essential for supplying oxygen and nutrients to regenerating tissue.

REFERENCES

Adamczyk, A., Meulenkamp, B., Wilken, G., & Papp, S. (2020). Managing bone loss in open fractures. *OTA Int*, *3*(1), e059. https://doi.org/10.1097/oi9.0000000000000059

Ahmed, R. M., & Jayakumar, R. (2003). Peripheral nerve regeneration in RGD peptide incorporated collagen tubes. *Brain Research*, *993*(1-2), 208-216. https://doi.org/10.1016/j.brainres.2003.08.057

Ahn, J. D., Dubern, B., Lubrano-Berthelier, C., Clement, K., & Karsenty, G. (2006). Cart overexpression is the only identifiable cause of high bone mass in melanocortin 4 receptor deficiency. *Endocrinology*, *147*(7), 196-202. https://doi.org/https://doi.org/10.1210/en.2006-0281

Aisenbrey, E. A., & Murphy, W. L. (2020). Synthetic alternatives to Matrigel. *Nature Reviews Materials*(2058-8437 (Print)).

Albrektsson, T., & Johansson, C. (2001). Osteoinduction, osteoconduction and osseointegration. *European Spine Journal*, *10*, S96-S101. https://doi.org/10.1007/s005860100282

Alipour, M., Baneshi, M., Hosseinkhani, S., Mahmoudi, R., Jabari Arabzadeh, A., Akrami, M., Mehrzad, J., & Bardania, H. (2020). Recent progress in biomedical applications of RGD-based ligand: From precise cancer theranostics to biomaterial engineering: A systematic review. *Journal of Biomedical Materials Research Part A*, *108*(4), 839-850. https://doi.org/10.1002/jbm.a.36862

Allison, S. J., Baldock, P., Sainsbury, A., Enriquez, R., Lee, N. J., Lin, E.-J. D., Klugman, M., During, M., Eisman, J. A., Li, M., Pan, L. C., Herzog, H., & Gardiner, E. M. (2006). Conditional Deletion of Hypothalamic Y2 Receptors Reverts Gonadectomy-induced Bone Loss in Adult Mice*. *Journal of Biological Chemistry*, *281*(33), 23436-23444. https://doi.org/https://doi.org/10.1074/jbc.M604839200

Arvidson, K., Abdallah, B. A., L. A., Baldini, N., Cenni, E., Gomez-Barrena, E., Granchi, D., Kassem, M., Konttinen, Y. T., Mustafa, K., Pioletti, D. P., Sillat, T., & Finne-Wistrand, A. (2011). Bone regeneration and stem cells. *Journal of Cellular and Molecular Medicine*, *15*(4), 718-746. https://doi.org/https://doi.org/10.1111/j.1582-4934.2010.01224.x

Bădilă, A. E., Rădulescu, D. M., Niculescu, A. G., Grumezescu, A. M., Rădulescu, M., & Rădulescu, A. R. (2021). Recent Advances in the Treatment of Bone Metastases and Primary Bone Tumors: An Up-to-Date Review. *Cancers (Basel)*, *13*(16). https://doi.org/10.3390/cancers13164229

Bai, J., Liu, G., Gao, Y., Zhang, X., Niu, G., & Zhang, H. (2024). Co-culturing neural and bone mesenchymal stem cells in photosensitive hydrogel enhances spinal cord injury repair [Original Research]. *Frontiers in Bioengineering and Biotechnology*, *Volume 12* https://www.frontiersin.org/journals/bioengineering-and-biotechnology/articles/10.3389/fbioe.2024.1431420

Baldock, P. A., Lin, S., Zhang, L., Karl, T., Shi, Y., Driessler, F., Zengin, A., Hörmer, B., Lee, N. J., Wong, I. P. L., Lin, E. J. D., Enriquez, R. F., Stehrer, B., During, M. J., Yulyaningsih, E., Zolotukhin, S., Ruohonen, S. T., Savontaus, E., Sainsbury, A., & Herzog, H. (2014). Neuropeptide y attenuates stress-induced bone loss through suppression of noradrenaline circuits. *Journal of Bone and Mineral Research: The Official Journal of the American Society for Bone and Mineral Research*, *29*(10), 2238-2249. https://doi.org/https://doi.org/10.1002/jbmr.2205

Baldock, P. A., Sainsbury, A., Couzens, M., Enriquez, R. F., Thomas, G. P., Gardiner, E. M., & Herzog, H. (2002). Hypothalamic Y2 receptors regulate bone formation. *The Journal of Clinical Investigation*, *109*(7), 915-921. https://doi.org/https://doi.org/10.1172/jci14588

Baraniak, P. R., & McDevitt, T. C. (2012). Scaffold-free culture of mesenchymal stem cell spheroids in suspension preserves multilineage potential. *Cell Tissue Research*, *347*(3), 701-711. https://doi.org/https://doi.org/10.1007/s00441-011-1215-5

Baruffaldi, D., Palmara, G., Pirri, C., & Frascella, F. A.-O. (2021). 3D Cell Culture: Recent Development in Materials with Tunable Stiffness. *ACS Applied Bio Materials Journal*(2576-6422 (Electronic)).

Bertoni, L., Ferretti, M., Cavani, F., Zavatti, M., Resca, E., Benelli, A., & Palumbo, C. (2009). Leptin increases growth of primary ossification centers in fetal mice. *Journal of Anatomy*, *215*(5), 577-583. https://doi.org/https://doi.org/10.1111/j.1469-7580.2009.01134.x

Betz, R. R. (2002). Limitations of autograft and allograft: new synthetic solutions. *Orthopaedics*, *25*, S561-S570. https://doi.org/https://doi.org/10.3928/0147-7447-20020502-04

Blokhuis, T. J. (2017). Management of traumatic bone defects: Metaphyseal versus diaphyseal defects. *Injury*, *48*, S91-S93. https://doi.org/https://doi.org/10.1016/j.injury.2017.04.021

Boccaccini, A. R. (2005). 3 - Ceramics. In L. L. Hench & J. R. Jones (Eds.), *Biomaterials, Artificial Organs and Tissue Engineering* (pp. 26-36). Woodhead Publishing. https://doi.org/https://doi.org/10.1533/9781845690861.1.26

Born-Evers, G., Orr, A. L., Hulsey, E. Q., Squire, M. E., Hum, J. M., Plotkin, L., Sampson, C., Hommel, J., & Lowery, J. W. (2023). Examining the Role of Hypothalamus-Derived Neuromedin-U (NMU) in Bone Remodeling of Rats. *Life (Basel)*, *13*(4). https://doi.org/https://doi.org/10.3390/life13040918

Boyce, B. F., Yao, Z., & Xing, L. (2009). Osteoclasts have multiple roles in bone in addition to bone resorption. *Critical Reviews in Eukaryotic Gene Expression*, *19*(3), 171-180. https://doi.org/https://doi.org/10.1615/critreveukargeneexpr.v19.i3.10

Campana, V., Milano, G. P., E., Barba, M., Cicione, C., Salonna, G., Lattanzi, W., & Logroscino, G. (2014). Bone substitutes in orthopaedic surgery: from basic science to clinical practice. *Journal of Materials Science. Materials in Medicine*, *25*(10), 2445-2461. https://doi.org/https://doi.org/10.1007/s10856-014-5240-2

Carragee, E. J., Chu, G., Rohatgi, R., Hurwitz, E. L., Weiner, B. K., Yoon, S. T., Comer, G., & Kopjar, B. (2013). Cancer risk after use of recombinant bone morphogenetic protein-2 for spinal arthrodesis. *The Journal of Bone and Joing Surgery*, *95*(17), 1537-1545.

Castañeda-Corral, G., Jimenez-Andrade, J. M. B., A. P., Taylor, R. N., Mantyh, W. G., Kaczmarska, M. J., Ghilardi, J. R., & Mantyh, P. W. (2012). The majority of myelinated and unmyelinated sensory nerve fibers that innervate bone express the tropomyosin receptor kinase A. *Neuroscience*, *178*, 196-207. https://doi.org/https://doi.org/10.1016/j.neuroscience.2011.01.039

Castejón, O. J., Fuller, L., & Dailey, M. E. (2004). Localization of synapsin-I and PSD-95 in developing postnatal rat cerebellar cortex. *Developmental Brain Research*, *151*(1-2), 25-32. https://doi.org/https://doi.org/10.1016/j.devbrainres.2004.03.019

Chen, Q.-C., & Zhang, Y. (2022). The Role of NPY in the Regulation of Bone Metabolism [Review]. *Frontiers in Endocrinology*, *Volume 13 - 2022*. https://www.frontiersin.org/journals/endocrinology/articles/10.3389/fendo.2022.833485

Chen, S., Zhou, X., Li, T., & He, C. (2024). Vascularization and Innervation for Bone Tissue Engineering. *Accounts of Materials Research*, *5*(9), 1121-1133. https://doi.org/10.1021/accountsmr.4c00165

Chen, Z., Zhang, W., Wang, M., Backman, L. J., & Chen, J. (2022). Effects of Zinc, Magnesium, and Iron Ions on Bone Tissue Engineering. *ACS Biomaterials Science & Engineering*, *8*(6), 2321-2335. https://doi.org/https://doi.org/10.1021/acsbiomaterials.2c00368

Cheung, W. H., Miclau, T., Chow, S. K.-H., Yang, F. F., & Alt, V. (2016). Fracture healing in osteoporotic bone. *Injury*, *47*, S21-S26. https://doi.org/https://doi.org/10.1016/S0020-1383(16)47004-X

Chouirfa, H., Bouloussa, H., Migonney, V., & Falentin-Daudré, C. (2019). Review of titanium surface modification techniques and coatings for antibacterial applications. *Acta Biomaterialia*, *83*, 37-57. https://doi.org/https://doi.org/10.1016/j.actbio.2018.10.036

Clark, D., Nakamura, M., Miclau, T., & Marcucio, R. (2017). Effects of Aging on Fracture Healing. *Current Osteoporosis Reports*, *15*(6), 601-608. https://doi.org/https://doi.org/10.1007/s11914-017-0413-9

Clines, G. A. (2010). Prospects for osteoprogenitor stem cells in fracture repair and osteoporosis. *Current Opinion in Organ Transplantation*, *15*(1), 73-78. https://doi.org/https://doi.org/10.1097/MOT.0b013e328333d52c

Court-Brown, C. M., & Caesar, B. (2006). Epidemiology of adult fractures: A review. *Injury*, *37*(8), 691-697. https://doi.org/10.1016/j.injury.2006.04.130

Cui, X., Li, S., Gu, J., Lin, Z., Lai, B., Huang, L., Feng, J., Liu, B., & Zhou, Y. (2019). Retrospective study on the efficacy of bisphosphonates in tyrosine kinase inhibitor-treated patients with non-small cell lung cancer exhibiting bone metastasis. *Oncology Letters*, *18*(5), 5437-5447. https://doi.org/https://doi.org/10.3892/ol.2019.10870

Dard, M., Sewing, A., Meyer, J., Verrier, S., Roessler, S., & Scharnweber, D. (2000). Tools for tissue engineering of mineralized oral structures. *Clinical Oral Investigations*, *4*(2), 126-129.

De Prins, A., Allaoui, W., Medrano, M., Van Eeckhaut, A., Ballet, S., Smolders, I., & De Bundel, D. (2020). Effects of neuromedin U-8 on stress responsiveness and hypothalamus-pituitary-adrenal axis activity in male C57BL/6J mice. *Hormones and Behaviour*, *121*. https://doi.org/https://doi.org/10.1016/j.yhbeh.2019.104666

Deguchi, M., Tsuji, S., Katsura, D., Kasahara, K., Kimura, F., & Murakami, T. (2021). Current Overview of Osteogenesis Imperfecta. *Medicina (Kaunas)*, *57*(5). https://doi.org/10.3390/medicina57050464

Ding, W.-G., Zhang, Z.-M., Zhang, Y.-H., Jiang, S.-D., Jiang, L.-S., & Dai, L.-Y. (2010). Changes of substance P during fracture healing in ovariectomized mice. *Regulatory Peptides*, *159*(1), 28-34. https://doi.org/https://doi.org/10.1016/j.regpep.2009.11.004

Doeppner, T. R., Herz, J., Görgens, A., Schlechter, J., Ludwig, A. K., Radtke, S., de Miroschedji, K., Horn, P. A., Giebel, B., & Hermann, D. M. (2015). Extracellular Vesicles Improve Post-Stroke Neuroregeneration and Prevent Postischemic Immunosuppression. *Stem Cells Translational Medicine*, *4*(10), 1131-1143. https://doi.org/https://doi.org/10.5966/sctm.2015-0078

Dong, Z., & Zhao, X. (2021). Application of TPMS structure in bone regeneration. *Engineered Regeneration*, *2*, 154-162. https://doi.org/https://doi.org/10.1016/j.engreg.2021.09.004

Ducy, P., & Karsenty, G. (2010). The two faces of serotonin in bone biology. *Journal of Cell Biology*, *191*(1), 7-13. https://doi.org/https://doi.org/10.1083/jcb.201006123

El-Masri, B. M., Andreasen, C. M., Laursen, K. S., Kofod, V. B., Dahl, X. G., Nielsen, M. H., Thomsen, J. S., Brüel, A., Sørensen, M. S., Hansen, L. J., Kim, A. S., Taylor, V. E., Massarotti, C., McDonald, M. M., You, X., Charles, J. F., Delaisse, J.-M., & Andersen, T. L. (2024). Mapping RANKL- and OPG-expressing cells in bone tissue: the bone surface cells as activators of osteoclastogenesis and promoters of the denosumab rebound effect. *Bone Research*, *12*(1), 62. https://doi.org/10.1038/s41413-024-00362-4

Elefteriou, F. (2018). Impact of the Autonomic Nervous System on the Skeleton. *Physiological Reviews*, *98*(3), 1083-1112. https://doi.org/https://doi.org/10.1152/physrev.00014.2017

Encinas, R., Sharpe, J., Bakaes, Y., Mazoue, C., Jackson, B., & Gonzalez, T. (2023). Fibula Stress Fractures: A Systematic Review. *Foot & Ankle Specialist*. https://doi.org/https://doi.org/10.1177/19386400231184124

Erikstein, B. S., Hagland Hr Fau - Nikolaisen, J., Nikolaisen J Fau - Kulawiec, M., Kulawiec M Fau - Singh, K. K., Singh Kk Fau - Gjertsen, B. T., Gjertsen Bt Fau - Tronstad, K. J., & Tronstad, K. J. (2011). Cellular stress induced by resazurin leads to autophagy and cell death via

production of reactive oxygen species and mitochondrial impairment. *Journal of Cell Biochemistry*(1097-4644 (Electronic)).

Feng, X., & McDonald, J. M. (2011). Disorders of bone remodeling. *Annual Review of Pathology: Mechanisms of Disease*, *6*, 121-145. https://doi.org/https://doi.org/10.1146/annurev-pathol-011110-130203

Ferraz, M. P. (2023). Bone Grafts in Dental Medicine: An Overview of Autografts, Allografts and Synthetic Materials. . *Materials (Basel)*, *16*(11), 4117. https://doi.org/https://doi.org/10.3390/ma16114117

Ferretti, G., Romano, A., Sirabella, R., Serafini, S., Maier, T. J., & Matrone, C. (2022). An increase in Semaphorin 3A biases the axonal direction and induces an aberrant dendritic arborization in an in vitro model of human neural progenitor differentiation. *Cell & Bioscience*, *12*(1), 182. https://doi.org/10.1186/s13578-022-00916-1

Firdaus Hussin, M. S., Abdullah, H. Z., Idris, M. I., & Abdul Wahap, M. A. (2012). Extraction of natural hydroxyapatite for biomedical applications-A review. *Heliyon*, *8*(8). https://doi.org/https://doi.org/10.1016/j.heliyon.2022.e10356

Fitzpatrick, V., Martín-Moldes, Z., Deck, A., Torres-Sanchez, R., Valat, A., Cairns, D., Li, C., & Kaplan, D. L. (2021). Functionalized 3D-printed silk-hydroxyapatite scaffolds for enhanced bone regeneration with innervation and vascularization. *Biomaterials*, *276*, 120995. https://doi.org/https://doi.org/10.1016/j.biomaterials.2021.120995

Florencio-Silva, R., Sasso, G. R., Sasso-Cerri, E., Simões, M. J., & Cerri, P. S. (2015). Biology of Bone Tissue: Structure, Function, and Factors That Influence Bone Cells. *Biomed Research International*, *2015*. https://doi.org/https://doi.org/10.1155/2015/421746

Fraile-Martínez, O., García-Montero, C., Coca, A., Álvarez-Mon, M. A., Monserrat, J., Gómez-Lahoz, A. M., Coca, S., Álvarez-Mon, M., Acero, J., Bujan, J., García-Honduvilla, N., Asúnsolo, Á., & Ortega, M. (2021). Applications of Polymeric Composites in Bone Tissue Engineering and Jawbone Regeneration. . *Polymers (Basel)*, *13*(19). https://doi.org/10.3390/polym13193429

Franquinho, F., Liz, M. A., Nunes, A. F., Neto, E., Lamghari, M., & Sousa, M. M. (2010). Neuropeptide Y and osteoblast differentiation–the balance between the neuro-osteogenic network and local control. *The FEBS journal*, *277*(18), 3664-3674.

GBD 2019, F. C. (2021). Global, regional, and national burden of bone fractures in 204 countries and territories, 1990-2019: a systematic analysis from the Global Burden of Disease Study 2019. *The Lancet Healthy Longevity*, *2*(9), e580-e592. https://doi.org/https://doi.org/10.1016/s2666-7568(21)00172-0

Gianfagna, F., Cugino, D., Ahrens, W., Bailey, M. E. S., Bammann, K., Herrmann, D., Koni, A. C., Kourides, Y., Marild, S., Molnár, D., Moreno, L. A., Pitsiladis, Y. P., Russo, P., Siani, A., Sieri, S., Sioen, I., Veidebaum, T., & Iacoviello, L. (2013). Understanding the links among neuromedin U gene, beta2-adrenoceptor gene and bone health: an observational study in European children. *PLOS One*, *8*(8). https://doi.org/https://doi.org/10.1371/journal.pone.0070632

Gonzalez-Perez, F., Hernández, J., Heimann, C., Phillips, J. B., Udina, E., & Navarro, X. (2018). Schwann cells and mesenchymal stem cells in laminin- or fibronectin-aligned matrices and regeneration across a critical size defect of 15 mm in the rat sciatic nerve. *Journal of Neurosurgery: Spine*, *28*(1). https://doi.org/https://doi.org/10.3171/2017.5.spine161100

Gorter, E. A., Reinders, C. R., Krijnen, P., Appelman-Dijkstra, N. M., & Schipper, I. B. (2021). The effect of osteoporosis and its treatment on fracture healing a systematic review of animal and clinical studies. *Bone Rep*, *15*, 101117. https://doi.org/10.1016/j.bonr.2021.101117

Hall, P. E., Lathia Jd Fau - Caldwell, M. A., Caldwell Ma Fau - Ffrench-Constant, C., & Ffrench-Constant, C. (2008). Laminin enhances the growth of human neural stem cells in defined culture media. *BMC Neuroscience*(1471-2202 (Electronic)).

Hamidouche, Z., Fromigué, O., Ringe, J., Ringe, J., Häupl, T., Vaudin, P., Pagès, J.-C., Srouji, S., Livne, E., & Marie, P. J. (2009). Priming integrin alpha5 promotes human mesenchymal stromal cell osteoblast differentiation and osteogenesis. *Proceedings of the National Academy of Sciences of the United States of America*, *106*(44), 18587-18591.

Hayashi, M., Nakashima, T., Taniguchi, M., Kodama, T., Kumanogoh, A., & Takayanagi, H. (2012). Osteoprotection by semaphorin 3A. *Nature*, *485*, 69-74. https://doi.org/https://doi.org/10.1038/nature11000

Heinzel, J., Längle, G., Oberhauser, V., Hausner, T., Kolbenschlag, J., Prahm, C., Grillari, J., & Hercher, D. (2020). Use of the CatWalk gait analysis system to assess functional recovery in rodent models of peripheral nerve injury - a systematic review. *Journal of Neuroscience Methods.*, *345*. https://doi.org/https://doi.org/10.1016/j.jneumeth.2020.108889

Herber, V., Okutan, B., Antonoglou, G., N, G. S., & Payer, M. (2021). Bioresorbable Magnesium-Based Alloys as Novel Biomaterials in Oral Bone Regeneration: General Review and Clinical Perspectives. *Journal of Clinical Medicine*, *10*(9). https://doi.org/https://doi.org/10.3390/jcm10091842

Hofman, M., Rabenschlag, F., Andruszkow, H., Andruszkow, J., Möckel, D., Lammers, T., Kolejewska, A., Kobbe, P., Greven, J., Teuben, M., Poeze, M., & Hildebrand, F. (2019). Effect of neurokinin-1-receptor blockage on fracture healing in rats. *Scientific Reports*, *9*(1), 9744. https://doi.org/10.1038/s41598-019-46278-6

Horsnell, H., & Baldock, P. A. (2016). Osteoblastic Actions of the Neuropeptide Y System to Regulate Bone and Energy Homeostasis. *Current Osteoporosis Reports*, *14*(1), 26-31. https://doi.org/10.1007/s11914-016-0300-9

Huang, X., Wang, J., Xie, H., Zhang, Y., Wang, W., Yu, W., Liu, Y., & Ma, X. (2010). Microcapsules embedded with three-dimensional fibrous scaffolds for cell culture and tissue engineering. *Tissue Engineering. Park C, Methods*, *16*(5), 1023-1032. https://doi.org/https://doi.org/10.1089/ten.tec.2009.0545

Hubrecht, R. C., & Carter, E. (2019). The 3Rs and Humane Experimental Technique: Implementing Change. *Animals (Basel)*, *9*(10). https://doi.org/https://doi.org/10.3390/ani9100754

Ida-Yonemochi, H., Yamada, Y., Yoshikawa, H., & Seo, K. (2017). Locally Produced BDNF Promotes Sclerotic Change in Alveolar Bone after Nerve Injury. *PLOS One*, *12*(1). https://doi.org/https://doi.org/10.1371/journal.pone.0169201

Idelevich, A., Sato, K., Avihai, B., Nagano, K., Galien, A., Rowe, G., Gori, F., & Baron, R. (2020). Both NPY-Expressing and CART-Expressing Neurons Increase Energy Expenditure and Trabecular Bone Mass in Response to AP1 Antagonism, But Have Opposite Effects on Bone Resorption. *Journal of Bone and Mineral Research*, *35*(6), 1107-1118. https://doi.org/10.1002/jbmr.3967

Igwe, J. C., Jiang, X. P., Frane, Ma, L., Adams, D. J., Baldock, P. A., & Pilbeam, C. C. K., Ivo. (2009). Neuropeptide Y is expressed by osteocytes and can inhibit osteoblastic activity. *Journal of Cell Biochemistry*, *108*(3), 621-630. https://doi.org/https://doi.org/10.1002/jcb.22294

Iwata, M., K.T., M., Shirayama, Y., Yamamoto, A., & Kawahara, R. (2005). A study of a dendritic marker, microtubule-associated protein 2 (MAP-2), in rats neonatally treated neurosteroids, pregnenolone and dehydroepiandrosterone (DHEA). *Neuroscience Letters*, *386*(3), 145-149. https://doi.org/https://doi.org/10.1016/j.neulet.2005.06.004

Jäger, M., Böge, C., Janissen, R., Rohrbeck, D., Hülsen, T., Lensing-Höhn, S. K., R., & Herten, M. (2013). Osteoblastic potency of bone marrow cells cultivated on functionalized biometals with cyclic RGD-peptide. *Journal of Biomedical Materials Research Part A*, *101*(10), 2905-2914.

Jamshidi-adegani, F., Al-Hashmi, S., Vakilian, S., Al-kindi, J., Al-Fahdi, F., Al-Broumi, M., Al-Hadhrami, A., Alwahaibi, N., Shalaby, A., Gibbons, S., Al-Harrasi, A., & Al-Rawahi, W. (2024). Enhanced bone tissue regeneration via mesenchymal stem cells-laden

Alginate/GelMa 3D-Bioprinted scaffold treated with Haplophyllum tuberculatum extract. *Journal of Traditional and Complementary Medicine*. https://doi.org/https://doi.org/10.1016/j.jtcme.2024.11.016

Ji, Y., Mao, Y., Lin, H., Wang, Y., Zhao, P., Guo, Y., Gu, L., Fu, C., Chen, X., Lv, Z., Wang, N., Li, Q., & Bei, C. (2024). Acceleration of bone repairation by BMSCs overexpressing NGF combined with NSA and allograft bone scaffolds. *Stem Cell Research & Therapy*, *15*(1), 194. https://doi.org/10.1186/s13287-024-03807-z

Jinawath, S., Polchai, D., & Yoshimura, M. (2002). Low-temperature, hydrothermal transformation of aragonite to hydroxyapatite. *Materials Science and Engineering: C*, *22*(1), 35-39. https://doi.org/https://doi.org/10.1016/S0928-4931(02)00110-8

Karanth, D., Puleo, D., Dawson, D., Holliday, L., & Sharab, L. (2023). Characterization of 3D printed biodegradable piezoelectric scaffolds for bone regeneration. *Clinical and Experimental Dental Research*, *9*(2), 398-408. https://doi.org/https://doi.org/10.1002/cre2.712

Khor, E. C., & Baldock, P. (2012). The NPY System and its Neural and Neuroendocrine Regulation of Bone. *Current Osteoporosis Reports*, *10*(2), 160-168. https://doi.org/10.1007/s11914-012-0102-7

Kim, C., Lee, J. W., Heo, J. H., Park, C., Kim, D. H., Yi, G. S., Kang, H. C., Jung, H. S., Shin, H., & Lee, J. (2022). Natural bone-mimicking nanopore-incorporated hydroxyapatite scaffolds for enhanced bone tissue regeneration. *Biomterials Research*, *26*(1). https://doi.org/https://doi.org/10.1186/s40824-022-00253-x

Kim, H., Kumbar, S. G., & Nukavarapu, S. P. (2020). Biomaterial-directed cell behavior for tissue engineering. *Current Opinion in Biomedical Engineering*, *17*. https://doi.org/https://doi.org/10.1016/j.cobme.2020.100260

Kim, K., Eo, M., Nguyen, T., & Kim, S. (2019). General review of titanium toxicity. *International Journal of Implant Dentistry*, *5*(1), 10. https://doi.org/https://doi.org/10.1186/s40729-019-0162-x

Kim, W.-S., Park, B.-S., Park, S.-H., Kim, H.-K., & Sung, J.-H. (2009). Antiwrinkle effect of adipose-derived stem cell: Activation of dermal fibroblast by secretory factors. *Journal of Dermatological Science*, *53*(2), 96-102. https://doi.org/https://doi.org/10.1016/j.jdermsci.2008.08.007

Kim, Y.-J., Seo, D. H., Lee, S. H., Lee, S.-H., An, G.-H., Ahn, H.-J., Kwon, D., Seo, K.-W., & Kang, K.-S. (2018). Conditioned media from human umbilical cord blood-derived mesenchymal stem cells stimulate rejuvenation function in human skin. *Biochemistry and Biophysics Reports*, *16*, 96-102. https://doi.org/https://doi.org/10.1016/j.bbrep.2018.10.007

Kulangara, K., Adler, A. F., Wang, H., Chellappan, M., Hammett, E., Yasuda, R., & Leong, K. W. (2014). The effect of substrate topography on direct reprogramming of fibroblasts to induced neurons. *Biomaterials*, *35*(20), 5327-5336. https://doi.org/https://doi.org/10.1016/j.biomaterials.2014.03.034

Kusumbe, A. P., Ramasamy, S. K., & Adams, R. H. (2014). Coupling of angiogenesis and osteogenesis by a specific vessel subtype in bone. *Nature*, *507*(7492), 323-328. https://doi.org/https://doi.org/10.1038/nature13145

Kwakwa, K. A., & Sterling, J. A. (2017). Integrin αvβ3 Signaling in Tumor-Induced Bone Disease. . *Cancers (Basel)*, *9*(7), 84.

Lee, N. J., Nguyen, A. D., Enriquez, R. F., Doyle, K. L., Sainsbury, A., Baldock, P. A., & Herzog, H. (2010). Osteoblast specific Y1 receptor deletion enhances bone mass. *Bone*, *48*(3), 461-467. https://doi.org/https://doi.org/10.1016/j.bone.2010.10.174

Lee, N. J., Nguyen, A. D., Enriquez, R. F., Luzuriaga, J., Bensellam, M., Laybutt, R., Baldock, P. A., & Herzog, H. (2015). NPY signalling in early osteoblasts controls glucose homeostasis. *Molecular Metabolism*, *4*(3), 164-174. https://doi.org/https://doi.org/10.1016/j.molmet.2014.12.010

Lehmann, T. P., Juzwa, W., Filipiak, K., Sujka-Kordowska, P., Zabel, M., Głowacki, J., Głowacki, M., & Jagodziński, P. P. (2016). Quantification of the asymmetric migration of the lipophilic dyes, DiO and DiD, in homotypic co-cultures of chondrosarcoma SW-1353 cells. *Mol Med Rep*, *14*(5), 4529-4536. https://doi.org/10.3892/mmr.2016.5793

Li, J., M, A., J, B., P, A., Stark, A., & Kreicbergs, A. (2010). Occurrence of substance P in bone repair under different load comparison of straight and angulated fracture in rat tibia. *Journal of Orthopaedic Research*, *12*, 1643-1650.

Li, J., Zhao, Y., Chen, S., Wang, S., Zhong, W., & Zhang, Q. (2024). Research Hotspots and Trends of Bone Xenograft in Clinical Procedures: A Bibliometric and Visual Analysis of the Past Decade. . *Bioengineering (Basel)*, *10*(8), 929. https://doi.org/https://doi.org/10.3390/bioengineering10080929

Li, X., Liu, X., Josey, B., Chou, C. J., Tan, Y., Zhang, N., & Wen, X. (2014). Short Laminin Peptide for Improved Neural Stem Cell Growth. *Stem Cells Translational Medicine*, *3*(5), 662-670. https://doi.org/10.5966/sctm.2013-0015

Lian, M., Qiao, Z., Qiao, S., Zhang, X., Lin, J., Xu, R., Zhu, N., Tang, T., Huang, Z., Jiang, W., Shi, J., Hao, Y., Lai, H., & Dai, K. (2024). Nerve Growth Factor-Preconditioned Mesenchymal Stem Cell-Derived Exosome-Functionalized 3D-Printed Hierarchical Porous Scaffolds with Neuro-Promotive Properties for Enhancing Innervated Bone Regeneration. *ACS Nano*, *18*(10), 7504-7520. https://doi.org/10.1021/acsnano.3c11890

Lim, H. S., Kim, C. K., Park, Y. S., Moon, Y. W., Lim, S. J., & Kim, S. M. (2016). Factors Associated with Increased Healing Time in Complete Femoral Fractures After Long-Term Bisphosphonate Therapy. *Journal of Bone Joint Surgery America*, *98*(23), 1978-1987. https://doi.org/https://doi.org/10.2106/JBJS.15.01422

Lin, Y., Huang, S., Zou, R., Gao, X., Ruan, J., Weir, M. D., Reynolds, M. A., Qin, W., Chang, X., Fu, H., & Xu, H. H. K. (2019). Calcium phosphate cement scaffold with stem cell co-culture and prevascularization for dental and craniofacial bone tissue engineering. *Dental Materials*, *35*(7), 1031-1041. https://doi.org/https://doi.org/10.1016/j.dental.2019.04.009

Liu, F., Wei, B., Xu, X., Ma, B., Zhang, S., Duan, J., Kong, Y., Yang, H., Sang, Y., Wang, S., Tang, W., Liu, C., & Liu, H. (2021). Nanocellulose-Reinforced Hydroxyapatite Nanobelt Membrane as a Stem Cell Multi-Lineage Differentiation Platform for Biomimetic Construction of Bioactive 3D Osteoid Tissue In Vitro. *Advanced Healthcare Materials*, *10*(8). https://doi.org/https://doi.org/10.1002/adhm.202001851

Lomas, R., Chandrasekar, A., & Board, T. N. (2013). Bone allograft in the U.K.: perceptions and realities. *HIP International*, *23*(5), 427-433. https://doi.org/https://doi.org/10.5301/hipint.5000018

Longhin, E. M., El Yamani, N., Rundén-Pran, E., & Dusinska, M. (2022). The alamar blue assay in the context of safety testing of nanomaterials. *Frontiers in Toxicology*(2673-3080 (Electronic)).

Lucas, A., Gaudé, J., Carel, C., Michel, J. F., & Cathelineau, G. (2001). A synthetic aragonite-based ceramic as a bone graft substitute and substrate for antibiotics. *International Journal of Inorganic Materials*, *3*(1), 87-94. https://doi.org/https://doi.org/10.1016/S1466-6049(00)00058-1

Lupsa, B. C., & Insogna, K. (2015). Bone Health and Osteoporosis. *Endocrinol Metab Clin North Am*, *44*(3), 517-530. https://doi.org/10.1016/j.ecl.2015.05.002

Lv, X., Gao, F., & Cao, X. (2022). Skeletal interoception in bone homeostasis and pain. *Cell Metabolism*, *34*(12), 1914-1931. https://doi.org/https://doi.org/10.1016/j.cmet.2022.09.025

Ma, W., & Suh, W. H. (2019). Cost-Effective Cosmetic-Grade Hyaluronan Hydrogels for ReNcell VM Human Neural Stem Cell Culture. *Biomolecules*, *9*(10). https://doi.org/https://doi.org/10.3390/biom9100515

Ma, W., Zhang, X., Shi, S., & Zhang, Y. (2013). Neuropeptides stimulate human osteoblast activity and promote gap junctional intercellular communication. *Neuropeptides*, *47*(3), 179-186. https://doi.org/https://doi.org/10.1016/j.npep.2012.12.002

Ma, Y., Wang, H., Wang, Q., Cao, X., & Gao, H. (2023). Piezoelectric conduit combined with multi-channel conductive scaffold for peripheral nerve regeneration. *Chemical Engineering Journal*, *452*(3), 139424. https://doi.org/https://doi.org/10.1016/j.cej.2022.139424

Ma, Z. J., Yang, J. J., Lu, Y. B., Liu, Z. Y., & Wang, X. X. (2020). Mesenchymal stem cell-derived exosomes: Toward cell-free therapeutic strategies in regenerative medicine. *World Journal of Stem Cells*, *12*(8), 814-840. https://doi.org/https://doi.org/10.4252/wjsc.v12.i8.814

Machado, C. V., Telles, P. D., & Nascimento, I. L. (2013). Immunological characteristics of mesenchymal stem cells. *Revista Brasileira de Hematologia e Hemoterapia*, *35*(1), 62-67. https://doi.org/https://doi.org/10.5581/1516-8484.20130017

Madsen, J. E., Hukkanen, M., Nordsletten, L., Konttinen, Y. T., Santavirta, S., Polak, J. M., & Aspenberg, P. (1996). Sensory nerve ingrowth during bone graft incorporation in the rat. *Acta Orthopaedica Scandinavica*, *67*(3), 217-220. https://doi.org/https://doi.org/10.3109/17453679608994676

Martino, M. M., Mochizuki M Rothenfluh, D. A., Rempel, S. A., Hubbell, J. A., & Barker, T. H. (2009). Controlling integrin specificity and stem cell differentiation in 2D and 3D environments through regulation of fibronectin domain stability. *Biomaterials*, *30*(6), 1089-1097.

McCabe, N. P., De, S., Vasanji, A., Brainard, J., & Byzova, T. V. (2007). Prostate cancer specific integrin alphavbeta3 modulates bone metastatic growth and tissue remodeling. *Oncogene*, *26*(4), 6238-6243.

Meli, L., Barbosa, H. S. C., Hickey, A. M., Gasimli, L., Nierode, G., Diogo, M. M., Linhardt, R. J., Cabral, J. M. S., & Dordick, J. S. (2014). Three dimensional cellular microarray platform for human neural stem cell differentiation and toxicology. *Stem Cell Research*, *13*(1), 36-47. https://doi.org/https://doi.org/10.1016/j.scr.2014.04.004

Miron, R. J., Hedbom, E., Saulacic, N., Zhang, Y., Sculean, A., Bosshardt, D. D., & Buser, D. (2011). Osteogenic potential of autogenous bone grafts harvested with four different surgical techniques. *Journal of Dental Research*, *90*(12), 1428-1433. https://doi.org/https://doi.org/10.1177/0022034511422718

Monchau, F., Hivart, P., Genestie, B., Chai, F., Descamps, M., & Hildebrand, H. F. (2013). Calcite as a bone substitute. Comparison with hydroxyapatite and tricalcium phosphate with regard to the osteoblastic activity. *Materials Science and Engineering: C*, *33*(1), 490-498. https://doi.org/https://doi.org/10.1016/j.msec.2012.09.019

Mondal, S., Park, S., Choi, J., Vu, T. T. H., Doan, V. H. M., Vo, T. T., Lee, B., & Oh, J. (2023). Hydroxyapatite: A journey from biomaterials to advanced functional materials. *Advances in Colloid and Interface Science*, *321*, 103013. https://doi.org/https://doi.org/10.1016/j.cis.2023.103013

Moreira, C. A., Dempster, D. W., & Baron, R. (2019). *Anatomy and Ultrastructure of Bone – Histogenesis, Growth and Remodeling*. . MDText.com, Inc.

Motyl, K. J., & Rosen, C. J. (2012). Understanding leptin-dependent regulation of skeletal homeostasis. *Biochimie*, *94*(10), 2089-2096. https://doi.org/https://doi.org/10.1016/j.biochi.2012.04.015

Munshi, S., Twining, R. C., & Dahl, R. (2014). Alamar blue reagent interacts with cell-culture media giving different fluorescence over time: Potential for false positives. *Journal of Pharmacological and Toxicological Methods*, *70*(2), 195-198. https://doi.org/https://doi.org/10.1016/j.vascn.2014.06.005

Nauth, A., Schemitsch, E., Norris, B., Nollin, Z., & Watson, J. T. (2018). Critical-Size Bone Defects: Is There a Consensus for Diagnosis and Treatment? *Journal of Orthopaedic Trauma*, *31*, S7-S11. https://doi.org/10.1097/BOT.0000000000001115

Ngo, T. D., Kashani, A., Imbalzano, G., Nguyen, K. T. Q., & Hui, D. (2018). Additive manufacturing (3D printing): A review of materials, methods, applications and challenges. *Composites Part B: Engineering*, *143*, 172-196. https://doi.org/https://doi.org/10.1016/j.compositesb.2018.02.012

Nguyen, T. T., Hu, C. C., Sakthivel, R., Nabilla, S. C., Huang, Y. W., Yu, J., Cheng, N. C., Kuo, Y. J., & Chung, R. J. (2022). Preparation of gamma poly-glutamic acid/hydroxyapatite/collagen composite as the 3D-printing scaffold for bone tissue engineering. *Biomaterials Research*, *26*(1), 21. https://doi.org/https://doi.org/10.1186/s40824-022-00265-7

Ni, M., & Ratner, B. D. (2003). Nacre surface transformation to hydroxyapatite in a phosphate buffer solution. *Biomaterials*, *24*(23), 4323-4331. https://doi.org/https://doi.org/10.1016/S0142-9612(03)00236-9

Nierode, G. J., Gopal, S., Kwon, P., Clark, D. S., Schaffer, D. V., & Dordick, J. S. (2018). High-throughput identification of factors promoting neuronal differentiation of human neural progenitor cells in microscale 3D cell culture. *Biotechnology and Bioengineering*, *116*(1), 160-180. https://doi.org/https://doi.org/10.1002/bit.26839

Nierode, G. J., Perea, B. C., McFarland, S. K., Pascoal, J. F., Clark, D. S., Schaffer, D. V., & Dordick, J. S. (2016). High-Throughput Toxicity and Phenotypic Screening of 3D Human Neural Progenitor Cell Cultures on a Microarray Chip Platform. *Stem Cell Reports*, *7*(5), 970-982. https://doi.org/https://doi.org/10.1016/j.stemcr.2016.10.001

Nociari, M. M., Shalev, A., Benias, P., & Russo, C. (1998). A novel one-step, highly sensitive fluorometric assay to evaluate cell-mediated cytotoxicity. *Journal of Immunological Methods*, *213*(2), 157-167. https://doi.org/https://doi.org/10.1016/S0022-1759(98)00028-3

Oftadeh, R., Perez-Viloria, M., Villa-Camacho, J. C., Vaziri, A., & Nazarian, A. (2015). Biomechanics and mechanobiology of trabecular bone: a review. *Journal of Biomechanical Engineering*, *137*(1). https://doi.org/https://doi.org/10.1115/1.4029176

Oguić, M., Čandrlić, M., Tomas, M., Vidaković, B., Blašković, M., Jerbić Radetić, A. T., Zoričić Cvek, S., Kuiš, D., & Cvijanović Peloza, O. (2023). Osteogenic Potential of Autologous Dentin Graft Compared with Bovine Xenograft Mixed with Autologous Bone in the Esthetic Zone: Radiographic, Histologic and Immunohistochemical Evaluation. . *International Journal of Molecular Sciences*, *24*(7). https://doi.org/https://doi.org/10.3390/ijms24076440

Oliveira, É. R., Nie, L., Podstawczyk, D., Allahbakhsh, A., Ratnayake, J., Brasil, D. L., & Shavandi, A. (2021). Advances in Growth Factor Delivery for Bone Tissue Engineering. . *International Journal of Molecular Sciences*, *22*(2), 903. https://doi.org/https://doi.org/10.3390/ijms22020903

Osuchukwu, O. A., Salihi, A., Abdullahi, I., Obada, D. O., Abolade, S. A., Akande, A., Csaki, S., & Dodoo-Arhin, D. (2023). Datasets on the elastic and mechanical properties of hydroxyapatite: A first principle investigation, experiments, and pedagogical perspective. *Data in Brief*, *48*. https://doi.org/https://doi.org/10.1016/j.dib.2023.109075

Panseri, S., Montesi, M., Hautcoeur, D., Dozio, S. M., Chamary, S., De Barra, E., Tampieri, A., & Leriche, A. (2021). Bone-like ceramic scaffolds designed with bioinspired porosity induce a different stem cell response. *Journal of Materials Science. Materials in Medicine*, *32*(1), 3. https://doi.org/https://doi.org/10.1007/s10856-020-06486-3

Park, E. J., Truong, V.-L., Jeong, W.-S., & Min, W.-K. (2024). Brain-Derived Neurotrophic Factor (BDNF) Enhances Osteogenesis and May Improve Bone Microarchitecture in an Ovariectomized Rat Model. *Cells*, *13*(6). https://doi.org/10.3390/cells13060518

Pinho, T. S., Silva, D., Ribeiro, J. C., Marote, A., Lima, R., Batista, S. J., Melo, R., Ribeiro, C., Cunha, C. B., Moreira, I. S., Lanceros-Mendez, S., & Salgado, A. J. (2023). Enhanced neuronal differentiation by dynamic piezoelectric stimulation. *Journal of Biomedical Materials Research Part A*, *111*(1), 35-44.

Pokharel, R. K., Paudel, S., & Lakhey, R. B. (2022). Iliac Crest Bone Graft Harvesting: Modified Technique for Reduction of Complications. *Journal of Nepal Medical Association*, *60*(247), 325-328. https://doi.org/https://doi.org/10.31729/jnma.7086

Polinder, S., Haagsma, J., Panneman, M., Scholten, A., Brugmans, M., & Van Beeck, E. (2016). The economic burden of injury: Health care and productivity costs of injuries in the Netherlands. *Accid Anal Prev*, *93*, 92-100. https://doi.org/10.1016/j.aap.2016.04.003

Qi, J., Wang, Y., Chen, L., Chen, L., Wen, F., Huang, L., Rueben, P., Zhang, C., & Li, H. (2023). 3D-printed porous functional composite scaffolds with polydopamine decoration for bone regeneration. *Regenerative Biomaterials*, *10*. https://doi.org/https://doi.org/10.1093/rb/rbad062

Qi, Y., Fu, M., & Herzog, H. (2016). Y2 receptor signalling in NPY neurons controls bone formation and fasting induced feeding but not spontaneous feeding. *Neuropeptides*, *55*, 91-97. https://doi.org/https://doi.org/10.1016/j.npep.2015.09.009

Rajabi, A. H., Jaffe, M., & Arinzeh, T. L. (2015). Piezoelectric materials for tissue regeneration: A review. *Acta Biomaterialia*, *24*, 12-23. https://doi.org/https://doi.org/10.1016/j.actbio.2015.07.010

Rajani, R., & Gibbs, C. P. (2012). Treatment of Bone Tumors. *Surg Pathol Clin*, *5*(1), 301-318. https://doi.org/10.1016/j.path.2011.07.015

Reid, I. R., Baldock, P. A., & Cornish, J. (2018). Effects of Leptin on the Skeleton. *Endocrine Reviews*, *39*(6), 938-959. https://doi.org/10.1210/er.2017-00226

Ripamonti, U. (1996). Osteoinduction in porous hydroxyapatite implanted in heterotopic sites of different animal models. *Biomterials*, *17*(1), 31-35. https://doi.org/https://doi.org/10.1016/0142-9612(96)80752-6

Ronchi, G., Fregnan, F., Muratori, L., Gambarotta, G., & Raimondo, S. (2023). Morphological Methods to Evaluate Peripheral Nerve Fiber Regeneration: A Comprehensive Review. . *International Journal of Molecular Sciences*, *24*(3). https://doi.org/https://doi.org/10.3390/ijms24031818

Roohani-Esfahani, S.-I., Newman, P., & Zreiqat, H. (2016). Design and Fabrication of 3D printed Scaffolds with a Mechanical Strength Comparable to Cortical Bone to Repair Large Bone Defects. *Scientific Reports*, *6*(1). https://doi.org/10.1038/srep19468

Ruehe, B., Niehues, S., Heberer, S., & Nelson, K. (2009). Miniature pigs as an animal model for implant research: bone regeneration in critical-size defects. *Oral Surgery, Oral Medicine, Oral Pathology, Oral Radiology, and Endodontics*, *108*(5), 699-706. https://doi.org/https://doi.org/10.1016/j.tripleo.2009.06.037

Safari, B., Davaran, S., & Aghanejad, A. (2021). Osteogenic potential of the growth factors and bioactive molecules in bone regeneration. *International Journal of Biological Macromolecules*, *175*, 544-557. https://doi.org/https://doi.org/10.1016/j.ijbiomac.2021.02.052

Sato, S., Hanada, R., Kimura, A., Abe, T., Matsumoto, T., Iwasaki, M., Inose, H., Ida, T., Mieda, M., Takeuchi, Y., Fukumoto, S., Fujita, T., Kato, S., Kangawa, K., Kojima, M., Shinomiya, K.-i., & Takeda, S. (2007). Central control of bone remodeling by neuromedin U. *Nature Medicine*, *13*(10), 1234-1240. https://doi.org/10.1038/nm1640

Schlesinger, P. H., Blair, H. C., Beer Stolz, D., Riazanski, V., Ray, E. C., Tourkova, I. L., & Nelson, D. J. (2019). Cellular and extracellular matrix of bone, with principles of synthesis and dependency of mineral deposition on cell membrane transport. *American Journal of Physiology Cell Physiology*, *318*(1), 111-124. https://doi.org/https://doi.org/10.1152/ajpcell.00120.2019

Schmidt, A. H. (2021). Autologous bone graft: Is it still the gold standard? *Injury*, *52*, S18-S22. https://doi.org/https://doi.org/10.1016/j.injury.2021.01.043

Schnell, S. A., Staines, W. A., & Wessendorf, M. W. (1999). Reduction of lipofuscin-like autofluorescence in fluorescently labeled tissue. *The Journal of Histochemistry and*

Cytochemistry: Official Journal of the Histochemistry Society, *47*(6), 719-730. https://doi.org/https://doi.org/10.1177/002215549904700601

Sharan, K., & Yadav, V. K. (2014). Hypothalamic control of bone metabolism. *Best Practice & Research Clinical Endocrinology & Metabolism*, *28*(5), 713-723. https://doi.org/https://doi.org/10.1016/j.beem.2014.04.003

Shi, H., & Chen, M. (2024). The brain–bone axis: unraveling the complex interplay between the central nervous system and skeletal metabolism. *European Journal of Medical Research*, *29*(1), 317. https://doi.org/10.1186/s40001-024-01918-0

Shi, J., Dai, W., Gupta, A., Zhang, B., Wu, Z., Zhang, Y., Pan, L., & Wang, L. (2022). Frontiers of Hydroxyapatite Composites in Bionic Bone Tissue Engineering. *Materials (Basel, Switzerland)*, *15*(23). https://doi.org/10.3390/ma15238475

Shi, Y.-C., & Baldock, P. A. (2012). Central and peripheral mechanisms of the NPY system in the regulation of bone and adipose tissue. *Bone*, *50*(2), 430-436. https://doi.org/https://doi.org/10.1016/j.bone.2011.10.001

Shi, Y., He, R., Deng, X., Shao, Z., Deganello, D., Yan, C., & Xia, Z. (2020). Three-dimensional biofabrication of an aragonite-enriched self-hardening bone graft substitute and assessment of its osteogenicity in vitro and in vivo. *Biomaterials Translational*, *1*(1), 69-81. https://doi.org/https://doi.org/10.3877/cma.j.issn.2096-112X.2020.01.007

Shin, S. R., & Tornetta, P. r. (2016). Donor Site Morbidity After Anterior Iliac Bone Graft Harvesting. *Journal of Orthopaedic Trauma*, *30*(6), 340-343. https://doi.org/https://doi.org/10.1097/BOT.0000000000000551

Smit, T., Koppen, S., Ferguson, S. J., & Helgason, B. (2021). Conceptual design of compliant bone scaffolds by full-scale topology optimization. *Journal of the Mechanical Behaviour of Biomedical Materials*, *143*. https://doi.org/https://doi.org/10.1016/j.jmbbm.2023.105886

Snyder, B. R., Chiu, A. M., Prockop, D. J., & Chan, A. W. S. (2010). Human multipotent stromal cells (MSCs) increase neurogenesis and decrease atrophy of the striatum in a transgenic mouse model for Huntington's disease. *PLOS One*, *5*(2). https://doi.org/https://doi.org/10.1371/journal.pone.0009347

Song, Y., Subramanian, K., Berberich, M. J., Rodriguez, S., Latorre, I. J., Luria, C. M., Everley, R., Albers, M. W., Mitchison, T. J., & Sorger, P. K. (2019). A dynamic view of the proteomic landscape during differentiation of ReNcell VM cells, an immortalized human neural progenitor line. *Scientific Data*, *6*. https://doi.org/https://doi.org/10.1038/sdata.2019.16

Sousa, D. M., Martins, P. S., Leitão, L., Alves, C. J., Gomez-Lazaro, M., Neto, E., Conceição, F., Herzog, H., & Lamghari, M. (2020). The lack of neuropeptide Y-Y(1) receptor signaling modulates the chemical and mechanical properties of bone matrix. *FASEB Journal*, *34*(3), 4163-4177.

Steijvers, E., Ghei, A., & Xia, Z. (2022). Manufacturing artificial bone allografts: a perspective. *Biomaterials Translational*, *3*(1), 65-89. https://doi.org/https://doi.org/10.12336/biomatertransl.2022.01.007

Steijvers, E., Shi, Y., Lu, H., Zhang, W., Zhang, Y., Zhao, F., Wang, B., Hughes, L., Barralet, J. E., Degli-Alessandrini, G., Kraev, I., Johnston, R., Shao, Z., Ebetino, F. H., Triffitt, J. T., Russell, R. G. G., Deganello, D., Cao, X., & Xia, Z. (2025). Rapid assessment of the osteogenic capacity of hydroxyapatite/aragonite using a murine tibial periosteal ossification model. *Bioactive Materials*, *45*, 257-273. https://doi.org/https://doi.org/10.1016/j.bioactmat.2024.11.025

Subbiah, R., & Guldberg, R. E. (2019). Materials Science and Design Principles of Growth Factor Delivery Systems in Tissue Engineering and Regenerative Medicine. *Advanced Healthcare Materials*, *8*(1).

Sun, X., Liu, C., Shi, Y., Li, C., Sun, L., Hou, L., & Wang, X. (2019). The assessment of xenogeneic bone immunotoxicity and risk management study. *Biomedical Engineering Online*, *18*, 108. https://doi.org/https://doi.org/10.1186/s12938-019-0729-z

Tang, P., Duan, C., Wang, Z., Wang, C., Meng, G., Lin, K., Yang, Q., & Yuan, Z. (2017). NPY and CGRP Inhibitor Influence on ERK Pathway and Macrophage Aggregation during Fracture Healing. *Cellular Physiology and Biochemistry*, *41*(4), 1457-1467.

Tomlinson, R. E., Li, Z., Zhang, Q., Goh, B. C., Li, Z., Thorek, D. L. J., Rajbhandari, L., Brushart, T. M., Minichiello, L., Zhou, F., Venkatesan, A., & Clemens, T. L. (2016). NGF-TrkA Signaling by Sensory Nerves Coordinates the Vascularization and Ossification of Developing Endochondral Bone. *Cell Reports*, *16*(10), 2723-2735. https://doi.org/https://doi.org/10.1016/j.celrep.2016.08.002

Toyofuku, T., Yoshida, J., Sugimoto, T., Zhang, H., Kumanogoh, A., Hori M, & Kikutani, H. (2005). FARP2 triggers signals for Sema3A-mediated axonal repulsion. *Nature Neuroscience*, *12*, 1712-1719. https://doi.org/https://doi.org/10.1038/nn1596

Tse, J. R., & Engler, A. J. (2010). Preparation of hydrogel substrates with tunable mechanical properties. *Curr Protoc Cell Biol*, *Chapter 10*, Unit 10.16. https://doi.org/10.1002/0471143030.cb1016s47

Uemura, M., Refaat, M. M., Shinoyama, M., Hayashi, H., Hashimoto, N., & Takahashi, J. (2010). Matrigel supports survival and neuronal differentiation of grafted embryonic stem cell-derived neural precursor cells. *Journal of Neuroscience Research*, *88*(3), 542-551. https://doi.org/https://doi.org/10.1002/jnr.22223

Vuola, J., Göransson H Fau - Böhling, T., Böhling T Fau - Asko-Seljavaara, S., & Asko-Seljavaara, S. (1996). Bone marrow induced osteogenesis in hydroxyapatite and calcium carbonate implants. *Biomaterials*(0142-9612 (Print)).

Wang, Z., Zhang, M., Liu, Z., Wang, Y., Dong, W., Zhao, S., & Sun, D. (2022). Biomimetic design strategy of complex porous structure based on 3D printing Ti-6Al-4V scaffolds for enhanced osseointegration. *Materials & Design*, *218*. https://doi.org/https://doi.org/10.1016/j.matdes.2022.110721

Watanabe, J., & Akashi, M. (2008). Integration approach for developing a high-performance biointerface: Sequential formation of hydroxyapatite and calcium carbonate by an improved alternate soaking process. *Applied Surface Science*, *255*(2), 344-349. https://doi.org/https://doi.org/10.1016/j.apsusc.2008.06.103

Watt, S. M., Gullo, F., van der Garde, M., Markeson, D. C., Rosalba, Khoo, C. P., & Zwaginga, J. J. (2013). The angiogenic properties of mesenchymal stem/stromal cells and their therapeutic potential. *British Medical Bulletin*, *108*(1), 25-53. https://doi.org/https://doi.org/10.1093/bmb/ldt031

Weber, C. D., Migliorini, F., Delbrück, H., & Hildebrand, F. (2022). Surgical Management of an Osteomyelitis Associated Subchondral Bone Defect in the Pediatric Knee Based on Arthroscopy, "Ossoscopy" and Bone Grafting-A Case Report. *Life (Basel)*, *12*(11). https://doi.org/10.3390/life12111754

Wee, N. K. Y., Sinder, B. P., Novak, S., Wang, X., Stoddard, C., Matthews, B. G., & Kalajzic, I. (2019). Skeletal phenotype of the neuropeptide Y knockout mouse. *Neuropeptides*, *73*, 78-88. https://doi.org/https://doi.org/10.1016/j.npep.2018.11.009

Wu, A.-M., Bisignano, C., James, S. L., Abady, G. G., Abedi, A., Abu-Gharbieh, E., Alhassan, R. K., Alipour, V., Arabloo, J., Asaad, M., Asmare, W. N., Awedew, A. F., Banach, M., Banerjee, S. K., Bijani, A., Birhanu, T. T. M., Bolla, S. R., Cámera, L. A., Chang, J.-C., . . . Vos, T. (2021). Global, regional, and national burden of bone fractures in 204 countries and territories, 1990–2019: a systematic analysis from the Global Burden of Disease Study 2019. *The Lancet Healthy Longevity*, *2*(9), e580-e592. https://doi.org/10.1016/S2666-7568(21)00172-0

Wu, K., Huang, D., & Huang, X. (2023). The effects of semaphorin 3A in bone and cartilage metabolism: fundamental mechanism and clinical potential. *Frontiers in Cell and Developmental Biology*. https://doi.org/https://doi.org/10.3389/fcell.2023.1321151

Wu, Y., Cheng, M., Jiang, Y., Zhang, X., Li, J., Zhu, Y., & Yao, Q. (2023). Calcium-based biomaterials: Unveiling features and expanding applications in osteosarcoma treatment. *Bioactive Materials*(2452-199X (Electronic)).

Wu, Z., Li, Q., Xie, S., Shan, X., & Cai, Z. (2020). In vitro and in vivo biocompatibility evaluation of a 3D bioprinted gelatin-sodium alginate/rat Schwann-cell scaffold. *Materials Science and Engineering: C*, *109*. https://doi.org/https://doi.org/10.1016/j.msec.2019.110530

Xia, Z., Shi, Y., He, H., Pan, Y., & Liu, C. (2018). Development of Biodegradable Bone Graft Substitutes Using 3D Printing. In C. Liu & H. He (Eds.), *Developments and Applications of Calcium Phosphate Bone Cements* (pp. 517-545). Springer Singapore. https://doi.org/10.1007/978-981-10-5975-9_13

Xiao, Y., Han, C., Wang, Y., Zhang, X., Bao, R., Li, Y., Chen, H., Hu, B., & Liu, S. (2023). Interoceptive regulation of skeletal tissue homeostasis and repair. *Bone Research*, *11*(1), 48. https://doi.org/10.1038/s41413-023-00285-6

Xu, H.-Q., Liu, J.-C., Zhang, Z.-Y., & Xu, C.-X. (2022). A review on cell damage, viability, and functionality during 3D bioprinting. *Military Medical Research*, *9*(1), 70. https://doi.org/10.1186/s40779-022-00429-5

Xu, J., Li, Z., Tower, R., Negri, S., Wang, Y., Meyers, C. X., Sono, T., Qin, Q., Lu, A., Xing, X., McCarthy, E. F., Clemens, T. L., & James, A. W. (2022). NGF-p75 signaling coordinates skeletal cell migration during bone repair. *Science Advances*, *8*(11). https://doi.org/https://doi.org/10.1126/sciadv.abl5716

Yang, M., Zhang, Z.-C., Liu, Y., Chen, Y.-R., Deng, R.-H., Zhang, Z.-N., Yu, J.-K., & Yuan, F.-Z. (2021). Function and Mechanism of RGD in Bone and Cartilage Tissue Engineering [Review]. *Frontiers in Bioengineering and Biotechnology*, *Volume 9 - 2021*. https://www.frontiersin.org/journals/bioengineering-and-biotechnology/articles/10.3389/fbioe.2021.773636

Ye, J., & Gong, P. (2020). NGF-CS/HA-coating composite titanium facilitates the differentiation of bone marrow mesenchymal stem cells into osteoblast and neural cells. *Biochemical and Biophysical Research Communications*, *531*(3), 290-296. https://doi.org/https://doi.org/10.1016/j.bbrc.2020.06.158

Ye, J., Huang, B., & Gong, P. (2021). Nerve growth factor-chondroitin sulfate/hydroxyapatite-coating composite implant induces early osseointegration and nerve regeneration of peri-implant tissues in Beagle dogs. *Journal of Orthopaedic Surgery and Research*, *16*(1), 51. https://doi.org/10.1186/s13018-020-02177-5

Ye, L., Xu, J., Mi, J., He, X., Pan, Q., Zheng, L., Zu, H., Chen, Z., Dai, B., Li, X., Pang, Q., Zou, L., Zhou, L., Huang, L., Tong, W., Li, G., & Qin, L. (2021). Biodegradable magnesium combined with distraction osteogenesis synergistically stimulates bone tissue regeneration via CGRP-FAK-VEGF signaling axis. *Biomaterials*, *275*, 120984. https://doi.org/https://doi.org/10.1016/j.biomaterials.2021.120984

Yeo, T., Ko, Y.-G., Kim, E. J., Kwon, O. K., Chung, H. Y., & Kwon, O. H. (2021). Promoting bone regeneration by 3D-printed poly(glycolic acid)/hydroxyapatite composite scaffolds. *Journal of Industrial and Engineering Chemistry*, *94*, 343-351. https://doi.org/https://doi.org/10.1016/j.jiec.2020.11.004

Yılmaz, E., Gökçe, A., Findik, F., Gulsoy, H. O., & İyibilgin, O. (2018). Mechanical properties and electrochemical behavior of porous Ti-Nb biomaterials. *Journal of Mechanical Behaviours of Biomedical Materials*, *87*, 59-67. https://doi.org/https://doi.org/10.1016/j.jmbbm.2018.07.018

Yoon, B. S., Moon, J.-H., Jun, E. K., Kim, J., Maeng, I., Kim, J. S., Lee, J. H., Baik, C. S., Kim, A., Cho, K. S., Lee, J. H., Lee, H. H., Whang, K. Y., & You, S. (2009). Secretory Profiles and Wound

Healing Effects of Human Amniotic Fluid–Derived Mesenchymal Stem Cells. *Stem Cells and Development*, *19*(6), 887-902. https://doi.org/10.1089/scd.2009.0138

Yoshimura, M., Sujaridworakun, P., Koh, F., Fujiwara, T., Pongkao, D., & Ahniyaz, A. (2004). Hydrothermal conversion of calcite crystals to hydroxyapatite. *Materials Science and Engineering: C*, *24*(4), 521-525. https://doi.org/https://doi.org/10.1016/j.msec.2004.01.005

Youseflee, P., Ranjbar, F. E., Bahraminasab, M., Ghanbari, A., Faradonbeh, D. R., Arab, S., Alizadeh, A., & Nooshabadi, V. T. (2022). Exosome loaded hydroxyapatite (HA) scaffold promotes bone regeneration in calvarial defect: an in vivo study. *Cell and Tissue Banking*, *24*, 389-400.

Yuan, M., Hu, X., Yao, L., Jiang, Y., & Li, L. (2022). Mesenchymal stem cell homing to improve therapeutic efficacy in liver disease. *Stem Cell Research & Therapy*, *13*(1), 179. https://doi.org/https://doi.org/10.1186/s13287-022-02858-4

Zagho, M. M., Hussein, E. A., & Elzatahry, A. A. (2018). Recent Overviews in Functional Polymer Composites for Biomedical Applications. . *Polymers (Basel)*, *10*(7), 739. https://doi.org/https://doi.org/10.3390/polym10070739

Zhang, Y., Chen, H., Long, X., & Xu, T. (2021). The effect of neural cell integrated into 3D co-axial bioprinted BMMSC structures during osteogenesis. *Regenerative Biomaterials*, *8*(5). https://doi.org/10.1093/rb/rbab041

Zhao, R., Yang, R., Cooper, P. R., Khurshid, Z., Shavandi, A., & Ratnayake, J. (2021). Bone Grafts and Substitutes in Dentistry: A Review of Current Trends and Developments. . *Molecules*, *26*(10). https://doi.org/https://doi.org/10.3390/molecules26103007

Zhao, Y., Cai, Y., Wang, W., Bai, Y., Liu, M., Wang, Y., Niu, W., Luo, Z., Xia, L., Zhu, J., Zhao, F., Tay, F. R., & Niu, L. (2025). Periosteum-bone inspired hierarchical scaffold with endogenous piezoelectricity for neuro-vascularized bone regeneration. *Bioactive Materials*, *44*, 339-353. https://doi.org/https://doi.org/10.1016/j.bioactmat.2024.10.020

Zopf, D. A., Mitsak, A. G., Flanagan, C. L., Wheeler, M., Green, G. E., & Hollister, S. J. (2014). Computer aided-designed, 3-dimensionally printed porous tissue bioscaffolds for craniofacial soft tissue reconstruction. *Otolaryngology–Head and Neck Surgery*, *152*(1), 57-62. https://doi.org/https://doi.org/10.1177/0194599814552065

Zustiak, S. P., & Leach, J. B. (2010). Hydrolytically Degradable Poly(Ethylene Glycol) Hydrogel Scaffolds with Tunable Degradation and Mechanical Properties. *Biomacromolecules*, *11*(5), 1348-1357. https://doi.org/10.1021/bm100137q